UNIVERSITY OF TRENTO

International PhD Program in Biomolecular Sciences

Department of Cellular, Computational

and Integrative Biology – CIBIO

33 Cycle

"The role of mitochondria in reduced penetrance of heterozygous Parkin mutations"

Tutor: Prof. Simona Casarosa

Department of Cellular, Computational, and Integrative Biology - CIBIO, University of Trento, Trento, Italy

Advisor: Dr. Andrew A. Hicks

Institute for Biomedicine, Eurac Research; Affiliated Institute of the University of Lübeck, Bolzano, Italy

Ph.D. Thesis of

Maria Paulina Castelo R.

Institute for Biomedicine, Eurac Research

Academic Year 2019-2020

Abstract

Parkinson´s Disease (PD) is the most common neurodegenerative movement disorder, estimated to affect up to 2% of the population over 65 years of age (Lin et al., 2019; Santos et al., 2019). *Parkin (PRKN)* mutations are the most common known cause of autosomal recessive early-onset PD, accounting for up to 77% of cases with an age of onset ≤20 years (Lucking et al., 2000), and parkin dysfunction represents a risk factor for sporadic PD (Dawson & Dawson, 2014). *Parkin* variants have been identified in numerous families with different genetic backgrounds (Hedrich et al., 2004) and include more than 170 mutations consisting of copy number variations (deletions or multiplications of exons), small deletions/insertions, as well as single nucleotide polymorphisms (missense, nonsense, or splice site variations) (Corti et al., 2011). Importantly, a large number of patients carry exon rearrangements that result in protein truncation (Hedrich et al., 2001). Parkin is an E3 ubiquitin ligase, mostly known for its role in facilitating the selective clearance of dysfunctional mitochondria (mitophagy), and for its involvement in several other cellular processes like mitochondrial biogenesis, free radical metabolism, and inflammation (Celardo et al., 2014). Homozygous or compound-heterozygous mutations in the *Parkin* gene result in highly penetrant symptom expression, while heterozygous mutations have been predicted to predispose to disease symptoms with highly reduced penetrance (Huttenlocher et al., 2015; Weissbach et al., 2017). The presence of heterozygous *Parkin* mutations is one of the reported potential genetic risk factors for PD; (Huttenlocher et al., 2015; Klein et al., 2007). Considering the reported frequency of heterozygous mutations in the population (up to 3%), it is essential to have better estimates of the penetrance of these variants, and to investigate which risk markers manifest in carriers and are potentially useful for identifying those individuals at greater risk of neurodegeneration later in life. Furthermore, it is of great importance to test the causal link between heterozygous pathogenic mutations in *Parkin* and expressivity of molecular phenotypes in cellular models derived from mutation carriers. This was addressed in this thesis by (1) identifying *Parkin* mutation carriers in the population-based CHRIS study and characterizing them for the presence of PD risk markers; and (2) by evaluating mitochondrial integrity, including mitochondrial DNA variation and mitochondrial function, in diverse cellular models of heterozygous *Parkin* mutation carriers. I was able to show that heterozygous *Parkin* mutation carriers in the general population have increased occurrence of diabetes and decreased heart rate. Moreover, in a subset of individuals, I have identified an altered molecular

phenotype, characterized by disparities at the level of mtDNA integrity and mitochondrial function in blood and two different cellular models derived from the mutation carriers. To adequately understand individual disease conversion, there is a need for more longitudinal studies with putatively healthy individuals carrying *Parkin* mutations and more in-depth clinical phenotyping.

Table of Contents

Index of Figures

Index of Tables

1. Introduction

1.1 Parkinson´s Disease

Parkinson´s Disease (PD) is the most common neurodegenerative movement disorder, estimated to affect up to 2% of the population over 65 years of age (Lin et al., 2019; Santos et al., 2019). In industrialized countries, a prevalence of 0.3% in the entire population has been estimated, rising to 1% in the population over 60 years, and further reaching 3% among people over 80 years. Additionally, the incidence rates of PD vary between 8 and 18 per 100,000 person-years (de Lau & Breteler, 2006; Lee & Gilbert, 2016).

The earliest reports on shaky palsy date between the years 138 - 201 AD, and the first comprehensible description of the disease was done by the renowned English surgeon James Parkinson in his study “An essay on the shaking palsy” in 1817 (Ovallath & Deepa, 2013). Parkinson´s work on shaking palsy was recognized and further characterized by the neurologist Jean-Martin Charcot who named the disorder "maladie de Parkinson" (Parkinson´s disease) (Corti et al., 2011; Ovallath & Deepa, 2013).

The neuropathological hallmarks of PD include the progressive loss of dopaminergic (DA) neurons in the *substantia nigra pars compacta* (SNpc) and the formation of intracytoplasmic proteinaceous inclusions known as Lewy bodies (LBs). In addition, LBs localize in other brain regions such as the dorsal motor nucleus of the vagus and locus coeruleus, and contain the protein α-synuclein, neurofilaments, ubiquitin, among other compounds (Forno, 1996; Kumar et al., 2020; Spillantini et al., 1998). These circumstances lead to a deficient production of the neurotransmitter dopamine in the basal ganglia, translating into a movement disorder characterized by classical parkinsonian motor symptoms (Mendoza-Velasquez et al., 2019). Coupled with the aggregation of α-synuclein, the pathophysiological and pathogenic mechanisms characterizing PD include mitochondrial dysfunction, oxidative stress, aberrant clearance of defective proteins by the autophagy-lysosomal pathway (e.g., α-synuclein), deficits of proteosomal system function, and neuroinflammation (Havelund et al., 2017; Kuan et al., 2021).

PD is clinically characterized by cardinal motor manifestations as resting tremor, muscle rigidity, bradykinesia and postural instability, the latter often appearing as the disease progresses

(Forno, 1996; Moustafa et al., 2016). Motor symptoms usually present after more than 50% of affected neurons have degenerated (Cheng et al., 2010).

Nonetheless, PD has also been associated with several non-motor symptoms, which often precede the motor symptoms by years or even decades (Kouli et al., 2018). Several non-motor symptoms have been reported and include sleep disturbances (e.g., REM sleep behaviour disorder, insomnia), autonomic dysfunction (e.g., constipation sympathetic neuron denervation), sensory and neuropsychiatric complications (e.g., anxiety, depression), among others (Wishart & Macphee, 2011). Non-motor symptoms have a great impact on the quality of life of PD patients, contributing enormously to disability and impairment (Cheon et al., 2009). Despite this, health care quite often focuses on motor symptoms, resulting in poor recognition and treatment of non-motor symptoms (Wishart & Macphee, 2011).

A growing body of evidence supports the possibility that PD originates peripherally in the autonomic nervous system and/or in the olfactory bulb, followed by a pathological spreading through the central nervous system until reaching/affecting the SNpc (Borghammer & Van Den Berge, 2019). This peripheral origin, considered pre-motor or prodromal state, is characterized by non-motor symptoms due to neurodegenerative processes outside of the SNpc. Such symptoms could aid the early detection of PD, representing a unique opportunity to identify the individuals at high risk before the massive neurodegeneration occurs. Therefore, this very early stage is currently under the research spotlight, and efforts are being undertaken to improve its recognition as it could represent an ideal time point for therapeutic intervention (Kouli et al., 2018; Moscovich et al., 2020; Prasuhn et al., 2021).

Currently, there is no disease-modifying therapy for PD. The available treatments aim to tackle the symptoms and mostly focus on restoring the levels of dopamine in the striatum or act on striatal post-synaptic dopamine receptors. Such effects are achieved with drugs that are metabolized to dopamine, that activate the dopamine receptor, or that prevent the breakdown of endogenous dopamine (Zahoor et al., 2018). For this, several drugs are used including L-Dopa (levodopa), dopamine agonists, inhibitors of monoamine oxidase (MAO)-B and catechol-o-methyltransferase (COMT) and amantadine (Oertel & Schulz, 2016; Zahoor et al., 2018). Over the past 50 years, the treatment for the motor symptoms has been optimized using pharmacotherapy, deep brain stimulation of the subthalamic nucleus or the globus pallidus internus, and physiotherapy. Nonetheless, being a long-term duration disease, patients live

under medication regimes, which often turn into problematic side effects such as motor fluctuations and dyskinesia (Fahn, 2000). Further investigation on novel therapies is ongoing with the hope of finding a disease-modifying approach.

PD has been broadly accepted as a multifactorial disorder, with both genetic and environmental factors playing an important role, and age being the biggest risk factor for developing the disease (Bloem et al., 2021; Kouli et al., 2018). Environmental factors such as pesticides and rural living have been linked to the risk of developing PD. Of note, certain substances such as MPTP (1-methyl-4-phenyl tetrahydropyridine) (a molecule structurally similar to the herbicide Paraquat) can cause nigrostriatal cell death and lead to atypical parkinsonism. Furthermore, inverse associations have been reported between the risk of PD and cigarette smoking, coffee drinking, calcium channel blockers and statins consumption (Balestrino & Schapira, 2020). Aging remains the biggest risk factor for developing idiopathic PD (iPD, i.e. with an unknown etiology). The research of mechanisms leading to cell death in PD have progressed greatly during the past years, nevertheless the specific age-related factors that may predispose some individuals to develop this neurodegenerative disorder remain unclear (Reeve et al., 2014). Even though most of the PD cases are classified as sporadic, a minority of cases (5 - 10%) have a clear monogenic, autosomal dominant or recessive, inheritance pattern. Family history is a risk factor for PD and the relative risk in first-degree relatives of PD cases increases by approximately 2 to 3-fold compared to controls (Balestrino & Schapira, 2020; Kovalchuke et al., 2019).

1.1.1 Genetic causes of PD

Back in 1997, a study carried out in an Italian family and three Greek kindreds resulted in the discovery of the missense variant A53T (Ala53Thr substitution) in the *SNCA* gene (encoding alpha-synuclein), becoming the first gene linked to PD (Polymeropoulos et al., 1997). To date, variants in more than 20 genes have been reported to cause PD. At the same time, the relevance of some of these genes and variants is still under investigation (Blauwendraat et al., 2020). Table 1 shows a list of mutations that have been reported to cause PD, with information regarding gene, type of mutation, inheritance, proposed disease mechanism, age of onset, frequency, among others. From the 21 genes listed, 10 present a very high confidence as irrefutable PD-linked genes, based on information obtained from multiple independent families, functional evidence, and absence of negative reports. Four of these genes (*SNCA*, *LRRK2*, *GBA*, *VPS35*) are

accountable for an autosomal dominant inheritance fashion, and closely resemble iPD (clinically and pathologically), while the remaining six (*PRKN, PARK7, PINK1, ATP13A2, FBX07, PLA2G6*) are responsible for autosomal recessive mode of inheritance and are causative of atypical and juvenile forms (Blauwendraat et al., 2020).

The *SNCA* gene encodes α-synuclein, and mutations in this gene can increase the protein´s predisposition to misfolding and aggregation, affect its quantity or alter its post-transcriptional modifications or interactions (Balestrino & Schapira, 2020). Mutations in *LRRK2* have shown to interfere with autophagy and slow α-synuclein degradation, contributing to its accumulation (Friedman et al., 2012). Notably, *LRRK2* and *SNCA* mutations also affect mitochondrial dynamics, trafficking, endoplasmic reticulum (ER)-mitochondrial tethering, calcium signalling, and mitophagy (Singh et al., 2019; Toyofuku et al., 2020; Vicario et al., 2018). Variants in the genes *GBA* and *VPS35* are likely involved in lysosomal and trafficking pathways. Impairment of mitochondrial function has been underpinned as a key mechanism of this pathology, and different genes implicated in familial forms of PD, including *PRKN (Parkin), PARK7 (DJ-1)* and *PINK1* are involved in the regulation of mitochondrial function (Balestrino & Schapira, 2020). *DJ-1* regulates calcium flux into the mitochondria to protect the cell from oxidative stress. Mutations in this reactive oxygen species (ROS) scavenger lead to disturbed mitochondrial respiration and membrane potential, increased ROS, and altered mitochondrial morphology (Hirota et al., 2015). Mutations in *Parkin* and *PINK1* are the first and second most frequent causes of autosomal recessive PD, respectively (Kitada et al., 1998; Lill, 2016; Valente et al., 2004). PINK1 and parkin work together in the mitochondrial quality control pathway (mitophagy pathway) to selectively degrade damaged mitochondria. PINK1, a serine/threonine kinase, “tags” damaged mitochondria, activating the mitophagy pathway and further recruiting the E3 ubiquitin ligase parkin (Balestrino & Schapira, 2020).

Even though several highly penetrant variants have been clearly linked to PD, the initiation of the pathology could be related to the contemporary presence of also other factors (both genetic and non-genetic). Interestingly, for some mutations in autosomal dominantly inherited PD genes, penetrance is markedly reduced. Conversely, heterozygous carriers of autosomal recessive PD mutations have been shown to manifest disease or subclinical phenotypes of disease, thus suggesting a more complex pathology scenario, where gene-environment, nuclear gene-mtDNA, and protein-protein interactions are able to modify the penetrance of genetic forms of PD (Zanon et al., 2018).

Table 1. *List of genes reported to cause PD (Blauwendraat et al., 2020)*

GENE	MUTATION	NOTE	YEAR OF DISCOVERY	PROPOSED DISEASE MECHANISM	INHERITANCE	FREQUENCY	NOMINATED BY GWAS	MULTIPLE INDEPENDENT FAMILIES REPORTED *	FUNCTIONAL EVIDENCE †	NEGATIVE REPORTS PUBLISHED ‡	CONFIDENCE AS ACTUAL PD GENE §
SNCA	Missense or multiplication	Often with dementia	1997, 2003	Gain of function or overexpression	Dominant	Very rare	Yes	++	++	+	Very high
PRKN	Missense or loss of function	Often early onset	1998	Loss of function	Recessive	Rare	No	++	++	+	Very high
UCHL1	Missense	--	1998	Loss of function?	Dominant	Unclear	No	-	+	--	Low
PARK7	Missense	Often early onset	2003	Loss of function	Recessive	Very rare	No	++	++	+	Very high
LRRK2	Missense	--	2004	Gain of function	Dominant	Common	Yes	++	++	+	Very high
PINK1	Missense or loss of function	Often early onset	2004	Loss of function	Recessive	Rare	No	++	++	+	Very high
POLG	Missense or loss of function	Atypical PD	2004	Loss of function?	Dominant	Rare	No	++	+	+	High
HTRA2	Missense	--	2005	Unclear	Dominant	Unclear	No	-	+	--	Low
ATP 13A2	Missense or loss of function	Atypical PD	2006	Loss of function	Recessive	Very rare	No	++	++	+	Very high
FBXO7	Missense	Often early onset	2008	Loss of function	Recessive	Very rare	No	++	++	+	Very high
GIGYF2	Missense	--	2008	Unclear	Dominant	Unclear	No	+	+	--	Low
GBA	Missense or loss of function	--	2009	Likely loss of function	Dominant (incomplete penetrance)	Common	Yes	++	++	+	Very high
PLA2G6	Missense or loss of function	Often early onset	2009	Loss of function	Recessive	Rare	No	++	++	+	Very high
EIF4G1	Missense	--	2011	Unclear	Dominant	Unclear	No	--	+	--	Low
VPS35	Missense	--	2011	Loss of function	Dominant	Very rare	No	++	+	+	Very high
DNAJC6	Missense or loss of function	Often early onset	2012	Loss of function	Recessive	Very rare	No	++	+	+	High
SYNJ1	Missense or loss of function	Often atypical PD	2013	Loss of function	Recessive	Very rare	No	++	+	+	High

DNAJC13	Missense	Same family as TMEM230	2014	Unclear	Dominant	Unclear	No	+	+	--	Low
TMEM 230	Missense	Same family as DNAJC13	2016	Loss of function?	Dominant	Unclear	No	--	+	--	Low
VPS13C	Missense or loss of function	--	2016	Loss of function	Recessive	Rare	Yes	++	+	+	High
LRP10	Missense or loss of function	--	2018	Loss of function?	Dominant	Unclear	No	--	+	--	Low

GWAS: genome-wide association study. PD: Parkinson's disease. * In this column, ++ denotes ≥4 families reported; + denotes ≥2 and <4 families reported; - denotes 1 family reported; - - denotes no families reported. † In this column, ++ denotes ≥4 disease-related reports; + denotes ≥1 and <4 disease-related reports; - denotes no disease-related reports. ‡ Reports that could not replicate this gene as a PD gene. In this column, + denotes no negative reports; - denotes ≥1 and <4 negative reports; - --denotes ≥4 negative reports. § Sum of the scores in the three preceding columns, with each + adding 1 and each - subtracting 1; very high denotes a score of ≥5; high denotes a score of 4; medium denotes a score of 2 or 3; low denotes a score of ≤1.

1.2 Parkin

1.2.1 Gene and protein

Over 20 years have passed since Kitada et al. identified *PARK2* (*PRKN*, *Parkin*; OMIM#600116) as a causative gene for familial PD in 1998 (Kitada et al., 1998). *Parkin* is the second largest gene in the human genome, spanning a 1.38 Mb region of chromosome 6 (6q26) with 12 exons, encoding a 465 amino acid protein (Corti et al., 2011; Hattori & Mizuno, 2017; Hauser et al., 2017). Since its discovery, parkinsonism-associated deletions have been reported for all exons, irrefutably showing that loss of parkin function causes disease (Corti et al., 2011). Moreover, the numerous mutations identified include large rearrangements, small deletions/insertions, and missense/nonsense variants (Corti et al., 2011; Kasten et al., 2018; Morais et al., 2016; Nuytemans et al., 2010).

Parkin protein is an E3 ubiquitin ligase in the ubiquitin-proteasome system, mostly known for its role in mitochondrial autophagy (mitophagy), facilitating the selective clearance of dysfunctional mitochondria (Celardo et al., 2014). This is carried out through the process of ubiquitination (a form of post-translational modification), where ubiquitin proteins (one or more) are conjugated to lysine residues of target proteins determining their cellular fate (Klein & Westenberger, 2012).

As depicted in Figure 1, parkin comprises an N-terminal ubiquitin-like (UbL) domain, followed by two RING finger domains (RING0 and RING1), an in-between-RING finger domain (IBR), a linker domain named repressor element of parkin (REP), and a C-terminal RING finger domain (RING2) (Seirafi et al., 2015; Trempe et al., 2013). This protein belongs to the RING-between-RING family of E3 ubiquitin ligases and functions as a hybrid of both RING-type and HECT-type E3

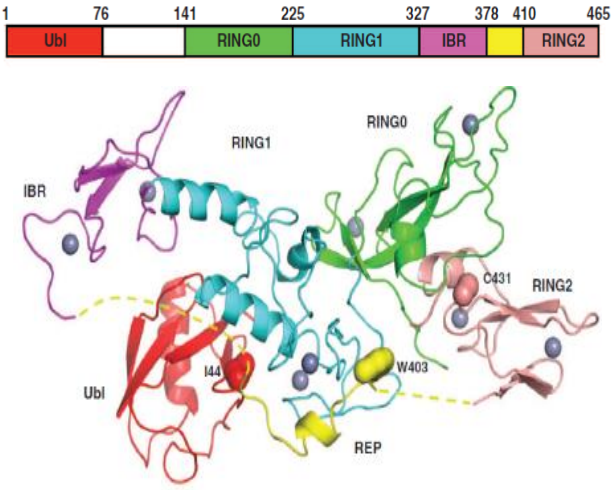

Figure 1. Parkin. *Top: Diagram of primary structure, showing linear domain organization of parkin. Bottom: Ribbon representation of the full-length structure, including the repressing REP α-helix (yellow) surrounded by unstructured regions (yellow dashed lines), zinc atoms (gray spheres), and each domain´s structural conformation (α-helix and β-strand). Under inactivated conditions, parkin adopts a tightly coiled conformation (Seirafi et al., 2015; Trempe et al., 2013).*

ligases (Seirafi et al., 2015). The RING1 domain binds E2 ubiquitin-conjugating enzymes, while the RING2 domain contains an active site cysteine residue that forms an intermediate thioester with ubiquitin prior to substrate transfer. The N-terminal UbL domain plays a role in substrate recognition and in the stability of the protein (Santos et al., 2019; Wenzel et al., 2011). In the overall structure, the RING2 domain is folded underneath the RING0 domain, hiding the active site contained in RING2 domain, thus conferring on parkin an auto-inhibited state. In order to shift from this inactive state to an active one, parkin interacts with ubiquitin, previously phosphorylated by PINK1 (Hauser et al., 2017; Santos et al., 2019). Adding ubiquitin to proteins can trigger a number of effects, including degradation through the proteasome, alteration of its cellular location, or changes in protein-protein interactions (promoting or preventing them) (Seirafi et al., 2015).

Parkin is essentially a cytosolic protein, as frequently reported, mediating ubiquitination in the cytosol. However, several studies have also shown parkin localizing to mitochondria (Kuroda et al., 2006; Narendra et al., 2008; Rothfuss et al., 2009), among other cellular locations (e.g., endoplasmic reticulum, outer nuclear membrane). Therefore, parkin is capable of ubiquitinating a wide range of protein targets, catalysing different types of ubiquitination (K63, K48, K11 and K6 linkages). Furthermore, parkin is able to ubiquitinate itself, promoting its own degradation (Santos et al., 2019). All this characterizes parkin as a multifunctional, complex protein involved in the regulation of numerous cellular processes through diverse protein substrates.

1.2.2 Function

As described above, one of the most studied functions of parkin is its involvement in the mitophagy pathway. Under normal conditions, PINK1 localizes to the mitochondria and is rapidly imported and translocated across the inner mitochondrial membrane (IMM), where it is cleaved by the IMM protease presenilin-associated rhomboid-like protein (PARL). Upon damaging conditions, mitochondria become depolarized (loss of membrane potential (MMP, $\Delta\psi$), and PINK1 is no longer imported through the outer mitochondrial membrane (OMM) transmembrane protein complexes, thus accumulating. This triggers PINK1's phosphorylating activity on its targets (i.e., ubiquitin and parkin) at serine 65 residue. This site-specific phosphorylation activates and recruits parkin to the OMM, where it starts "flagging" the

damaged mitochondria for sequestration and subsequent degradation through autophagy (Narendra et al., 2008; Rakovic et al., 2011; Vives-Bauza et al., 2010).

Another well described function of parkin is the control of the cell´s apoptotic response. Parkin ubiquitinates the apoptotic effector protein BAK, a member of the proapoptotic Bcl-2 family proteins, impairing its activation and further formation of lethal oligomers for the OMM destruction. Likewise, parkin suppresses BAX-mediated apoptosis through an indirect mechanism (Bernardini et al., 2019). Additionally, parkin is known for its role in mitochondrial biogenesis activation through ubiquitination and subsequently degradation of PARIS (parkin interacting substrate), which is a transcriptional repressor of the master regulator of mitochondrial biogenesis PGC1- α (peroxisome proliferator-activated receptor gamma coactivator 1α) (Shin et al., 2011). Furthermore, parkin might be able to modulate mtDNA transcription through interaction with TFAM (mitochondrial transcription factor A) at the mitochondrial genome (Kuroda et al., 2006; Rothfuss et al., 2009) and is involved in in the maintenance and integrity of the mitochondrial genome (Pickrell et al., 2015). In the last years, parkin has been linked to the role of mitochondria as a trigger of inflammation. In stress or injury situations, mtDNA is released from the mitochondrial matrix (and found in the cytosol or extracellular space), and perceived as foreign and potentially toxic, thus initiating an inflammatory response through the activation of the cyclic GMP-AMP synthase-stimulator of interferon genes (cGAS-STING), resulting in proinflammatory cytokine signalling (Sliter et al., 2018). More recently, parkin has been shown to negatively regulate inflammation via inhibition of RIPK3, an initiator of necroptosis (Lee et al., 2019). Additionally, PINK1 and parkin have been shown to play an active role in the innate immune response by suppressing mitochondrial-derived vesicles (MDVs) formation and the presentation of mitochondrial antigens. In this pathway, parkin prevents the recruitment of sorting nexin 9 (SNX9), a protein required to produce MDVs. In the absence of PINK1 or parkin, inflammation triggers mitochondrial antigen presentation in immune cells, suggesting an autoimmune mechanism for PD in individuals with mutations in *Parkin* (Matheoud et al., 2016). In addition, in response to oxidative stress, parkin stimulates the formation of MDVs filled with oxidized cargo, in a PINK1-dependent manner. Once formed, these vesicles are degraded in the lysosomes (McLelland et al., 2014).

Overall, the above-mentioned functions of parkin provide an overview on how this complex protein exerts numerous effects, which undeniably contribute to cellular homeostasis and

survival (Figure 2). Disease-associated variants in this gene can affect parkin function through different mechanisms impairing its activity, stopping the translation of a functional protein, turning insoluble and enhancing aggregation, hampering protein folding and stability, and/or affecting its ability to bind to cofactors and substrates (Santos et al., 2019).

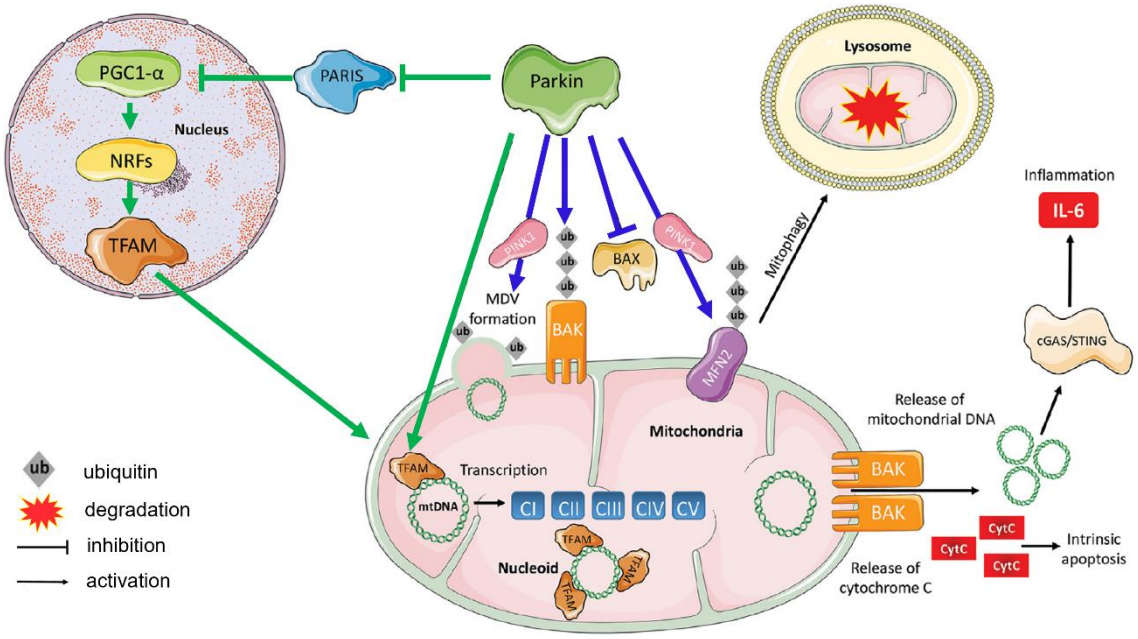

Figure 2. Scheme summarizing parkin´s most relevant cellular functions. *In mitophagy, PINK1 phosphorylates parkin promoting its recruitment to the OMM. Activated parkin adds phospho-ubiquitin to its targets (e.g., MFN2 and BAK) for further sequestering and degradation in the lysosome. Parkin inhibits BAX-mediated apoptosis and on its absence, BAK creates pores in the OMM driving the release of mitochondrial DNA (mtDNA) and cytochrome C (CytC). This in turn triggers inflammation and intrinsic apoptosis, respectively. Additionally, parkin influences biogenesis by inhibiting PARIS (PGC1-α inhibitor) or by interaction with TFAM. Parkin colocalizes with MDVs in a PINK1-dependent manner, stimulating their formation and further degradation in the lysosomes (Wasner et al., 2020). Green arrows indicate parkin actions at the transcriptional level, blue arrows at the post-transcriptional level.*

1.3 Relevance of parkin in PD

1.3.1 Parkin-linked PD

Parkin mutations are the most frequent cause of autosomal recessive early-onset PD worldwide, accounting for up to 77% of cases with an age of onset <20 years (Lucking et al., 2000), and parkin dysfunction represents also a risk factor for sporadic PD (Dawson & Dawson, 2014). *Parkin* mutations have been identified in numerous families with different genetic background (Hedrich et al., 2004) and include more than 170 mutations consisting of rearrangements and

copy number variations (CNVs), such as deletions and duplications of exons, small deletions/insertions, as well as single nucleotide polymorphisms (SNPs) that cause missense, nonsense or splice site mutations (Corti et al., 2011; Kasten et al., 2018). Of these, missense variants are the most frequently reported in PD patients, and they likely obstruct parkin protein function rather than disrupting protein expression (Yi et al., 2019). Importantly, a large number of patients carry exon deletions and duplications that result in protein truncation (Hedrich et al., 2001; Kasten et al., 2018). Figure 3 gives a detailed overview of all the reported locations of mutations in *Parkin* on the gene and protein levels, alongside their pathogenicity status (The Movement Disorder Society Genetic mutation database (MDSGene): www.mdsgene.org).

A)

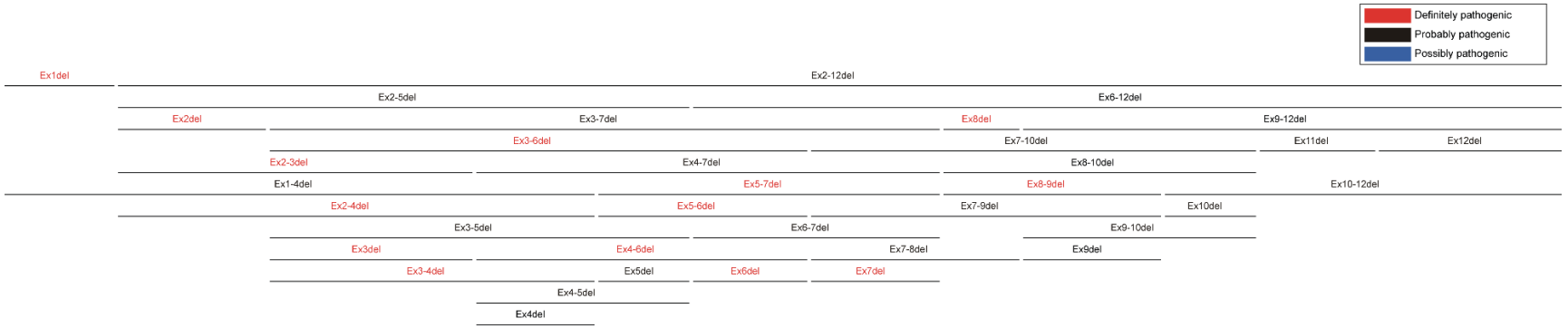
Definitely pathogenic
Probably pathogenic
Possibly pathogenic
Ex1del
Ex2-12del
Ex2-5del
Ex6-12del
Ex2del
Ex3-7del
Ex8del
Ex9-12del
Ex3-6del
Ex7-10del
Ex11del
Ex12del
Ex2-3del
Ex4-7del
Ex8-10del
Ex1-4del
Ex5-7del
Ex8-9del
Ex10-12del
Ex2-4del
Ex5-6del
Ex7-9del
Ex10del
Ex3-5del
Ex6-7del
Ex9-10del
Ex3del
Ex4-6del
Ex7-8del
Ex9del
Ex3-4del
Ex5del
Ex6del
Ex7del
Ex4-5del
Ex4del

B)

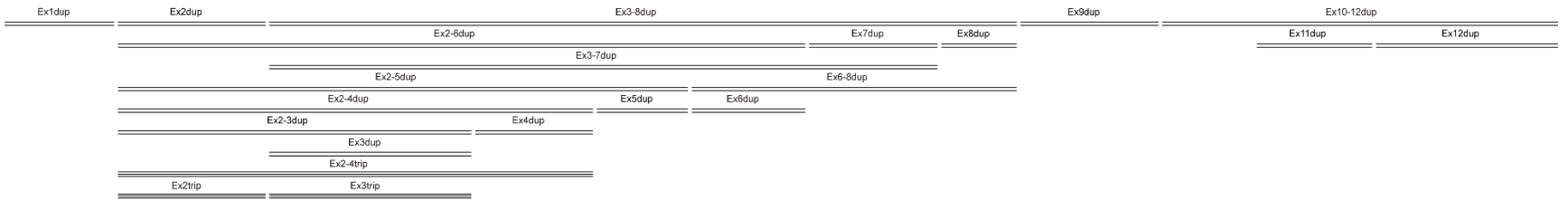
Ex1dup
Ex2dup
Ex3-8dup
Ex9dup
Ex10-12dup
Ex2-6dup
Ex7dup
Ex8dup
Ex11dup
Ex12dup
Ex3-7dup
Ex2-5dup
Ex6-8dup
Ex2-4dup
Ex5dup
Ex6dup
Ex2-3dup
Ex4dup
Ex3dup
Ex2-4trip
Ex2trip
Ex3trip

C)

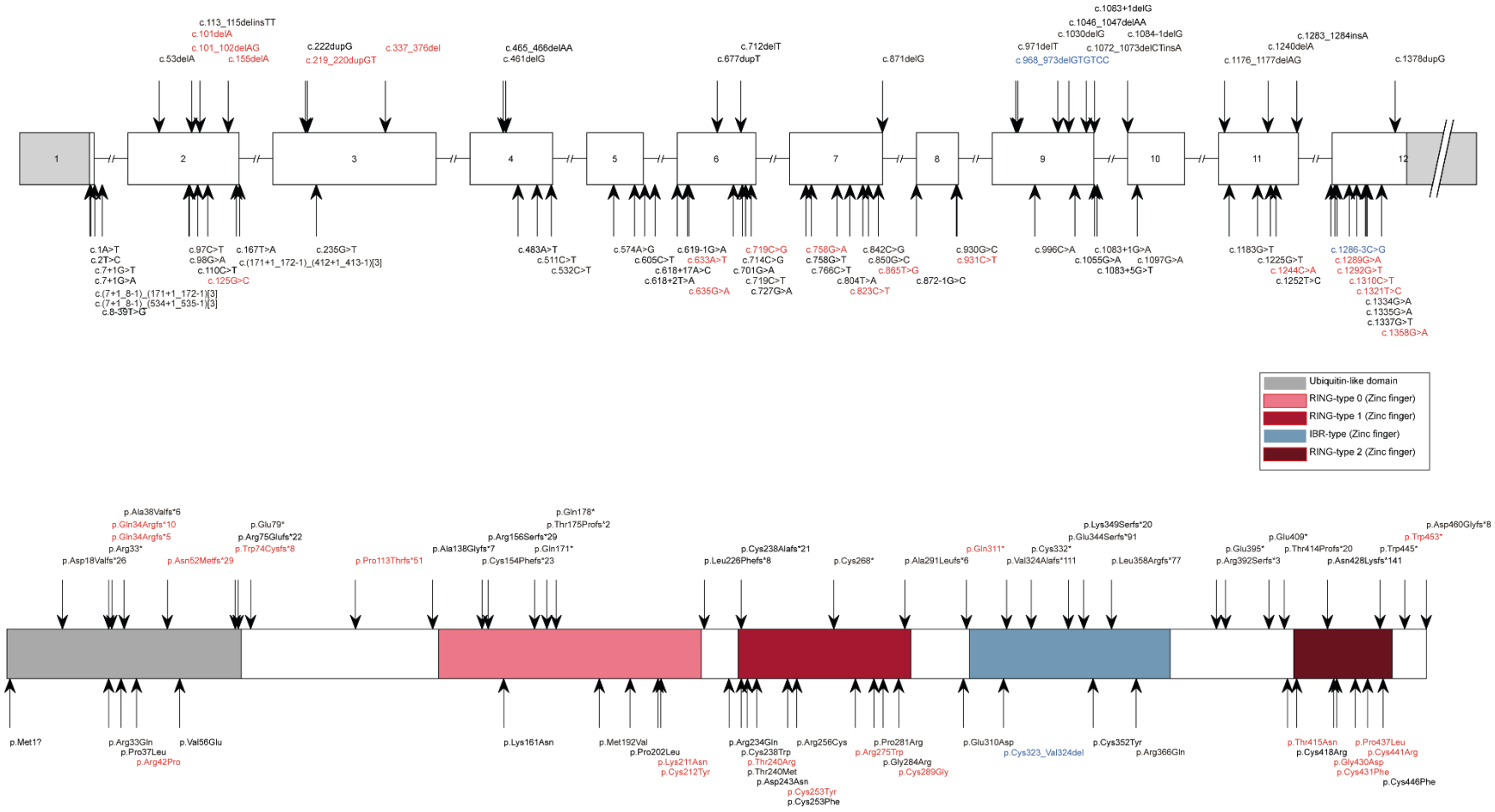

Figure 3. Schematic representation of mutations in Parkin. *Exon rearrangements: A) exon deletions, B) duplications and triplications. C) small deletions and single nucleotide variations at the gene and protein level (MDSGene, www.mdsgene.org).*

Early-onset PD usually starts in the third or fourth decade of patient´s life and presents as a less aggressive form of the disease. Some *Parkin* mutation carriers have an onset even in childhood, and homozygous mutations are the most frequent cause of juvenile PD (age at onset (AAO) ~ 21 years) (Klein & Westenberger, 2012). Normally, patients with early-onset PD show slower disease progression and a positive response to L-dopa, compared to idiopathic PD. However, during the course of disease, motor fluctuations occur frequently, and L-dopa-induced dyskinesia symptoms are common (Li et al., 2020).

The Movement Disorder Society Genetic mutation database (MDSGene), which summarizes and quantifies genetic and phenotypic data from relevant literature for hereditary movement disorders (Lill, 2016), currently lists 1,000 biallelic *Parkin* mutation carriers, from which 56% are male. The median AAO of all *Parkin* mutation carriers is 31 years (25^{th}/75^{th} percentile: 23/39 years; range: 3 – 73 years) (Wasner et al., 2020). Regarding the ethnicity, the majority of reported patients are of Asian origin (37%), followed by Caucasians and Hispanics (35.4% and 8.7%, respectively). The most common phenotypic signs are tremor, bradykinesia and dystonia. Lewy bodies or Lewy neurites are rarely seen in this subtype of PD, which differs in pathogenesis compared to the α-synuclein pathology (Li et al., 2020; Wasner et al., 2020). Non-motor signs and symptoms do occur in *Parkin* mutation carriers, but their reporting has been inconsistent over the years, resulting in data gaps. Nevertheless, meta-analyses of published PD patients with *Parkin* mutations reported that dementia is very rare, affecting less than 3% of the cases (Grunewald et al., 2013; Kasten et al., 2018). Overall, *Parkin*-linked PD is the most common form of early-onset PD across all ethnic groups, representing about 10 - 20% of cases of PD with AAO from 40 - 50 years (Domingo & Klein, 2018). Looking explicitly at heterozygous *Parkin* mutation carriers, to date 200 different mutations have been published. These include 18 variants in introns, 13 nonsense mutations, 69 missense mutations, 29 small insertions or deletions, and 71 exon rearrangements. Out of 1,155 mutation-positive index patients, two thirds carried at least one exon rearrangement (Wasner et al., 2020).

1.3.2 Penetrance of *Parkin* variants

Homozygous or compound heterozyous (biallelic) mutations in *Parkin* are causative for PD with highly penetrant symptom expression and early age at onset, but may manifest with a very late

onset in a subset of cases (Pramstaller et al., 2005). On the contrary, the more frequent heterozygous mutations in *Parkin* may predispose to PD with highly reduced penetrance (Huttenlocher et al., 2015; Ohlei et al., 2018; Vulinovic et al., 2018), with a similar pattern established for mutations in *GBA* (Avenali et al., 2020; Klein & Krainc, 2013). Heterozygous *Parkin* mutations are found more frequently in PD patients than in controls (Lubbe et al., 2021), where they are detected with a frequency up to 3.1% (Klein et al., 2007). Importantly, a reported potential genetic risk factor of PD is the presence of heterozygous *Parkin* mutations (Huttenlocher et al., 2015; Klein et al., 2007). Heterozygous mutation carriers present an extremely variable expressivity and include subtle motor signs, which do not allow for a definitive clinical diagnosis of PD (Kasten et al., 2018). Additionally, they might present parkinsonian features detectable only upon neuroimaging or electrophysiology (Heinzel et al., 2019; Lill, 2016).

Even though loss of function mutations in *Parkin* are confirmed contributors to the loss of dopaminergic neurons, the core mechanisms, which lead to the actual neurodegeneration, associated with PD, are still not fully understood (Santos et al., 2019). Nonetheless, deficiency resulting from mutations in *Parkin* have proven to disrupt mitochondrial performance, demonstrating the crucial role of these organelles in the onset of the disease (Mouton-Liger et al., 2017).

1.4 Mitochondria and PD

Over the past years, a growing number of studies has shown evidence supporting mitochondrial dysfunction as a central factor in the pathophysiology of PD. Most of the genetic PD loci are directly associated with mitochondria, and its dysfunction has been implicated as an integral disease component (Celardo et al., 2014; Hauser & Hastings, 2013; Trinh et al., 2021). The earliest report linking mitochondria and PD dates back to 1976, when scientists described a case report of a 23-year-old student who had injected a “sloppy batch” of self-synthesized 1-methyl-4-phenyl-4-propionoxy-piperine (MPPP), resulting in the development of PD-like motor symptoms. His autopsy revealed typical Lewy body pathology in the SNpc (Davis et al., 1979). A few years later, in 1982, the neurologist James William Langston and colleagues reported two incidents of drug abuse, where four patients showed typical signs of L-dopa-responsive

parkinsonism after injecting what they thought was “synthetic heroin”. The injected compound was MPTP, thus linking Langston’s findings with Davis’ case report (Langston et al., 1983). MPTP can pass the blood brain barrier (being a highly lipophilic compound) and is converted into the cation 1-methyl-4-phenylpyridinium (MPP^+) by monoamine oxidase B, a highly abundant enzyme in glial cells (Levitt et al., 1982). The cation MPP^+ selectively enters dopaminergic neurons through the dopamine transporter (Storch et al., 2004), where it concentrates selectively in mitochondria. MPP^+ inhibits respiratory complexes I, III and IV of the electron transport chain (Desai et al., 1996; Nicklas et al., 1985), thereby leading to a reduced ATP production, generation of ROS and finally neuronal impairment/death. The link between mitochondrial malfunction and PD was further corroborated some years later when reduced activities of complexes I, II and IV were found in post-mortem SNpc homogenates of PD patients (Schapira, 1993; Schapira et al., 1990). Moreover, the discovery that exposure to environmental inhibitors of the electron transport chain (ETC), like pesticides, was parkinsonism-related, further associated mitochondria with PD (Lin et al., 2019).

1.4.1 Mitochondrial structure and main functions

Mitochondria are highly dynamic intracellular organelles responsible for the efficient cellular energy generation, and their correct function determines cellular survival or death. The number of mitochondria present in human cells ranges from a few hundred to approximately one thousand, depending on the type of tissue (Jang & Lim, 2018). Mitochondria present a double-membraned structure, with outer and inner mitochondrial membranes (OMM, IMM) separated by an intermembrane space (IMS) with a pH of 7.2 - 7.4, and the central compartment enclosed by the IMM. This central compartment is the mitochondrial matrix and is surrounded by convoluted inner membrane folds named cristae (Ge et al., 2020); the high pH of 7.9 to 8.0 of the mitochondrial matrix generates the transmembrane electrochemical gradient that drives ATP synthesis (Llopis et al., 1998). Moreover, the mitochondrial matrix is the site where mtDNA replication occurs, as well as transcription, protein biosynthesis and several enzymatic reactions (Kuhlbrandt, 2015). The cristae extend into the matrix and happen to be the main sites of energy conversion. The OMM is distinguished for being porous, thus allowing the free transport of ions and small, uncharged molecules (no potential across it). On the other hand, the IMM is a tight diffusion barrier, which allows the transfer of ions and molecules only with the aid of specific

membrane transport proteins. This results in an electrochemical membrane potential of ~180 mV that builds up across the IMM (Kuhlbrandt, 2015). As depicted in Figure 4, the ETC is composed of transmembrane protein complexes I-V: the NADH ubiquinone oxidoreductase (complex I), succinate ubiquinone oxidoreductase (complex II), ubiquinone-cytochrome c reductase (complex III), cytochrome oxidase (complex IV) and ATP synthase (complex V). Complex I of the ETC is characterized by a particularly high complexity, comprising 14 central subunits and up to 32 accessory subunits. Its L-shaped structure is partly embedded in the IMM with the remaining portion protruding into the mitochondrial matrix (Zhao et al., 2019).

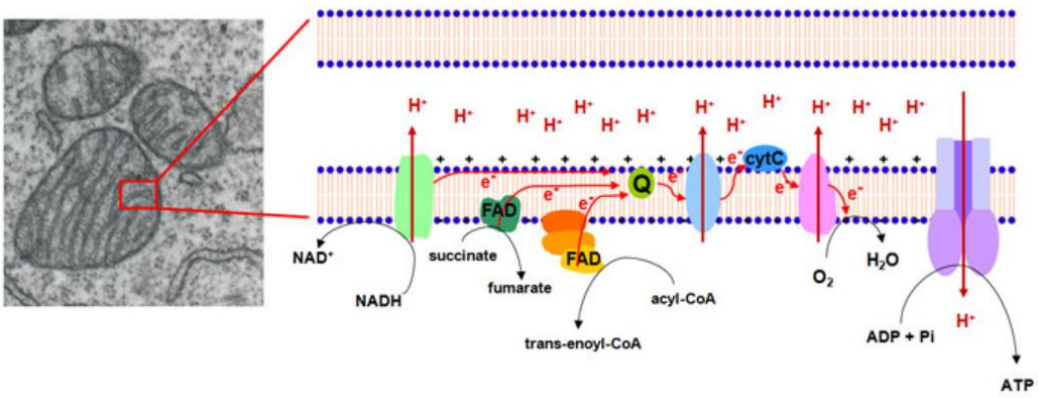

Figure 4. ETC in the inner mitochondrial membrane. *Left: Electron micrograph showing mitochondria. Right: representative scheme indicating the protein complexes in the ETC. Mitochondrial membranes in blue and red; NADH ubiquinone oxidoreductase in light green; succinate ubiquinone oxidoreductase in dark green; ubiquinone in green labeled with a Q; ubiquinone cytochrome c reductase in light blue; cytochrome c in dark blue labeled with cytC; cytochrome c oxidase in pink; and the ATP synthase complex in lila. The flux of electrons is represented by red arrows and e-, and the flux of protons is represented by red arrows and H^+ (Da Poian, 2010).*

Mitochondria are commonly referred to as the "powerhouses" of the cell, for their provision of ATP through the oxidative phosphorylation (OXPHOS) process. In all eukaryotes, mitochondria are the main source of ATP to drive fundamental cell functions (Kuhlbrandt, 2015). The reduced substrates NADH and FADH2, products of the tricarboxylic acid (TCA) cycle, donate electrons to the ETC in the IMM. Complexes I, III and IV use energy generated from redox reactions to pump protons across the IMM towards the IMS. Briefly, complex I feeds electrons from NADH through the respiratory chain and transfers them to a quinol in the membrane. Energy released from electron transfer is further used to pump four protons from the matrix into the cristae lumen. Complex III takes the electrons from the reduced quinol and transfers them to the electron carrier protein cytochrome c, while pumping one proton. Finally, complex IV transfers the

electrons from cytochrome c to molecular oxygen and contributes to the proton gradient by using up four protons per consumed oxygen molecule to produce water. Complex II transfers electrons directly from succinate to quinol without contributing to the proton gradient (Kuhlbrandt, 2015). This proton gradient generated from electron transportation (oxidation) drives the protons across the IMM through the F1F0-ATP Synthase (complex V), phosphorylating adenosine diphosphate (ADP) into ATP (Davies et al., 2011) (Figure 4). Of note, a consequence of the reaction between electrons of the respiratory chain and oxygen is the generation of free radicals. The possible toxic effect of these free radicals is "handled" by a variety of antioxidant molecules and enzymes which, when unbalanced, can result in oxidative stress (Celardo et al., 2014).

Apart from cellular respiration and ATP synthesis, these highly multifunctional organelles are responsible of several functions, including the biosynthesis of numerous macromolecules (e.g., lipids, proteins and nucleic acids), regulation of apoptosis, cell proliferation, cell motility, ROS and cytoplasmic Ca^{2+} buffering, and they serve as key anchoring scaffolds for intracellular signaling networks (Ge et al., 2020). Mitochondria exist as dynamic networks shifting from innumerable punctate organelles to cell-wide tubular networks thanks to their complex fission/fusion machinery. The function of these organelles is strictly regulated through the coordinated expression of mitochondrial and nuclear genes.

Mitochondria carry their unique circular genome (mtDNA), as reflection of their evolutionary origin as endosymbiotic bacteria, containing multiple copies in the matrix (Jang & Lim, 2018). mtDNA copy numbers vary among different cell or tissue types responding to metabolic and bioenergetic demands, as well as a consequence or cause of specific pathological conditions (D'Erchia et al., 2015). mtDNA is a double stranded circular macromolecule of 16,569 base pairs compacted into supramolecular assemblies called nucleoids. The mitochondrial genome has been commonly thought to be uniparentally inherited from the mother; nevertheless, some evidence suggested that in rare cases the father might pass on his mtDNA to the offspring (Luo et al., 2018), which was however challenged by more recent studies (Lutz-Bonengel & Parson, 2019; Wei & Chinnery, 2020). The mitochondrial genome (Figure 5) contains 37 genes and encodes 2 unique rRNAs (12S and 16S), 22 transfer RNAs (tRNAs), and 13 polypeptides required to assemble the respiratory chain complexes. Additionally, it contains a major non-coding region called D-Loop, holding the promoter components HSP1, HSP2 and LSP (Winklhofer & Haass,

2010). On the other hand, the nuclear genome encodes more than 1,000 proteins needed for the remaining components of the ETC, as well as proteins involved in various mitochondrial functions (Jang & Lim, 2018). Mutations in the mtDNA or nuclear genes alter the sequences of mitochondrial proteins, leading to mitochondrial dysfunction. Mitochondria normally contain more than one type of genome, the wild type mtDNA and mtDNA carrying variants. This is referred to as heteroplasmy. A small percentage of mutant mtDNA coexisting with multiple copies of wild type mtDNA is not enough to translate into disease. However, if the percentage of mutated mtDNA goes over a certain threshold (typically >70%), mitochondrial disease appears (Jang & Lim, 2018).

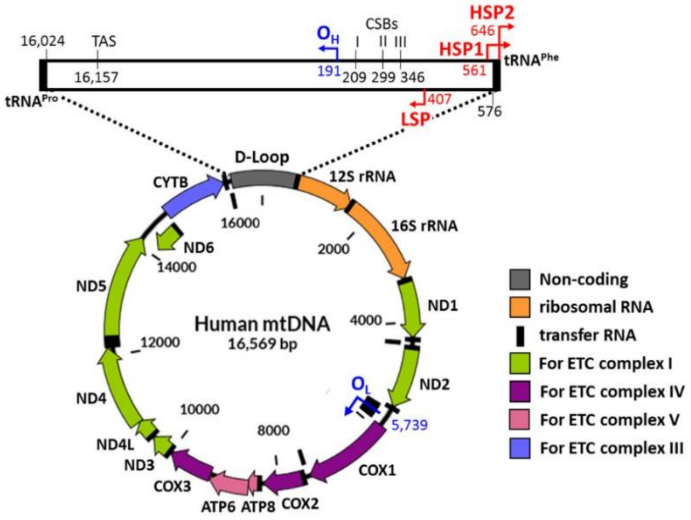

Figure 5. Schematic diagram of human mitochondrial DNA, illustrating the enclosed genes (Jang & Lim, 2018).

1.4.2 Mitochondrial dysfunction in PD

After discovering and further corroborating the clear link between mitochondrial dysfunction and PD over 30 years ago, the majority of familial PD genes have been found to be associated either directly or indirectly with mitochondrial function, further implicating it as an integral disease component (Park et al., 2018). Pathogenic mutations in these genes are known to affect mitochondrial performance on several fronts (Figure 6) including the disruption of the respiratory chain complexes, loss of mitochondrial membrane potential, unbalance of the organelle´s dynamics, quality control disequilibrium, impairment of mitochondrial biogenesis, compromised morphology, among others (Lin et al., 2019; Park et al., 2018). In fact, both sporadic and familial PD seem to converge at the level of mitochondrial integrity (Winklhofer & Haass, 2010).

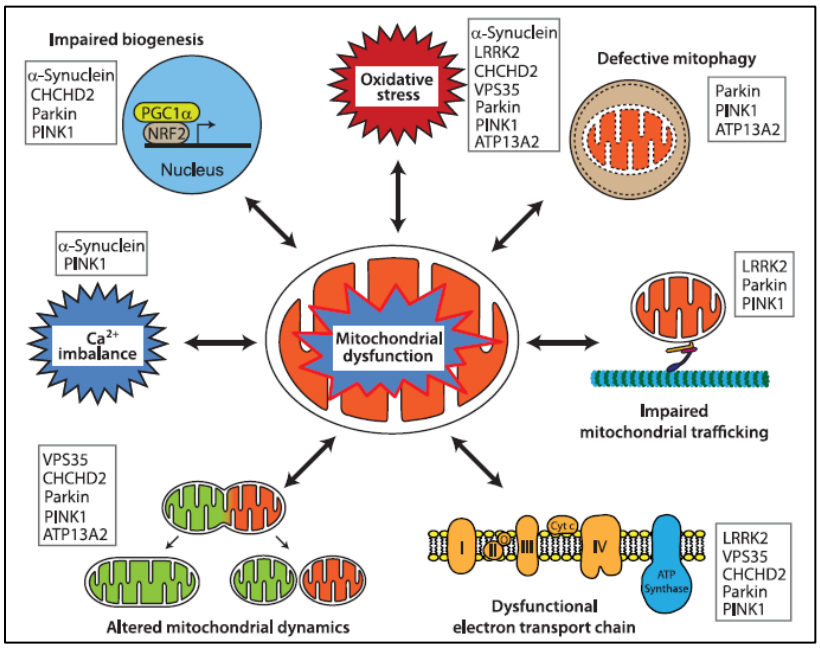

Figure 6. Mitochondrial dysfunction in PD. *Representative pathways involved in PD pathophysiology (Park et al., 2018).*

Respiratory chain complex impairment

Inhibiting key mitochondrial proteins of the respiratory chain, such as complex I, has been known to cause parkinsonian like symptoms since its inhibition with MPP^+ was demonstrated to cause loss of SNpc neurons (Langston et al., 1983). Once the link between mitochondrial ETC dysfunction and PD was established, subsequent investigation further related other environmental toxins, such as pesticides, herbicides, insecticides (paraquat and rotenone) to PD, which are now used frequently for PD toxin models (Kung Lin et al., 2019). During the past decades, several clinical studies have identified impairment in mitochondrial respiration linked to PD patients. Hattori *et al*. observed reduction in complex I activity or protein levels in *postmortem* SNpc tissues (Hattori et al., 1991). Interestingly, this impairment has been observed also in other parts of the PD brain and even in other tissues like fibroblasts, lymphocytes, or skeletal muscles (Haas et al., 1995; Parker et al., 2008). Moreover, Bender et al. reported that approximately 3% of SNpc neurons in PD patients are complex IV (COX)-deficient (Bender et al., 2006). Respiratory deficiency may lead to compromised ATP production, which can affect the excitability of neurons in the SNpc known to have high-energy demands, further increasing their vulnerability (Reeve et al., 2014). Moreover, complex I dysfunction results in increased ROS

production, directly contributing to oxidative stress and damage, which has also been observed in PD (Schapira et al., 1990). Particularly, when assessing mitochondrial respiration in *Parkin* mutant models (Damiano et al., 2014; Haylett et al., 2016; Kumar et al., 2020), increasing evidence reveals an altered rate of oxygen consumption. Mitochondrial respiration assessment represents a solid indicator of functional bioenergetic capacity and of overall cellular health (Haylett et al., 2016).

Defects in mitochondrial biogenesis

PGC1α is a transcriptional coactivator known as the master regulator of biogenesis in mitochondria, transcribing several downstream target genes responsible for mitochondrial maintenance and respiration, including nuclear respiratory factors (NRFs) and estrogen related receptors (ERRs) (Wasner et al., 2020). PD related genes, such as *Parkin* and *PINK1* have a role in mitochondrial biogenesis through its interaction with PGC1α. Parkin is involved in several functions related to mitochondria maintenance (Section 1.2.2), and this is achieved by regulating their biogenesis and degradation via mitophagy. Under stable physiological conditions, parkin facilitates the degradation of PARIS, a repressor of PGC1α activity, which leads to translocation of PGC1α and transcriptional activation of mitochondrial-associated genes. Consequently, loss of parkin function generates PARIS accumulation and successive inhibition of the transcription of PGC1α and its downstream targets (Shin et al., 2011; Zheng et al., 2017). This is the scenario observed in the brain of patients with autosomal recessive juvenile PD, linked to mutations in *Parkin* or *PINK1*.

Oxidative stress

Mitochondria produce ~90% of cellular ROS, which associates them directly to oxidative stress. The OXPHOS process through the ETC is the major source of ROS in eukaryotes (Zhang et al., 2019). Under physiological conditions, ROS participate as central players in the cellular signaling network (Mittler et al., 2011). Molecular oxygen is reduced to water by the ETC´s complexes but a small percentage of the oxygen is converted to superoxide (O^{-}_{2}) by complexes I and III. The produced superoxide is converted to hydrogen peroxide (H_2O_2) by the enzyme manganese superoxide dismutase (MnSOD), and some mitochondrial enzymes (e.g., glutathione

peroxidase), as well as non-mitochondrial enzymes (e.g., peroxisomal catalase), catalyze the reduction of H_2O_2 to water and molecular oxygen. However, unfavorable situations can cause ROS production to surpass the antioxidant capacity of the cell, resulting in oxidative stress. Oxidative stress leads to irreversible damage to macromolecules (e.g., proteins, lipids, nucleic acids, carbohydrates), changing their structures and consequently their functions, ultimately leading to cell death. Markers of oxidative stress, including high levels of oxidatively modified lipids, proteins and DNA have been found in the SNpc of patients with PD (Keeney et al., 2006). Moreover, levels of protein nitration were also found to be increased in PD brains (Cenini et al., 2019; Hauser & Hastings, 2013). Importantly, a systemic deficiency in complex I is evident in many PD patients, and oxidative stress caused by reactive metabolites of dopamine and alterations in the levels of iron and glutathione in the SNpc accompany mitochondrial dysfunction (Hauser & Hastings, 2013). Increased oxidative stress was found also in PD patients with *Parkin* mutations (Ge et al., 2020; Kamienieva et al., 2021). DA neurons in the SNpc are particularly vulnerable to oxidative stress due to their unmyelinated axons with numerous synapses, their autonomous pacemaking activity involving cytosolic calcium oscillations, and increased levels of cytosolic dopamine and its metabolites (Poewe et al., 2017).

Mitophagy impairment

Mitochondrial clearance through mitophagy is one of the most well studied pathways of PD pathogenesis. This autophagic process, occurring explicitly in mitochondria, leads the dysfunctional organelles towards degradation in the autophagosomes (Rodolfo et al., 2018). Mitochondrial turnover via mitophagy is of great importance to maintain neuronal health since this process sequesters, degrades and recycles cellular material (Lin et al., 2019). It is widely known that abnormal mitophagy is linked to neurodegeneration, considering that several PD-related proteins are involved in the regulation and execution of this function. Mainly, the PINK1-parkin pathway, which regulates ubiquitin dependent mitophagy (Valdinocci et al., 2019), implicates the role of mitophagy in the pathogenesis of PD (Vives-Bauza et al., 2010). In 2008, Richard Youle´s laboratory first identified the relationship between parkin and mitophagy (Narendra et al., 2008), and subsequent studies showed PINK1 also participating in this process (Matsuda et al., 2010; Vives-Bauza et al., 2010). The role of *Parkin* mutations in mitophagy was confirmed in induced pluripotent stem cell (iPSC)-derived DA neurons (Kumar et al., 2020; Suzuki

et al., 2017). Furthermore, parkin has been reported to show reduced solubility in sporadic PD, which compromises its performance in the autophagy system (Liu et al., 2019; Lonskaya et al., 2013).

Alterations of mitochondrial dynamics

The dynamic properties of mitochondria such as fission, fusion, trafficking, biogenesis, and degradation are critical to all cells and can be particularly important to neuronal function (Van Laar & Berman, 2009). Mitochondria actively divide (fission) and fuse continuously, and in neurons they are actively transported along the cell through axons and dendrites (Okamoto & Shaw, 2005; Saxton & Hollenbeck, 2012). Fusion and fission functions are of great importance to maintain mitochondrial integrity, electrical and biochemical connectivity, turnover, and to segregate, stabilize and protect the mtDNA (Westermann, 2012). The balance between these two processes is crucial for function and morphology based on the cells' needs (Van Laar & Berman, 2009). Mediators of fission and fusion include the GTPase Dynamin-related protein 1 (Drp1), which is directly recruited by the fission adaptor proteins MiD49/51 (Palmer et al., 2011), translocating to the OMM and mediating mitochondrial fission, together with proteins like hFis1 (Hoppins et al., 2007). On the other hand, fusion is mediated by the outer membrane proteins mitofusin 1 and 2 (MFN1 and MFN2) and the inner membrane optic atrophy protein (Opa1) (Van Laar & Berman, 2009). In *Drosophila* neurons, Verstreken *et al.* identified mutations in *DRP1*, resulting in disrupted distribution of mitochondria within the cell, which were unable to support neurotransmission at the synapses (Verstreken et al., 2005). Additionally, it has been shown that the overexpression of parkin or PINK1 rescues mitochondrial fragmentation induced by overexpression of DRP1 or alpha-synuclein or by rotenone treatment (Kamp et al., 2010). When considering the role of mitochondrial dynamics in PD, it is important to understand that fusion and fission are not isolated events, but are tightly interconnected with other maintenance and homeostasis functions such as biogenesis and degradation (Van Laar & Berman, 2009).

1.4.3 Role of mitochondrial DNA mutations in PD

mtDNA replicates independently from the nuclear DNA, and it is characterized by an increased vulnerability to mutations due to a less efficient DNA repair mechanism and the lack of

protective histones. Moreover, the close proximity to the ETC could make it particularly vulnerable to ROS damage. Additionally, somatic mtDNA mutations accumulate during aging in various tissues such as brain and muscle (Winklhofer & Haass, 2010). Typically, mutations in the mtDNA cause symptoms in post-mitotic cells with high-energy demand such as neurons, skeletal and cardiac muscle cells. Specific mutations in the mtDNA have been found in patients with different forms of parkinsonism, associated with mitochondrial disorders, thus mtDNA mutations are suspected to contribute to complex I deficiency in PD (Zanon et al., 2018). Studies performed in *postmortem* brains or peripheral tissues (blood and skeletal muscle) of PD patients have led to the identification of three different types of mtDNA alterations: point mutations, deletions and copy number alterations (Simon et al., 2000; W. Wei et al., 2017). Nevertheless, no specific rare PD-linked mutation has been identified yet. However, a high proportion of multiple heteroplasmic mtDNA deletions were found to accumulate in the SNpc and other brain regions with age and were significantly more abundant in PD patients (Bender et al., 2006; Kraytsberg et al., 2006). In a recent study by Grünewald *et al.*, conducted on human brain tissue, a reduction of mtDNA copy number was observed in single neurons of PD patients, compared to controls, and this was even more pronounced in neurons with severe complex I deficiency (Grunewald et al., 2016). Interestingly, in the "MitoPark mouse", in which the mitochondrial transcription factor TFAM is selectively removed in DA neurons, a reduced mtDNA expression as well as respiratory chain deficiency leading to OXPHOS impairment was observed. This in turn resulted in a parkinsonism phenotype, characterized by DA neuron degeneration and motor deficits (Ekstrand & Galter, 2009). These data provide evidence for a role of mtDNA alterations in impairment of mitochondrial function and neurodegeneration.

2. Aims

Homozygous or compound-heterozygous mutations in the *Parkin* gene result in highly penetrant symptom expression, while heterozygous mutations may predispose to disease symptoms with highly reduced penetrance (Huttenlocher et al., 2015; Weissbach et al., 2017). Considering the frequency (up to 3%) of heterozygous *Parkin* mutation carriers in the population, it is of great importance to obtain accurate estimates of the penetrance of these variants and to investigate, which risk markers are manifesting in heterozygous mutation carriers that are able to influence the penetrance, and thus be potentially useful for identifying those individuals at greater risk of clinical symptoms later in life. To further elucidate the role of heterozygous mutation in this recessive gene, it is of great importance to test the causal link between heterozygous pathogenic mutations in *Parkin* and expressivity of molecular phenotypes in cellular models derived from mutation carriers.

Therefore, the following specific aims were addressed in this thesis:

1) To identify *Parkin* mutation carriers in the population-based CHRIS study and characterize them for the presence of PD risk markers
2) To evaluate mitochondrial integrity, including mitochondrial DNA variation and mitochondrial function, in diverse cellular models of heterozygous *Parkin* mutation carriers.

3. Study participants, materials and methods

3.1 Study participants

In the present study, participants enrolled in the Cooperative Health Research in South Tyrol (CHRIS) study were investigated. The CHRIS study is a longitudinal population-based study targeting the population of Vinschgau/Val Venosta in South Tyrol, to investigate the genetic and molecular basis of age-related common chronic conditions and their interaction with genes, lifestyle and environment in the general population (Pattaro et al., 2015). The CHRIS study is a joint initiative with the South Tyrolean healthcare system conducted under the leadership of the Institute for Biomedicine, Eurac Research, and was approved by the Ethics Committee of the Healthcare System of the Autonomous Province of South Tyrol.

For the molecular assessment of mitochondrial performance, 21 CHRIS participants originating from four families (Figure 7) were investigated in the present study. From these, 11 carried a heterozygous *Parkin* mutation and ten were healthy individuals (matched by close age) without *Parkin* mutations from the same families. For these 21 study participants, lymphoblastoid cell lines (LCLs) and/or induced pluripotent stem cell (iPSC)-derived neurons were generated (Tables 2 and 3). None of the study participants fulfilled the diagnostic criteria for PD, which was assessed with a screening questionnaire for parkinsonism (Pramstaller et al., 1999). In addition, human iPSC lines from two PD patients (iPSC-B125 and iPSC-2011) and one control individual (iPSC SFC084-03-02) were included in the functional analyses for comparison. iPSC-B125 line was previously generated at the Institute of Neurogenetics of the University of Lübeck (Zanon et al., 2017), and the iPSC-2011 line was generated in our laboratory at the Institute for Biomedicine (Zanon et al., 2019). The control iPSC line SFC084-03-02 was established through the StemBANCC consortium.

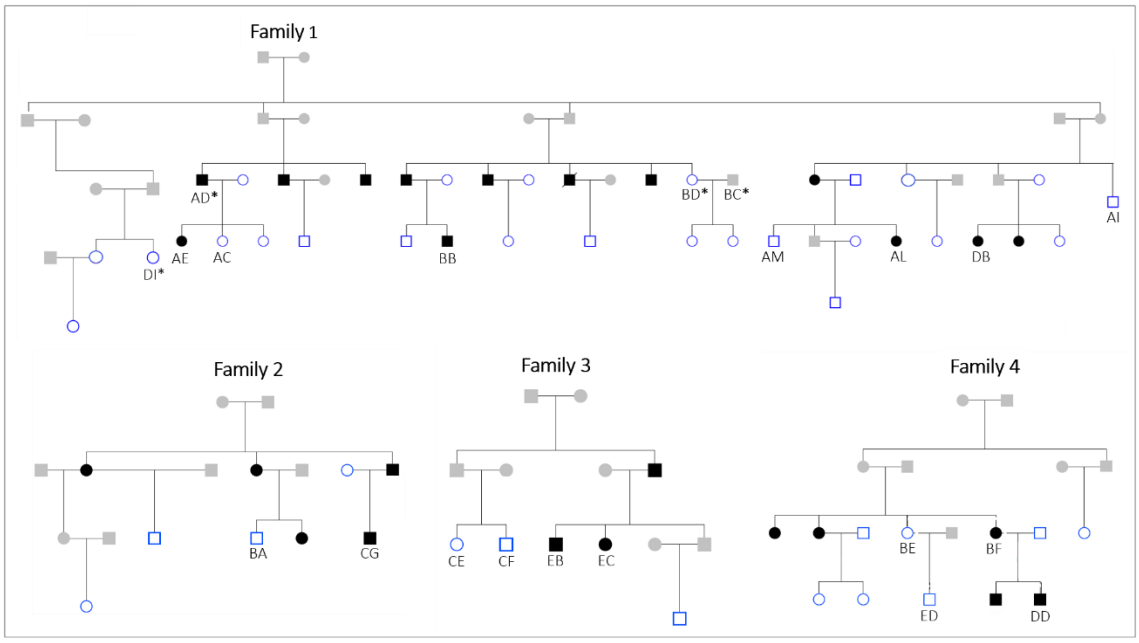

Figure 7. Pedigrees of four families including participants enrolled in the CHRIS study, spanning five generations. *Individuals with a heterozygous exon 7 deletion in the Parkin gene are shown in black. The 20 study participants, for which LCLs were generated in this study are indicated with their ID; the 4 participants, for which iPSC lines were generated in this study are indicated with an asterisk (*). Circles = women; squares = men; slashed symbol = deceased; grey = not recruited and no information available.*

Table 2. *Demographic data, genotypic and phenotypic information of individuals from the CHRIS study, for which lymphoblastoid lines were generated in this study*

ID	*Sex*	*Age at examination*	*Heterozygous Parkin mutation*	*SN hyperechogenicity*	*Subtle motor signs (UPDRS-III)*	*Hypomimia*
AE	female	40	Exon 7 deletion	NO	NO	
DB	female	39	Exon 7 deletion	NO	YES	+
AL	female	34	Exon 7 deletion	YES	NO	
BD	male	69	Exon 7 deletion	YES	YES	+
BB	male	32	Exon 7 deletion	NO	NO	
AD	male	68	Exon 7 deletion	YES	YES	+
BF	female	58	Exon 7 deletion	NO	NO	
DD	male	37	Exon 7 deletion	YES	NO	
EC	female	54	Exon 7 deletion	YES	NO	
EB	male	61	Exon 7 deletion	YES	NO	
CG	male	46	Exon 7 deletion	YES	YES	+
AM	male	42	/	NO	NO	
AI	male	75	/	YES	NO	

BC	female	80	/	NO	NO	
AC	female	42	/	NO	NO	
BE	female	57	/	YES	YES	+
ED	male	37	/	NO	NO	
CF	male	46	/	YES	YES	(+)
CE	female	44	/	NO	NO	
BA	male	47	/	YES	NO	

SN: *substantia nigra; UPDRS-III: Unified Parkinson's Disease Rating Scale (UPDRS)-Part III;*

SN hyperechogenicity, subtle motor signs, and hypomimia are regarded as markers for prodromal PD (Fereshtehnejad et al., 2019; Heinzel et al., 2019).

Table 3. *Demographic data, genotypic and phenotypic information of individuals from the CHRIS study, for which iPSCs were generated in this study*

ID	*Sex*	*Age*	*Mutation*	*SN hyperechogenicity*	*Subtle motor signs (UPDRS-III)*	*Hypomimia*
AD	male	68	Heterozygous exon 7 deletion	YES	YES	+
BD	male	69	Heterozygous exon 7 deletion	YES	YES	+
BC	female	80	/	NO	NO	
DI	female	56	/	YES	NO	
*B125**	male	64	Exon 9 homozygous delA (p.Val324AlafsTer111 - rs1562519380)	n.a.	n.a.	n.a.
*2011**	female	n.a.	Homozygous exon 3 deletion	n.a.	n.a.	n.a.
*SFC**	female	n.a.	/	n.a.	n.a.	n.a.

SN: *substantia nigra*; UPDRS-III: Unified Parkinson's Disease Rating Scale (UPDRS)-Part III; n.a.: not available.

SN hyperechogenicity, subtle motor signs, and hypomimia are regarded as markers for prodromal PD (Fereshtehnejad et al., 2019; Heinzel et al., 2019).

*These lines were not generated in this study but were included in the functional analyses for comparison: iPSC-B125 and iPSC-2011 are PD lines, iPSC-SFC084-03-02 is a healthy control line.

3.2 Materials and Methods

This chapter describes all the techniques established and performed in the laboratory of the Institute for Biomedicine as part of this thesis.

3.2.1 Isolation of Peripheral Blood Mononuclear Cells

The starting material for the experiments in this study was peripheral blood, collected by venous puncture in EDTA-buffered collection tubes, from all participants. Peripheral Blood Mononuclear Cells (PBMCs) were isolated from the blood sample and further used to generate the cell models for mitochondrial performance assessment. Using PBMCs as starting material for research is advantageous since this cell type can be collected in a minimally invasive approach. The mononucleated cell fraction was separated from the other blood components (i.e. plasma, erythrocytes, and platelets) using Histopaque – 1077 reagent (Sigma Aldrich), a polysucrose and sodium diatrizoate medium with a density of 1.077 g/mL, and 50 mL Leucosep tubes (Greiner Bio-one). This method facilitates the isolation and further recovery of viable PBMCs from whole blood samples and was carried out following the manufacturers' instructions. In detail, for each participant, 18 mL of venous peripheral blood were collected in Vacutainer EDTA collection tubes and processed within 24 hours after collection. The blood was diluted with sterile PBS, up to 35 mL and carefully poured onto the membrane (porous barrier) of the Leucosep tube (containing 15 mL of Histopaque solution below the membrane). The tube was then centrifuged for 10 min at 1,000 x g at room temperature (RT) in a swinging bucket rotor (intermediate acceleration 6, brakes 0). After centrifugation, the sequence of layers previously mentioned appeared as follows (from top to bottom): plasma, enriched cell fraction (interphase consisting of PBMCs), separation medium, porous barrier, separation medium, pellet (erythrocytes and granulocytes). Next, the plasma fraction was collected and discarded to facilitate the collection of the enriched cell fraction (PBMCs), which was carefully harvested and transferred to another centrifugation tube. The collected cells were washed with 20 mL of sterile PBS and subsequently centrifuged for 10 min at 250 x g (fast acceleration, intermediate break 6). This step was repeated twice, and the final pellet was resuspended in 5 mL of sterile PBS. Following, isolated PBMCs were counted with trypan blue (Thermo Fisher Scientific) in order to evaluate cell viability by using the Neubauer counting chamber (BlauBrand). Trypan blue is a

stain used in a 1:1 ratio to selectively color dead cells. After counting, multiple aliquots of isolated PBMCs, containing approximately 1 x 10^7 cells were frozen in 1 mL of freezing medium (Table 5) and stored in liquid nitrogen until usage.

3.2.2 Immortalization of Peripheral Blood Mononuclear Cells

The availability of a continuous source of material (cells or DNA) from a single individual usually is a rate-limiting step in research. Lymphoblastoid cell lines (LCLs) can be established by infecting B-cells from peripheral blood with Epstein Barr Virus (EBV). *In vitro*, EBV infects mature resting B-lymphocytes, activating them and inducing their continuous proliferation (Mrozek-Gorska et al., 2019). This leads to the generation of "immortal" cells, which can be cultured and expanded continuously, thus fulfilling the much-needed requirement of constant supply of starting material for a variety of assays (Hussain & Mulherkar, 2012). To establish LCLs, a vial of previously cryopreserved PBMCs was thawed in the water bath at 37°C, and its content was carefully diluted in 10 mL of warm transformation medium (Table 5). Then, it was centrifuged for 10 min at 200 x g, and the supernatant was discharged. The resulting pellet was resuspended in the remaining solution (~100 µl), and 2 mL of culture supernatant from B95.8 cells (a marmoset cell line) expressing EBV were added immediately and mixed carefully. Next, cells were incubated at 37°C in 5% CO_2 atmosphere for 2.5 hours (carefully mixing 2 – 3 times during the incubation period). Finally, the cell containing tubes were centrifuged for 6 min at 200 x g, and the pellet was resuspended in 6 ml of transformation medium, containing phytohemagglutinin (PHA) (Sigma Aldrich). PHA is a T-cell mitogen used to induce the secretion of T-cell-assisted B-cell growth factors and the ultimate removal of T-cells (Penno et al., 1993; Sie et al., 2009). The cell solution was seeded in a 24-well plate (2 mL per well), and the EBV-infected cells were observed under the microscope on a daily basis to identify the rosette-like transformed LCLs forming clusters. One week after infection, clusters were visible and PHA was withdrawn from transformation medium. As time progressed (from 3 to 4 weeks), cellular clusters became larger until being visible macroscopically. Upon successful establishment, cell lines were expanded in LCLs growth medium (Table 5) for up to 6 weeks, and finally they were cryopreserved in freezing medium and stored in liquid nitrogen tanks. Multiple vials of lymphoblast aliquots per individual were stored to allow access to cultures with low passage numbers for future use. For experiments, cells were removed from storage by thawing in a 37°C

water bath, harvested by centrifugation, resuspended in growth medium and transferred to a fresh T75 flask.

3.2.3 Culture and passaging of Lymphoblastoid Cell Lines

Lymphoblastoid cell lines were cultured in Roswell Park Memorial Institute (RPMI) 1640 Medium (Biowest), supplemented with 10% Fetal bovine serum (FBS) (Sigma Aldrich) and 1% penicillin-streptomycin (Thermo Fisher Scientific), in T75 flasks. Cell culture medium was changed every third day, and cells were kept at 37°C in a saturated humidity atmosphere containing 5% CO_2. Cells were passaged upon reaching confluence. In detail, cells were seeded at concentrations of not less than 3 x 10^5 cells/mL and passaged at intervals not exceeding three days. First, confluent cells were transferred into a conical 15 mL tube and centrifuged for 5 min at 200 x g. The resulting pellet was resuspended in 2 mL of growth medium and split in a 1:3 ratio. Cells were kept in culture for no longer than 10 passages. Prior to commencing experiments, LCLs were cultured over a short time and as few passages (2 - 3) as possible. In addition, doubling time (DT) was calculated for each line before starting the experiment. DT was calculated according to the formula: DT = [0.693 *t /ln (N/N0)], where t = elapsed time, N0 = starting number of lymphoblasts, N = final number of lymphoblasts. DT is expressed in hours.

3.2.4 Cellular reprogramming

The generation of iPSCs from primary human PBMCs of *Parkin* mutation carriers (heterozygous exon 7 deletion) and non-carriers was performed by transfection with episomal plasmids (Meraviglia et al., 2015).

3.2.4.1 Preincubation of Peripheral Blood Mononuclear Cells

Isolated PBMCs from four individuals were thawed by shortly immersing the vials in a water bath at 37°C and immediately resuspending the cells in 1 mL of warm PBMCs medium (Table 5). Resuspended PBMCs were seeded and incubated at 37°C and 5% CO_2 in a humidified incubator for 48 hours, followed by medium change. PBMCs were incubated in PBMCs medium for 14 days before starting the reprogramming protocol. This protocol preferentially enriches for

erythroblast-like cells ($CD34^+$ hematopoietic stem/progenitor cells), due to their high proliferation rate. Thereby, PBMC medium contains specific growth factors aiming to select this cell type, discriminating against the others (Dowey et al., 2012; Meraviglia et al., 2015).

3.2.4.2 Generation and culture of induced Pluripotent Stem Cells (iPSCs)

In this thesis, the reprogramming of PBMCs into iPSCs was performed by transfection with episomal plasmids through electroporation, following the protocol detailed by Meraviglia et al., 2015. The electroporation procedure applies an electrical field on the cells in order to increase the permeability of the cell membrane, thus allowing the insertion of chemicals, drugs, or DNA into the cells. Electroporation was executed with the Neon® transfection system and Neon® transfection Kit (Thermo Fisher Scientific), following the manufacturer's instruction. In detail, the previously expanded PBMCs were collected in a 15 mL conical tube and counted using Acridine orange stain, with LUNA FL™ Fluorescence Cell Counter (Biosystems). 2.5 $x10^6$ cells were centrifuged at 300 x g for 10 min at RT and resuspended in 100 µl of transfection mix containing Resuspension Buffer T and 1 µg of each plasmid DNA. The four plasmids used in this protocol were (1) OCT3/4 and shRNA against p53, (2) SOX2 and KLF4, (3) L-MYC (non-oncogenic) and LIN28, and (4) EGFP (as transfection efficiency control). The transfection mix containing cells and plasmids was aspirated with the given pipette and vertically inserted in the tube section of the pipette station (electroporation instrument) containing 3 ml of the saline Electrolytic Buffer E2, as indicated in the protocol. PBMCs were efficiently electroporated with the following program: 1650 V, 10 msec, 3 pulses. Once electroporated, cells were transferred into one well of a 6-well plate containing pre-warmed PBMC medium and 0.25 mM of sodium butyrate (NaB). NaB is a small-molecule inhibitor of histone deacetylases (HDAC), which improves iPSC derivation by enhancing Oct4 transcriptional activity (Mali et al., 2010). Cells were incubated at 37°C, 5% CO_2 humidified environment, and medium was replaced every two days.

Picking and Expansion of iPSCs

After 3 days following electroporation, cells were seeded onto a monolayer of irradiated Mouse Embryonic Fibroblasts (MEFs). MEFs secrete several important growth factors into the medium (aiding maintenance of the pluripotency status) and provide a cellular matrix for iPSCs to grow

on. At this time point, PBMC medium was replaced with iPSC medium (Table 5), which was changed daily. After approximately 10-15 days post-transfection, the first iPSC colonies were visible and between 30-35 days from electroporation, colonies were ready for picking and replating. During the first passaging step, each iPSC colony was manually dissected with a needle under the stereo microscope in a safety hood, in order to obtain a grid, and smaller clumps were collected by pipetting and transferred individually into one well of a 12-well plate previously coated with MEFs. Next, iPSCs were cultured for 24h in iPSC medium with 10 ng/mL Fibroblast Growth Factor-basic (bFGF; Millipore) and 10 µM Y-27632 (Miltenyi Biotech), a highly potent and selective Rho-associated, coiled-coil containing protein kinase (ROCK) inhibitor. This small molecule enhances survival of iPSCs when they are dissociated to small clumps or single cells by preventing dissociation-induced apoptosis, thus increasing their efficiency (Emre et al., 2010). During the first 2-3 passages, manual picking is more efficient for expansion, compared to enzyme dissociation, to select fully undifferentiated, compact and tightly packed colonies. After initial picking, selected iPSC clones were further expanded through enzyme dissociation with Collagenase IV (1 mg/mL) (Gibco) by incubating at 37°C for 10 min. After incubation, colonies were not completely detached but only the edges were partially lifted. The enzyme solution was removed, and cells were rinsed with 1 ml of KO-DMEM (Gibco). Colonies were gently collected in a 15 mL conical tube and centrifuged at 100 x g for 2 min at RT. Next, iPSC colonies were resuspended in iPSC medium with 10 ng/ml bFGF (Millipore) and 10 µM Y-27632 (Miltenyi Biotech) and plated on a MEF coated 6-well plate (ratio 1:2 – 1:4).

Culture and passaging of iPSCs

iPSCs were maintained and expanded under feeder-free conditions by using Matrigel™ Growth Factor Reduced (GFR) Basement Membrane LDEV-Free Matrix (Corning) in mTeSR™1 complete medium (Stemcell) with 1% penicillin-streptomycin (Thermo Fisher Scientific). Cells were kept at 37°C in a saturated humidity atmosphere containing 5% CO_2, and medium was changed on daily basis. Passaging was performed at a maximum of 90% confluence by incubating with UltraPure™ 0.5mM EDTA (Invitrogen Life Technology), pH 8.0 for 3 min at 37°C. Cells were then harvested by adding mTeSR™1 complete medium. After incubation, colonies were not completely detached but only the edges were partially lifted. The enzyme solution was removed,

and cells were rinsed with cell culture medium. Cells were seeded at a ratio of 1:3-1:6 on Matrigel-coated cell culture plates as colonies in cell culture medium.

3.2.4.3 Characterization of iPSCs

Assessing the pluripotency potential of the generated iPSCs is a key step in the reprogramming process. All four lines were characterized when iPSC colonies were between 5-10 passages, by evaluating the expression of stemness markers and their pluripotency potential. Characterization was carried out through the following assays: alkaline phosphatase staining, immunofluorescence assay for expression of pluripotency markers, qPCR for transgene exclusion, qRT-PCR for gene expression analysis, and differentiation of iPSCs in Embryoid Bodies (EBs).

Alkaline Phosphatase

Alkaline phosphatase (AP) expression indicates undifferentiated cells with the potential to self-renew. AP is a hydrolase enzyme responsible for dephosphorylating molecules such as nucleotides, proteins, and alkaloids under alkaline conditions. Briefly, iPSC colonies were cultured from 3-5 days in iPSC medium and then fixed with 4% PFA for 15 min. Fixed cells were carefully washed with PBS to remove residual PFA and stained with a commercial alkaline phosphatase kit (Stemgent® Alkaline Phosphatase Staining Kit II) for 15-20 min in darkness, according to manufacturer´s instructions. Next, cells were washed twice with PBS and observed under a bright field microscope. Undifferentiated iPSCs present a red or purple staining, while differentiated cells appear colorless.

Immunofluorescence

Immunofluorescence staining was used to visualize the expression of pluripotency markers in the newly generated iPSC lines. Primary antibodies bind target proteins allowing for the analysis of their relative expression level in the cells. All four iPSC lines were grown on glass coverslips contained in a 24 well plate. The protocol for immunostaining was carried out following the manufacturer´s indications of the Pluripotent Stem Cell 4-Marker Immunocytochemistry Kit (Thermo Fischer Scientific). This kit contains primary and secondary antibodies and ready-to-use

buffers. Briefly, cells were fixed with the Fixative Solution provided by the kit for 15 min at RT. Then, Permeabilization Solution was added for 15 min, followed by Blocking Solution for other 30 min at RT. Next, the desired primary antibodies (Table 4) (anti-OCT4, anti-SSEA4, anti-SOX2, anti-TRA-1-60) were diluted in the Blocking Solution, yielding a 1X final dilution, and incubated overnight at 4°C. On the next day, cells were washed 3 times with Wash buffer (provided by the kit), and the secondary antibodies diluted in Blocking Solution were added to the cells for one hour at RT in the dark. Finally, cells are washed 3 times with PBS to remove the residual secondary antibody solution, and nuclei were stained with NucBlue™ Fixed Cell Stain (Thermo Fisher Scientific), before being mounted with Dako Fluorescence mounting medium. Images were acquired using a Leica SP8-X confocal microscope (Leica Microsystems), with a 40X or 63X oil immersion objective.

Table 4. *List of antibodies for immunofluorescence contained in the Pluripotent Stem Cell 4-Marker Immunocytochemistry Kit (Thermo Fischer Scientific)*

PRIMARY ANTIBODIES	DILUTION
RABBIT ANTI-OCT4	1:100
MOUSE ANTI-SSEA4 (IGG3)	1:100
RAT ANTI-SOX2	1:100
MOUSE ANTI-TRA-1-60 (IGM)	1:100
SECONDARY ANTIBODIES	
ALEXA FLUOR® 555 DONKEY ANTI-RABBIT	1:250
ALEXA FLUOR® 488 GOAT ANTI-MOUSE IGG3	1:250
ALEXA FLUOR® 488 DONKEY ANTI-RAT	1:250
ALEXA FLUOR® 555 GOAT ANTI-MOUSE IGM	1:250

Spontaneous Embryoid Bodies formation

iPSCs are differentiated into embryoid bodies (EBs) in order to assess their *in vitro* pluripotency potential. This was achieved with the following spontaneous differentiation protocol: iPSC colonies were collected after incubation with collagenase IV (1mg/ml) and then respuspended in EB medium (Table 5). Colonies were then cultured in suspension during 4 days in ultra-low attachment plates, to allow the formation of spheroidal three-dimensional EBs. Medium was changed every second day and on day 4, EBs were plated onto Matrigel™ coated plates and maintained in differentiation for 15-20 days. Differentiated cells were detached, pelleted and

processed for RNA extraction, to analyze expression of markers of the three germ layers through qRT-PCR (see section 3.2.10).

Gene expression analysis

To perform gene expression analysis, RNA samples, extracted from EBs, iPSCs, and iPSC-derived neurons, were retrotranscribed into cDNA and quantitative Real – Time PCR (qPCR) was performed as described below in sections 3.2.9 and 3.2.10.

Karyotyping

Karyotype analysis was performed in outsourcing by cytogenetic Q-banding analysis of 20 metaphases, at the Laboratory of Medical Genetics, Fondazione IRCCS Ca´Granda, Ospedale Maggiore Policlinico, Milan.

3.2.5 Neuronal differentiation

The direct differentiation of iPSCs into dopaminergic neurons was conducted as described previously (Kriks et al., 2011; Mazzulli et al., 2016), with minor modifications. iPSC colonies were disaggregated into single cells using accutase and replated onto matrigel (BD)-coated dishes in mTeSR™ 1 complete medium, supplemented with 10 µM ROCK inhibitor Y-27632 (Miltenyi Biotech) at a density of 57,000 – 62,000 cells/cm^2. Differentiation was started once iPSCs reached a confluence of 90% by adding knockout serum replacement (KSR) medium (Table 5) supplemented with SMAD pathway inhibitors SB431542 (SB, Miltenyi Biotech) and LDN-193189 (LDN, StemMACS). On days 1 to 5, KSR medium was added to the cells in the presence of SB, LDN, recombinant Human Sonic Hedgehog (SHH, R&D System), recombinant Human FGF-8a (FGF8, R&D System), and Purmorphamine (Pu, StemMACS). The Wnt pathway activator molecule CHIR99021 (CH, StemMACS) was included from days 3-12. During days 6-10 of differentiation, increasing amounts of Neurobasal medium plus B27 supplement (NB-B27 medium, Thermo Fisher Scientific) (Table 5) was added to the KSR medium (25%, 50%, 75%), and upon day 7, SHH, FGF8 and Pu were withdrawn. On day 11, maturation of DA neurons was initiated by adding recombinant Human BDNF (Peprotech), ascorbic acid (Sigma Aldrich),

recombinant Human TGF-ß3 (Peprotech), cyclic-AMP (EnzoLifescience) and DAPT (Tocris) as previously reported (Kriks et al., 2011; Perrier et al., 2004). Cells were passaged between days 12 – 15 *en bloc* (Mazzulli et al., 2016), and between days 20 - 25 of differentiation cells were replated as single cells onto plastic dishes or live imaging chamber slides, previously coated with poly-D-lysine (Sigma Aldrich) and laminin (Sigma Aldrich), in neural differentiation medium with factors.

Table 5. *Detailed composition of culture media*

CULTURE MEDIA	
EB DIFFERENTIATION MEDIUM	Knockout DMEM (KO-DMEM, Thermo Fisher Scientific), 20% defined fetal bovine serum (FBS) (Sigma Aldrich), 1 mM NEAAs, 1% Penicillin/Streptomycin (Thermo Fisher Scientific), 20 mM L-Glutamine, 0.1 mM β-mercaptoethanol
FREEZING MEDIUM	90% FBS, 10% DMSO
IPSC MEDIUM	Knockout DMEM (KO-DMEM), 20% KO-Serum Replacement (KOSR), 1 mM NEAAs, 1% Penicillin/Streptomycin (Thermo Fisher Scientific), 20 mM L-Glutamine, 0.1 mM β-mercaptoethanol, 10 ng/ml bFGF
LCL GROWTH MEDIUM	RPMI 1640 w/L-Glutamine (Biowest), 10% fetal bovine serum (FBS), 1% penicillin/streptomycin (Thermo Fisher Scientific)
MEF MEDIUM	Dulbecco's Modified Eagle Medium (DMEM) high glucose, 10% fetal bovine serum (FBS), 1mM sodium pyruvate, 1% nonessential amino acid solution (MEM - NEAA) and 1% penicillin/streptomycin (P/S) (Thermo Fisher Scientific)
KSR MEDIUM	Knockout DMEM (Thermo Fisher Scientific), 15% knockout serum (Life Technologies), 1% L- glutamine (Life Technologies), 1% nonessential amino acids (Life Technologies), 0.2% b-mercaptoethanol (Life Technologies), 1% penicillin/streptomycin (P/S) (Thermo Fisher Scientific)
NB-B27 MEDIUM	Neurobasal medium (Life Technologies), B27 Supplement 1X, 1% L-glutamine (Life Technologies), 1% penicillin/streptomycin (P/S) (Thermo Fisher Scientific)
PBMC MEDIUM	IMDM and Ham's F-12 (ratio 1:1), 1% of Insulin-Transferrin-Selenium-Ethanolamine (ITS-X), 1% of Chemically Defined Lipid Concentrate (CDL), 1% Penicillin/Streptomycin, 0.005% of L-ascorbic acid, 0.5% of Bovine Serum Albumin (BSA), 1-Thioglycerol (final concentration 200 µM), Stem Cell Factor SCF (100 ng/ml), Interleukin-3 IL-3 (10 ng/ml), Erythropoietin EPO (2 U/ml), Insulin-like Growth Factor IGF-1 (40 ng/ml), Dexamethasone (1 µM) and holo-transferrin (100 µg/ml) (Meraviglia et al., 2015)
TRANSFORMATION MEDIUM	RPMI 1640 (Biowest), 20% FBS (Life Technologies), 1% L-Glutamine (Life Technologies), 1% penicillin/streptomycin (P/S) (Thermo Fisher Scientific), 5 ug/mL Phytohemagglutinin (PHA)*
RESPIRATION MEDIUM MIR05	EGTA (0.5 mM), magnesium dichloride (3 mM), lactobionic acid (60 mM), taurine (20 mM), potassium dihydrogenphosphate (10 mM), HEPES (20 mM),

sucrose (110 mM), and essential fatty acid free bovine serum albumin (1 g/l) in 250 mL MiliQ water, pH 7.1

3.2.6 Characterization of iPSC-derived dopaminergic neurons

Differentiated dopaminergic neurons were characterized using immunofluorescence as described in section 3.2.13. Parkin protein levels were assessed by means of Western blot, with the antibodies described in Table 7.

3.2.7 Mitochondrial protein levels upon CCCP treatment

In order to assess protein levels of MFN2 (mitofusin 2) and TOM70 (mitochondrial import receptor subunit) in iPSC-derived neurons upon dissipation of the mitochondrial membrane potential, a treatment with carbonyl cyanide 4-(trifluoromethoxy) phenylhydrazone (CCCP) (Sigma Aldrich) was performed. Neurons from heterozygous *Parkin* exon 7 deletion carriers, a *Parkin* PD line and non-carriers were cultured under basal conditions (no treatment) and treatment with 20 µM CCCP. The treatment was performed for 15 hours, and the protein levels of MFN2 and TOM70 were investigated by means of Western blotting as described in section 3.2.12.

3.2.8 Extraction of nucleic acids

Genomic DNA was isolated from PBMCs, LCLs, and iPSCs using the commercial kit "QIAamp DNA Blood Mini Kit". Cell pellets were collected and processed according to the manufacturer's instructions. Total RNA from iPSCs, embryoid bodies (EBs) and iPSC-derived neurons was obtained using Direct-zol RNA Miniprep Kit (Zymo Research), following the manufacturer's instructions. The concentration of eluted nucleic acids was measured using a NanoDrop 1000 (Thermo Fisher Scientific), and the ratios 260/280 and 260/230 were assessed (for "pure" nucleic acids, the first ration should be >1.8, while the second should range from 1.8 to 2.2).

3.2.8.1 RNA quality assessment

In order to determine the quality of total isolated RNA, as well as RNA integrity and purity, the Experion RNA StdSens Analysis Kit (BioRad) was used. The customized Experion RNA chip holds up to 12 samples, and within each chip, a series of microchannels connect the sample wells to a separation channel and buffer wells. A set of electrodes in the electrophoresis station applies a voltage across the microchannels, causing charged molecules in the samples to migrate and separate based on their size and charge. The assay was performed following the manufacturer´s protocol. Experion software plots the fluorescence intensity as a function of migration time, generating an electropherogram for each sample, further converting the electropherogram data into densitometric bands, which appear in a virtual gel. Additionally, the software also constructs RNA quality indicator (RQI), providing a quantitative indication of the integrity of the sample.

3.2.9 Reverse transcription

Briefly, 1000 ng of total RNA were reverse transcribed in a 20 µl reaction containing: 4µl of 5X VILO™ Reaction Mix (oligo(dT), random hexamers, MgCl2, mix of dNTPs); 2µl of 10X SuperScript® Enzyme Mix (enzyme SuperScript ™ III Reverse Transcriptase, RNase OUT™ Recombinant Ribonuclease Inhibitor (RNase inhibitor); RNAse free water (to 20 µl). The reaction was carried out in the thermocycler GeneAmp® PCR System 9700 (Applied Biosystems), with the following program: 25°C for 10 min, 42°C for 60 min, 85°C for 5 min. The reaction was then kept at 4°C.

3.2.10 Real – Time PCR (qPCR)

The Real-Time PCR or qPCR (Real-Time Polymerase Chain Reaction or quantitative PCR) is a variant of the classic method of PCR. PCR is a biochemical technique used for *in vitro* DNA amplification (Saiki et al., 1985). A DNA template can be exponentially amplified starting from a single or a few copies of DNA using two chemically synthesized primers (short DNA sequences), which bind complementary to the target sequence. A heat-stable DNA polymerase, like the Taq polymerase (originally isolated from the thermophilic eukaryote Thermus aquaticus), synthesizes the DNA portion located within the two primers. The three main repeating steps of

the reaction are (1) DNA denaturation, (2) primers annealing, and (3) elongation through DNA polymerase. During the first step, the two strands of the double stranded DNA are physically separated at a high temperature. Next, a decrease in temperature allows the annealing of the primers to the single strand DNA template, followed by the synthesis of a new DNA strand complementary to the DNA template, through the addition of deoxynucleotide triphosphates (dNTPs) complementary to the template in 5' to 3' direction. Quantitative PCR (qPCR) determines whether a target sequence (DNA or cDNA) is present in a sample and its quantity (number of copies present). This method uses fluorescent dyes to measure the amount of amplified product in real time. The use of fluorescence allows this method to be very sensible and precise to quantify nucleic acids. The PCR product is monitored in real-time as it is being bound to the fluorophore. Sybr Green, a commonly used fluorescent dye, which preferentially binds to double-stranded DNA, was used to monitor and quantify the amount of generated amplicons. The main repeating steps of the reaction constitute a single cycle of the amplification program, and the PCR product doubles each cycle, so multiple cycles are required to amplify the DNA target to millions of copies in order to obtain an appreciable quantity of products. The amplification reactions were performed in a final volume of 20 µl containing 10 µl of Sybr Green (2X All-in-One qPCR Mix by GeneCopoeia), 5 ng/µl of cDNA as template and 1 µl of primers (Table 6) at a final concentration of 0.5 µM. The amplification reaction was carried out using the CFX96 Real-Time System C1000™ Thermal Cycler (BioRad), with the following program: 95°C for 10 mins; // 40 cycles: 95°C for 10 sec; 60° C for 20 sec; 72° C 15 sec. Melting curve analysis: 72° to 95°C, increment 0.5°C, for 6 sec.

The deltadelta-Ct (ΔΔCt) method was used to quantify the differences in gene expression levels between two samples, and the Ct value of the target gene was normalized to the Ct value of a reference gene using the following equation: Fold change ≈ 2ΔΔCt = 2 exp (ΔCtsample A (target-reference) - ΔCtsample B (target-reference)).

This method was used to measure expression levels of the pluripotency markers NANOG, GDF3, OCT4, and SOX2 in iPSC lines and parental PBMCs for all 4 individuals. Moreover, the residual expression of the specific episomal plasmid EBNA-1 gene was determined with qPCR, as well as the expression level of lineage markers representative of the 3 germ layers (ectoderm: NCAM, PAX6; endoderm: SOX17; mesoderm: RUNX1, MYH6). All expression levels were normalized to

reference genes, and each reaction was performed in triplicates. The primer sequences used for the characterization of the newly generated iPSC lines are listed in Table 6.

Table 6. *List of primers 5´to 3´used for qPCR and ddPCR*

Primers	*Target*	*Forward/Reverse primer (5'-3')*
Episomal plasmid gene (episome silencing)	*EBNA-1*	TCAGGGCCAAGACATAGAGATG/GCCAATGCAACTTGGACGTT
House-Keeping gene (episome silencing)	*FBXO15*	GCCAGGAGGTCTTCGCTGTA/AATGCACGGCTAGGGTCAAA
Pluripotency Markers (qRT-PCR)	*NANOG*	TGAACCTCAGCTACAAACAG/TGGTGGTAGGAAGAGTAAAG
	GDF3	AAATGTTTGTGTTGCGGTCA/TCTGGCACAGGTGTCTTCAG
	SOX2	CCCAGCAGACTTCACATGT/CCTCCCATTTCCCTCGTTTT
	OCT4	GACAGGGGGAGGGGAGGAGCTAGG/CTTCCCTCCAACCAGTTGCCCCAAAC
Embryoid body formation and House-keeping gene (qRT-PCR)	*NCAM*	ATGGAAACTCTATTAAAGTGAACCTG/TAGACCTCATACTCAGCATTCCAGT
	PAX6	GTCCATCTTTGCTTGGGAAA/TAGCCAGGTTGCGAAGAACT
	SOX17	AAGGGCGAGTCCCGTATC/CGGCCGGTACTTGTAGTTG
	RUNX1	CCCTAGGGGATGTTCCAGAT/TGAAGCTTTTCCCTCTTCCA
	MYH6	TCAGCTGGAGGCCAAAGTAAAGGA/TTCTTGAGCTCTGAGCACTCGTCT
	ACTB	TGAAGTGTGACGTGGACATC/GGAGGAGCAATGATCTTGAT
mtDNA deletion and replication status	*ND1*	CCCTAAAACCCGCCACATCTAC/GAGCGATGGTGAGAGCTAAGGT
	ND4	CCATTCTCCTCCTATCCCTCAAC/CACAATCTGATGTTTTGGTTAAACTATATTT
	D-LOOP	CCCACACGTTCCCCTTAAATAA/CGTGAGTGGTTAATAGGGTGATAGAC
Targeted mutation analysis (ddPCR)	*PRKN (Parkin) exon 2*	dHsaCNS641949461
	PRKN (Parkin) exon 4	dHsaCNS336937253
	PRKN (Parkin) exon 6	dHsaCNS859410403
	PRKN (Parkin) exon 7	dHsaCNS525204420
House-Keeping Gene (ddPCR)	*RPP30*	dHsaCP2500350

3.2.11 Droplet digital PCR analysis

Droplet digital PCR (ddPCR) allows the quantification of nucleic acids with high precision and sensitivity. The principle of this technique relies on the use of microfluidic circuits and surfactant chemistry, where the DNA sample is randomly partitioned across 20,000 discrete droplets such that each droplet contains one or no copy of the template DNA. PCR amplification is performed using fluorescent probes specific for the target genes investigated allowing the detection of "positive" droplets. The portion of positive droplets identified is analyzed with Poisson statistics used to calculate the absolute concentration of the template DNA. With this method, it is possible to determine copy number variations (CNVs) to a higher degree of precision compared to what achieved with the traditional qPCR. In the present project, ddPCR was used to determine heterozygous deletions or duplications of exons in the *Parkin* gene. The assay was carried out on blood DNA for all individuals investigated in this study and on both iPSCs and parental PBMCs. Assay IDs are reported in Table 6, and RPP30 was used as internal control. Briefly, the master mix for the ddPCR reaction included 1X ddPCR SuperMix for probes (no dUTP; BioRad), 1X *Parkin* exon-specific primers/probe (FAM), 1X *RPP30* primers/probe (HEX), together with 25 ng sample DNA and RNAse/DNAse-free water added to a final reaction volume of 20 µl. The samples were thoroughly mixed, and 20 µl of reaction mix were transferred into a sample well of a DG8™ cartridge. Droplet generation oil for probes (BioRad) was then added to the cartridge, which was placed into the QX200 Droplet Generator™ (BioRad). After droplet generation, droplets were carefully transferred into a ddPCR 96-well plate (BioRad), and the plate was sealed for 5 sec at 175° C using a PX1™ PCR Plate Sealer (BioRad). Subsequent amplification was performed in the GeneAmp® PCR System 9700 (Applied Biosystems) with a ramp rate of 2°C/second. First, the enzyme was activated at 95°C for 10 min, followed by 40 cycles of denaturation at 94° C for 30 sec, and 60° C for 1 min. The enzyme was deactivated at 98°C for 10 min, and the reaction was finally kept at 4°C. Droplets were read using a QX200 droplet reader™ (BioRad), and the ddPCR data were analyzed using the QuantaSoft™ Analysis Pro software version 1.0 (BioRad). Manual thresholds were applied for both *Parkin* and *RPP30*.

3.2.12 Western blot

Western Blot is a well-established molecular technique used to evaluate the expression of specific proteins in cells and tissues. This procedure involves multiple steps (1) sample preparation, which comprises: preparation of cell lysate, protein extraction and quantification,

(2) electrophoretic separation of proteins based on the molecular weight on a polyacrylamide gel matrix (SDS-PAGE) and protein transfer onto a membrane (nitrocellulose or polyvinylidene fluoride (PVDF)), (3) incubation with primary antibody, coupled with a light signal inducing secondary antibody (conjugated with horseradish peroxidase, HRP) and detection.

Sample preparation

For Western Blot analysis, whole cell homogenates were used. To prepare whole cell lysates from different cell sources, cell pellets were resuspended in the appropriate volume of cold RIPA buffer (Thermo Fisher Scientific) supplemented with protease inhibitors cOmplete™ Protease Inhibitor Cocktail (Roche) and phosphatase inhibitors PhosSTOP EASYpack (Roche), to prevent the digestion of the sample by activation of endogenous proteases and phosphatases, followed by incubation for 30 min on ice. Next, lysates were centrifuged for 15 min at 14,200 x g at 4°C. The supernatant, containing the cell proteins, was transferred into a new tube and further quantified using BCA Protein Assay Kit (Thermo Fisher Scientific) according to the manufacturer's protocol. The absorbance was measured using VICTOR™ X3 Multilabel Plate Reader (PerkinElmer) at 562 nm. Sample protein concentration was calculated from the BCA standard calibration curve (0-2.5 µg/µL).

SDS-PAGE and protein transfer

Between 8 and 10 µg of protein lysates were loaded per well on the SDS-PAGE gel. The desired amount of proteins was mixed with 4X NuPAGE LDS Sample buffer and 10X NuPAGE Sample Reducing Agent (ratio 1:10) (Thermo Fisher Scientific). RIPA-buffer was added as needed to obtain an equal volume for all samples. Next, the samples were denaturated by incubating for 5 min at 95°C. After denaturation, 10 µl of sample mixture were loaded on a NuPAGE 4-12% Bis-Tris Gel (Thermo Fisher Scientific). Molecular weight standard Precision Plus Protein WesternC Blotting Standards (BioRad) was loaded on the same gel. The electrophoresis was performed in Running buffer (Table 8) at 100 V for 5 min, followed by 150 V for 90 min and 300 mA. Proteins were transferred to a nitrocellulose or PVDF membrane (BioRad). Briefly, sponges and filter paper were pre-soaked in Transfer buffer (Table 8) before assembling the transfer blot unit. The Western blot "sandwich" was structured as follows: two sponges, blotting paper, SDS-PAGE gel,

nitrocellulose membrane, blotting paper, three sponges. The transfer was run at 32 V and 200 mA for 70 min in an XCell II™ Blot Module (Thermo Fisher Scientific) containing Transfer buffer. As a final step, the quality of the transfer procedure was assessed by staining the membrane with a Ponceau solution. Ponceau (Sigma Aldrich), a sodium salt dye, allows a rapid detection of the protein bands on nitrocellulose or PVDF membranes, and the coloration is reversible upon washing with TBS-T 1X (Table 8).

Antibody incubation and detection

Once proteins were transferred to the membranes, the blots were blocked with Blocking buffer I or II (Table 8) for 1 h. The primary antibody (Table 7) was diluted to an appropriate concentration in Blocking buffer, and the blots were incubated overnight at 4°C on agitation. On the following day, three washing steps in TBS-T 1X for 5 min each, under agitation conditions, were performed, and the blots were incubated with the respective secondary antibodies for 1 h at RT. This was followed by other three washing steps in TBS-T 1X. Target proteins were detected by enhanced chemiluminescence using Clarity™ ECL Western Kit (BioRad), according to the manufacturers' protocol. The chemiluminescence signal was detected using the ChemiDoc™ Touch Imaging System (BioRad). Equal loading was assessed by use of an antibody against a housekeeping protein. The signal of the target protein was quantified by Image Lab 6.0 analyzer software (BioRad) by normalizing the expression of the target protein in relation to housekeeping proteins.

Table 7. *Antibodies for Western Blotting*

Primary antibodies	*Supplier*	*Dilution factor*	*Blocking Solution*
Mouse anti-MFN2	Abcam (Ab56889)	1:1,000	Blocking buffer II
Rabbit anti-SOD2 (D3X8P)	Cell Signaling (13141S)	1:1,000	Blocking buffer I
Mouse anti-Parkin	Abcam (77924)	1:5,000	Blocking buffer II
Mouse anti-Tubulin	Abcam (44928)	1:1,000	Blocking buffer I
Mouse anti-GAPDH	Milipore (MAB374)	1:5,000	Blocking buffer I
Rabbit anti-TOM70 A	Abcam (Ab135602)	1:1,000	Blocking buffer I
Rabbit anti-β-actin	Cell Signaling (4967S)	1:5,000	Blocking buffer I

Secondary antibodies			
Goat anti-mouse IgG, HRP conjugate	Millipore - Merck	1:5,000	Blocking buffer I
Goat anti-rabbit IgG, HRP conjugate	Millipore - Merck	1:10,000	Blocking buffer I

Table 8. *Solutions for Western Blotting*

Solutions	
Running buffer	50 NuPAGE MES Running buffer 20X (Thermo Fisher Scientific), 950 mL ddH2O
Transfer buffer	50 mL NuPAGE MES Transfer buffer 20X (Thermo Fisher Scientific), 100 mL MeOH, 850 mL ddH2O
Ponceau Red	0.1% Ponceau S, 5% acetic acid in ddH2O
TBS 10X	200 mM Tris, 9% NaCl, pH 7.5 in ddH2O
TBS-T 1X	100 mL TBS 10X, 0.1% Tween20, ddH2O to 1 liter
Blocking buffer I	5% Blotting-Grade Blocker in TBS-T 1X
Blocking buffer II	5% BSA in TBS-T 1X

3.2.13 Immunofluorescence

For immunocytochemical analysis, differentiated neurons were grown on a 16-well format chamber slide System Nunc™ Lab-Tek™ (Thermo Fisher Scientific), previously coated with poly-D-lysine (Sigma Aldrich) and laminin (Sigma Aldrich), and then fixed in a 4% paraformaldehyde solution in PBS for 10 min at room temperature. Next, cells were permeabilized in a 0.5% Triton X100 - PBS solution for 5 min and blocked for 1 h with Blocking solution (3% BSA in PBS) at RT. Immunostaining was then performed by addition of the primary antibodies (TH with GRP75 for assessment of mitochondrial network morphology, TH with TUBJ1 for iPSC-derived neurons characterization, Table 9) properly diluted in Blocking solution overnight at 4°C. On the next day, cells were washed three times for 5 min with PBS and further incubated with the appropriate fluorescently labelled secondary antibodies (goat anti-mouse Alexa Fluor 488-conjugated, goat anti-rabbit Alexa Fluor 555-conjugated, Thermo Fisher Scientific, Table 9), diluted 1:1,000 in Blocking solution for 1 h at RT. Finally, nuclei were stained by adding NucBlue™ Fixed Cell Stain (Thermo Fisher Scientific), and the slides were mounted with Dako Fluorecence mounting medium. Images were acquired using a SP8-X confocal microscope (Leica Microsystems), with a 63X oil immersion objective. Mitochondrial fragmentation was calculated using the filament

function in Imaris software (version 9.6.0, Bitplane) (Oxford Instruments). For each field, the total length of the modelled mitochondrial network was calculated and divided by the number of unconnected parts.

Table 9. *Antibodies for Immunofluorescence*

Primary antibodies	*Supplier*	*Dilution factor*
Rabbit anti-TH (MAB318)	Millipore - Merck	1:500
Rabbit anti-GRP75	Abcam	1:5,000
Mouse anti-TUBJ	Biolegend	1:1,000
Goat anti-mouse Alexa Fluor 488-conjugated	BioRad	1:1,000
Goat anti-rabbit Alexa Fluor 555-conjugated	BioRad	1:1,000

3.2.14 Flow cytometry

Flow cytometry is a well-established laser-based method, used to analyze the characteristics of cells or particles within a heterogeneous population. It is predominantly used to measure fluorescence intensity generated by fluorescently-labelled antibodies to detect proteins or ligands that bind to specific molecules. In this project, flow cytometry was used to assess mitochondrial membrane potential (MMP) and to detect the production of mitochondrial reactive oxygen species (ROS) in LCLs. Tetramethylrhodamine, methyl ester (TMRM, Image-iT™ Thermo Fisher Scientific) was used as membrane potential indicator. TMRM is a cell-permeant dye that accumulates in healthy active mitochondria with intact membrane potential, generating a bright signal. Upon loss of MMP, TMRM does not accumulate and the signal reduces or vanishes. In order to exclude dead cells from the analyzed sample, VivaFix™ Cell Viability Assay (Biorad) was used together with TMRM. To assess ROS production (specifically mitochondrial superoxide) in LCLs, MitoSOX™ Red reagent (Thermo Fisher Scientific) was used. MitoSox Red is a fluorogenic dye used for highly selective detection of superoxide in the mitochondria of live cells. It permeates the cell membrane and rapidly targets mitochondria, where it is oxidized by superoxide and exhibits red fluorescence. LCLs were co-stained with MitoSox Red and Mito Tracker™ Green (MTG), a green-fluorescence stain that specifically

localizes to mitochondria regardless of their membrane potential, in order to facilitate the selection of the cell population of interest for the acquisition and analysis. Stained LCLs were interrogated using an S3e Cell Sorter (Biorad), operated by the ProSort™ Software, version 1.6. Briefly, 5 x 10^5 cells were resuspended in 0.5 mL of RPMI 1640 (Biowest) medium containing either 100 nM TMRM and 1X VivaFix dye for MMP assessment or 2.5 µM MitoSox Red and 200 nM MTG for ROS production detection. After incubation in the dark at 37° C and 5% CO_2 for 30 min, cells were washed with fresh PBS and resuspended in 300 µl of warm PBS. Prior to acquisition with the flow cytometer, the cell solution was filtered with a 0.70 µm Corning® cell strainer. Fluorescence intensity of 20,000 events was quantified and analyzed using the FlowJo™ v10.6.1 software.

3.2.15 Staining with fluorescent dyes

To assess MMP, ROS production and mitochondrial morphology in iPSC-derived neurons under live imaging conditions, 2x10^5 cells per well were seeded after day 25 of differentiation as single cells on an 8-well live imaging chamber slide (ibidi GmBH) previously coated with poly-D-lysine (Sigma Aldrich) and laminin (Sigma Aldrich). Neurons were kept in culture with NB-B27 medium supplemented with factors and imaged between days 40 and 50 of differentiation. First, cells were washed once with pre-warmed HBSS 1X (Thermo Fisher Scientific), followed by incubation with a staining solution containing either 100 nM TMRM to assess MMP, 2.5 µM MitoSox Red to evaluate ROS production, or 100 nM MTG to evaluate mitochondrial morphology, at 37°C and 5% CO_2 for 30 min. Considering that primary neurons do not express multidrug resistance (MDR) transporters, which may limit the retention of TMRM in the organelle, it was not necessary to add a MDR inhibitor as Cyclosporin H during the assay (Connolly et al., 2018). MTG concentration, which could potentially be toxic to neurons, was determined considering the manufacturer´s guidelines and previous works on iPSC-derived neurons (Berenguer-Escuder et al., 2020; Shaltouki et al., 2015). Next, two washing steps with pre-warmed HBSS 1X were carefully performed, and cells were directly imaged in HBSS at 37°C and 5% CO_2 using a Leica SP8-X confocal microscope (Leica), with a 63X oil immersion objective. For mean intensity measurements of TMRM and MitoSox Red in thresholded images, Image J software was used (https://imagej.nih.gov/ij/index.html), a public domain Java-based image processing and analysis program developed at the National Institutes of Health and the Laboratory for Optical

and Computational Instrumentation. Mitochondrial fragmentation, acquired with 100 nM MTG staining, was calculated using the filament function in Imaris software (version 9.6.0, Bitplane) (Oxford Instruments).

3.2.16 High resolution respirometry

High-resolution respirometry (HRR) is an approach to measure respiration in several types of mitochondrial preparations and living cells. Mitochondrial oxygen consumption was measured in LCLs of heterozygous exon 7 deletion carriers and non-carriers, by means of HRR with the Oxygraph-2K (Oroboros Instruments, Innsbruck, Austria). The Oxygraph-2k (O2k) is a system composed of two separated 2-mL chambers, equipped with polarographic oxygen sensors capable of determining oxygen concentration (µM) and oxygen flux per cell [amol $O_2 \cdot s^{-1} \cdot cell^{-1}$], which were recorded in real-time using the manufacturer´s software DatLab7 (Oroboros Instruments, Innsbruck, Austria). This software was also used for post-experimental analysis. Temperature within the chambers, as well as the homogeneous oxygen distribution through constant stirring are crucial parameters to obtain accurate oxygen consumption measurements. Experiments were carried out under normoxic conditions (O_2 concentration at and below air saturation). Before the assay, air calibration was performed as described in the instrument´s manual, and temperature was set at 37°C ± 0.001°C (electronic Peltier regulation), under constant stirring at 750 rpm. Respirometry was performed in respiration medium MiR05 (Table 5), and manual titration of mitochondrial inhibitors and uncouplers was performed using Hamilton syringes (customized by Hamilton®). First, LCLs were collected between 48 and 72 hours after passaging in a 15 mL conical tube and counted using Acridine orange stain, with LUNA FL™ Fluorescence Cell Counter (Biosystems). Next, 5 x 10^6 cells were harvested at 200 x g for 5 min and resuspended in 50 µl of PBS. This solution of intact LCLs was added to each chamber, and the stopper was immediately placed to carefully close the chambers without disturbing the signal of the sensor. Mitochondrial respiration of intact LCLs was measured with the following multiple substrate-uncoupler-inhibitor titration protocol (SUIT-003, BioBlast, Figure 8): (1) ROUTINE corresponds to physiological respiration (depends on endogenous substrates), (2) LEAK respiration was induced by adding the ATP synthase inhibitor oligomycin (Omy, 10 nM; Sigma Aldrich) and corresponds to the non-phosphorylating resting state, when oxygen flux is compensating for the proton leak, (3) maximal capacity of the electron transfer

system was determined after uncoupling by stepwise titration (usually 1 – 2 steps) of the protonophore carbonyl cyanide-p-trifluoromethoxyphenylhydrazone (FCCP, U, 0.5 µM each step; Sigma Aldrich), (4) injection of complex I inhibitor rotenone (Rot, 0.5 µM; Sigma Aldrich) inhibited respiration of intact cells and allowed the determination of residual oxygen consumption, (5) addition of succinate (S, 10 mM; Acros Organics) served to test the intactness of cell membrane, and (6) the injection of the complex III-inhibitor antimycin A (Ama, 2.5 µM; Sigma Aldrich) led again to the assessment of the residual oxygen consumption. Respiratory fluxes were corrected for instrumental background considering the oxygen consumption by the oxygen sensors and the oxygen diffusion of the chamber, measured in a separate experiment recreating the same experimental conditions. Respiration related to ATP turnover was calculated as the difference between ROUTINE and LEAK respiration (R-L), and spare respiratory capacity was determined as the difference between maximal respiration and routine respiration (ET-R). The contents of each chamber were collected and frozen, for subsequent measurement of citrate synthase activity. Absolute respiration values were normalized for the total number of cells per chamber and citrate synthase activity.

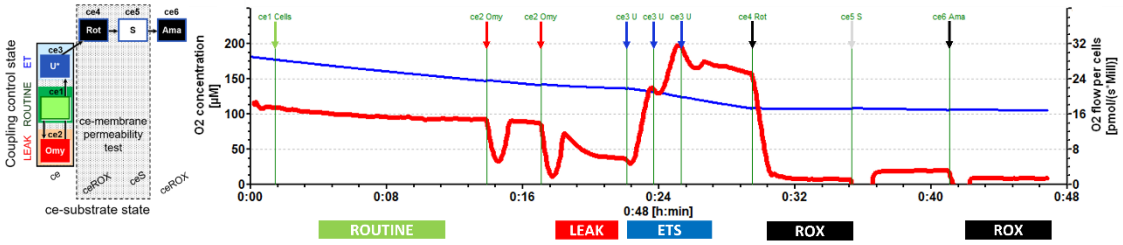

Figure 8. SUIT-003 protocol used to determine respiration of intact LCLs (Bioblast, www.bioblast.at/index.php/SUIT-003_O2_ce_D028) and its resulting trace. *Ce1: routine respiration (physiological coupling state after adding the cells in the chamber), ce2Omy: non-phosphorylating resting (Leak) state induced with titration of oligomycin, ce3U: noncoupled ET-state achieved with uncoupler titration, ce4Rot: residual oxygen consumption in ROX state after CI inhibition with rotenone, ce5S: succinate pathway control state (permeability test), ce6Ama: residual oxygen consumption in ROX state after CIII inhibition with antimycin A. Respirometry trace over time: blue indicates oxygen concentration (µM) and red represents oxygen flow per cells [amol $O_2 \cdot s^{-1} \cdot cell^{-1}$] on each respiratory state, induced by the addition of cells, substrates and inhibitors.*

3.2.17 Citrate synthesis activity

The enzyme citrate synthase (CS) is known as the pace-making enzyme in the Krebs Cycle. CS is localized in the mitochondrial matrix but it is nuclear encoded, and it is commonly used as a quantitative measure for the determination of intracellular density of mitochondria (Holloszy et

al., 1970). CS was assayed spectrophotometrically at 412 nm on the EnVision 2105 Multimode Plate Reader (Perkin-Elmer), according to the method described by Coore *et al*., with slight modifications (Coore et al., 1971). Following respirometry, LCLs were removed from the Oxygraph chamber and an aliquot of 0.5 mL was snap-frozen with liquid nitrogen and stored at -80° C. To perform CS activity measurements, first 110 µl of thawed cell solution (LCLs in MiR05) were mixed with 100 mM Tris buffer (pH 8.0) (Sigma Aldrich), 100 µM acetylcoenzyme A (Sigma Aldrich), 0.1% Triton X-100 (Sigma Aldrich) and 100 µM 5,5'-Dithiobis (2-nitrobenzoic acid) (DNTB, Sigma Aldrich) per well of a 96-well plate; the final reaction volume was 200 µL/well. After addition of these reagents, basal absorbance levels were measured for 1 min at 412 nm and 30°C. Next, the reaction was started by the addition of 100 µM oxaloacetate (Sigma Aldrich) to the mixture, and the CS activity was measured at 412 nm for 7 min at 30°C. The intensity of the absorbance is proportional to the CS activity, thus considered as the amount of mitochondria in the reaction. The assessment of CS activity was performed in duplicates for each sample and averaged values were used for normalization of respirometry results.

3.2.18 Extracellular Oxygen Consumption

Oxygen consumption is a well established measure of mitochondrial function. Aiming to provide an accurate model of neurons, derived from study participants, which are able to form synapses and transmit signals, I assessed oxygen consumption rates (OCR) on substrate-attached iPSC-derived neurons. For this, I used the extracellular oxygen consumption assay kit (Abcam, ab197243), according to the manufacturer's instructions. Briefly, at day 31 of differentiation, 2 x 10^5 iPSC-derived neurons were seeded on a 96-well black culture plate, previously coated with poly-D-lysine (Sigma Aldrich) and laminin (Sigma Aldrich), NB-B27 medium (Table 5) supplemented with neuronal differentiation factors. After replating, cells recovered for 72 hours prior preforming the respirometry measurements. For the assay, medium was replaced with 150 µl of fresh NB-B27 medium for basal OCR measurements, or with 150 µl of NB-B27 medium supplemented with 2.5 µM FCCP for maximal respiration measurements. Next, 10 µL of Extracellular O_2 consumption reagent were added to each well, except to the blank control. 100 µl of high-sensitivity mineral oil (pre-heated at 37°C) were promptly added to each well to limit back diffusion of ambient oxygen. Fluorescence intensities were measured immediately using the EnVision 2105 Multimode Plate Reader (Perkin-Elmer), pre-heated at 37°C. Fluorescence

intensity in each well was measured over 2-minutes intervals for a total of 200 min, at excitation/emission wavelengths = 355/642 nm. Respiration of cells results in oxygen depletion from the surrounding environment, causing an increase of fluorescence signal. Fluorescence intensity generated in each well was corrected with the blank control, and OCR was determined by selecting the linear portion of the signal profile (avoiding any initial lag or subsequent plateau) and applying the linear regression to determine the slope.

Right after performing the extracellular consumption assay, the CyQuant™ proliferation reagent assay (Thermo Fisher Scientific) was employed to determine the number of live cells in each well, according to manufacturer´s instructions, and fluorescence was read at excitation/emission wavelengths = 480/535 nm. The OCR calculated for each well was normalized to the cell number determined by CyQuant fluorescence dye. Fluorescence intensities detecting OCR are expressed as relative fluorescence units (RFU) *versus* time (min).

3.2.19 Statistical analyses

Statistical analyses were performed using GraphPad Prism 9. One-way ANOVA was used in experiments comparing three groups, followed by Tukey's *post-hoc* test to correct for multiple comparisons. For analyzing differences between two experimental groups, the non-parametric Mann-Whitney U test or a two-sided t-test were utilized. Threshold for significance was set at $p<0.05$. All experiments were performed in a minimum of three independent biological replicates.

4. Results

The present thesis is organized in three parts. The first part describes the identification of heterozygous *Parkin* mutation carriers in the CHRIS study and the penetrance of PD risk markers in these mutation carriers (section 4.1). The second part presents mtDNA analyses (section 4.2), and the third part comprises the functional evaluation of mitochondria in the lymphoblastoid cell lines of a subset of 20 individuals and in iPSC-derived neurons of four individuals (sections 4.3 and 4.4).

4.1 Frequency of heterozygous *Parkin* variants and penetrance of Parkinson's disease risk markers in the population-based CHRIS cohort

For n = 3,603 participants of the CHRIS study, exome sequence data were available. To identify carriers of pathogenic or likely pathogenic point mutations and small deletions/insertions in the exome sequence dataset, I used an in-house instance of the BRAVO (**Br**owse **A**ll **V**ariants **O**nline) browser, which is a web-based browser for genetic variation. All variants were annotated with the Ensembl Variant Effect Predictor (VEP) and the Combined Annotation Dependent Depletion (CADD) algorithms (Kircher et al., 2014; McLaren et al., 2016). I decided a CADD score cutoff of >20, which was more likely to capture predicted pathogenic variants by comparison with variants described in the MDSGene database.

In this exome sequence dataset, n = 164 individuals carrying one of 17 known or newly detected heterozygous mutations in *Parkin* were identified, which resulted in a carrier frequency of 4.55%. Two small frameshift deletions (delA in exon 9, p.Val324AlafsTer111 - rs1562519380); del CT in exon 2, p.Gln34ArgfsTer5 - rs55777503) were detected in 35 individuals, and 98 individuals carried one out of 11 single nucleotide variations (eight known and three novel) resulting in a missense mutation (Table 10). To search for predicted CNVs over the *Parkin* gene, the SNP & Variation Suite software (SVS version 8, Golden Helix) was used to examine the signal intensity information (LogR) from available chip genotyping data. To confirm predicted deletions or duplications of specific exons, DNA was further analyzed by ddPCR. Large exon rearrangements affecting exons 2, 3, 4 and 7 of the *Parkin* gene were identified and confirmed by ddPCR in 31 individuals (0.86%) (Table 10, Figure 9).

Table 10. *Heterozygous mutations in the Parkin gene identified in the exome sequence dataset of the CHRIS cohort (n=3,603)*

Parkin *mutation* *(DNA change / rsID)*	*Consequence*	*CADD score*	*Number of carriers*	*Carrier frequency (%)*	*Allele frequency (%)*	*gnomAD allele frequency (%)*
Exon 7 deletion	CNV, frameshift	/	24	0.67	0.33	
Exon 2 deletion	CNV	/	4	0.11	0.06	
Exon 2,3,4 duplication	CNV	/	2	0.06	0.03	
Exon 4 duplication	CNV	/	1	0.03	0.014	
GA / G (rs1562519380)	frameshift, p.Val324AlafsTer111	33	18	0.50	0.25	/
CCT / C (rs55777503)	frameshift, p.Gln34ArgfsTer5	32	17	0.47	0.23	0.02
G / A (rs34424986)	missense, p.Arg275Trp	30	59	1.64	0.82	0.19
G / A (rs150562946)	missense, p.Arg256Cys,	32	11	0.30	0.14	0.04
C / T (rs146173584)	missense, p.Asp243Asn,	24	10	0.28	0.14	0.026
C / T (rs748892763)	missense, p.Arg104Gln,	23	6	0.17	0.08	0.0012
G / A (rs55830907)	missense, p.Arg402Cys,	24	3	0.08	0.04	0.18
G / A (rs137853054)	missense, p.Thr240Met	24	3	0.08	0.04	0.034
G / C	missense, p.Cys441Trp	29	2	0.06	0.03	/
G / A (rs149953814)	missense, p.Pro437Leu	28	1	0.03	0.014	0.15
T / G (rs182893847)	missense, p.Met458Leu	24	1	0.03	0.014	0.028
T / C	missense, p.Tyr267Cys	28	1	0.03	0.014	/
C / T (c.8-1G>A)	splice acceptor	35	1	0.03	0.014	/

CNV, copy number variant

CADD (Combined Annotation Dependent Depletion): tool for scoring the deleteriousness of single nucleotide variants as well as insertion/deletion variants in the human genome; variants with a score of >20 were taken into consideration in this study (Kircher et al., 2014; McLaren et al., 2016)

gnomAD: Genome Aggregation Database (https://gnomad.broadinstitute.org/)

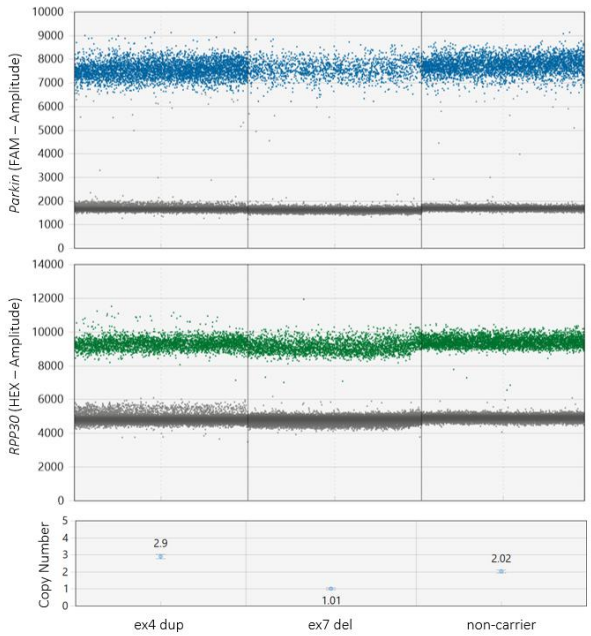

Figure 9. Confirmation of exon rearrangements in the Parkin gene by ddPCR. *Representative plots of ddPCR data output for individuals carrying a duplication in exon 4, a deletion in exon 7, and a non-carrier. Top: one-dimensional plots of droplets measured for fluorescence signal emitted from Parkin (FAM labeled; positive droplets in blue) and from the reference gene RPP30 (HEX labeled; positive droplets in green). Negative droplets are shown in black. Bottom: display of the calculated Parkin copy number, where the reference gene copy number was set to 2. Error bars represent 95% Poisson confidence* limits, *generated by QuantaSoft software.*

None of the 164 *Parkin* mutation carriers identified, fulfilled the criteria for a PD diagnosis. The heterozygous mutation carriers were further compared with 2,582 controls in terms of risk markers associated with PD. All risk markers described in (Heinzel et al., 2019), except for occupational solvent exposure and *substantia nigra* hyperechogenicity, were available for analysis. The descriptive analysis is presented in Table 11, reporting percentages for the binary variables and means, medians and inter-quartile range (IQR) for the continuous variables. Interestingly, a higher percentage of heterozygous *Parkin* mutation carriers shows diabetes mellitus (type II) (p=0.023), which is known to be associated with PD risk in multiple population-based prospective studies (Heinzel et al., 2019). In addition to the established PD risk markers, I included potential PD risk markers in the analyses, which I identified based on recent data in the literature. For these markers, I observed a trend for a lower heart rate in the *Parkin* mutation carriers (59.01 vs. 60.6, p=0.054) as compared to the controls.

Table 11. *Descriptive statistics of PD risk markers in heterozygous Parkin mutation carriers in the exome sequenced dataset of the CHRIS study*

PD risk markers	*CONTROLS (n=2,582)*						*MUTATION CARRIERS (n=164)*						p-*value*
Sex, n (%)													
Male	1,148 (44.46)						68 (41.46)						0.454
Female	1,434 (55.54)						96 (58.54)						
Pesticide exposure, n (%)													
Yes	497 (27.25)						30 (25.86)						0.745
No	1,327 (72.75)						86 (74.14)						
Non-use of caffeine, n (%)													
Yes	40 (15.21)						2 (12.50)						0.769
No	223 (84.79)						14 (87.50)						
Non-smoker, n (%)													
Yes	1,973 (80.79)						126 (80.77)						0.9938
No	469 (19.21)						30 (19.23)						
Diabetes (II), n (%)													
Yes	119 (4.85)						14 (8.97)						**0.023**
No	2,335 (95.15)						142 (91.03)						
	Mean	*SD*	*Median*	*IQR (25-75)*	*Min*	*Max*	*Mean*	*SD*	*Median*	*IQR (25-75)*	*Min*	*Max*	*p-value*
Age (years)	46.03	16.66	46.37	25.94	18.03	93.51	44.58	16.85	43.45	29.34	18.02	87.71	0.2948
Uric acid levels	5.14	1.35	5	1.9	1.4	11	5.23	1.30	5.2	1.9	2.4	8.4	0.2209

Physical activity	1376	955	1260	1505	0	3780	1444	948.89	1260	1610	0	3360	0.3336
CRP	0.24	0.38	0.13	0.21	0	7.15	0.28	0.48	0.11	0.245	0	3.46	0.7314
PC	259.52	57.52	254	74	73	516	267.92	73.57	257	78	149	732	0.5662
MPV	8.7	1.41	8.5	2	4.3	13.7	8.62	1.37	8.4	2.1	5.5	12.4	0.4906
PLR	8.09	2.94	7.60	3.30	1.79	39.83	8.23	3.05	7.47	3.11	3.35	21.08	0.8147
NLR	4.87	1.35	4.69	1.63	1.26	17.90	5.03	1.55	4.88	1.56	2.12	15.77	0.2677
Heart rate	60.60	9.73	60	12	34	120	59.01	8.87	59	13	41	86	0.0538
Systolic BP	119.58	16.82	117	21	84	201	117.51	15.12	117	19	90	167	0.2730
WBC	6.17	1.58	5.9	1.9	2.6	19.3	6.10	1.51	6	1.9	2.9	10.9	0.6535
Neutrophil counts	3.42	1.24	3.2	1.4	0.5	15.4	3.36	1.15	3.2	1.5	1.6	8.5	0.5798
Serum albumin	4.59	0.30	4.6	0.40	3.3	5.9	4.57	0.33	4.6	0.5	3.5	5.6	0.1652
Sodium	140.50	2.30	140	3	132	155	140.57	2.39	141	3	134	148	0.6593

PD risk markers from Heinzel et al (Heinzel et al., 2019) are underlined

Physical activity was measured as minutes per week

Additional potential PD risk markers were chosen based on Qiu et al. (Qiu et al., 2019) (CRP), Kocer et al. (Kocer et al., 2013) (Platelet count (PC), Mean platelet volume (MPV), Moghaddam et al. (Sanjari Moghaddam et al., 2018) (Platelet to lymphocyte ratio (PLR), Neutrophil to lymphocyte ratio (NLR), Iwaki et al. (Iwaki et al., 2020) (heart rate, systolic blood pressure (BP), white blood cell (WBC), neutrophil counts, serum albumin, sodium, height)

Data reported here are not corrected for multiple comparison

4.2 mtDNA analyses

4.2.1 Mitochondrial DNA deletion and transcriptional activity in individuals with a heterozygous *Parkin* mutation

A possible role of parkin in mitochondrial DNA (mtDNA) maintenance has been described previously in the literature (Pickrell et al., 2015; Shin et al., 2011). To expand the mtDNA characterization of individuals carrying a heterozygous mutation in *Parkin*, I looked at their mtDNA and specifically quantified the presence of mtDNA major arc deletions and the proportion of transcriptionally active mtDNA molecules, compared to non-carriers. A triplex real-time PCR assay was performed for n=91 mutation carriers and n=75 non-carriers to detect simultaneously three targets within the mitochondrial genome (*ND1* [NADH dehydrogenase 1], *ND4*, and D-Loop) (Grunewald et al., 2016). To detect mtDNA major arc deletions, the cellular concentration of *MT-ND4* (situated within the common major arc deletion) and *MT-ND1* (situated in the minor arc) was compared and MT-ND4:MT-ND1 ratio calculated, thus obtaining the proportion of wildtype mtDNA molecules without somatic major arc deletions. Quantification of the 7S DNA, which binds the D-Loop during mtDNA transcription and replication, was carried out through the simultaneous amplification of a portion of the D-Loop and MT-ND1, to calculate the D-Loop:MT-ND1 ratio. The quantification of mtDNA major arc deletions showed no deletion accumulation (Figure 10) in the mtDNA of individuals carrying a heterozygous *Parkin* mutation (*Parkin*+/PD-) (MT-ND4:MT-ND1 is decreased in the presence of mtDNA deletions). On the other hand, when quantifying the presence of 7S DNA, I observed significantly reduced levels in the heterozygous *Parkin* mutation carriers ($p= 0.047$) compared to non-carriers. This result suggests an impaired mtDNA integrity and homeostasis, possibly as a consequence of parkin deficiency due to the mutation on one allele.

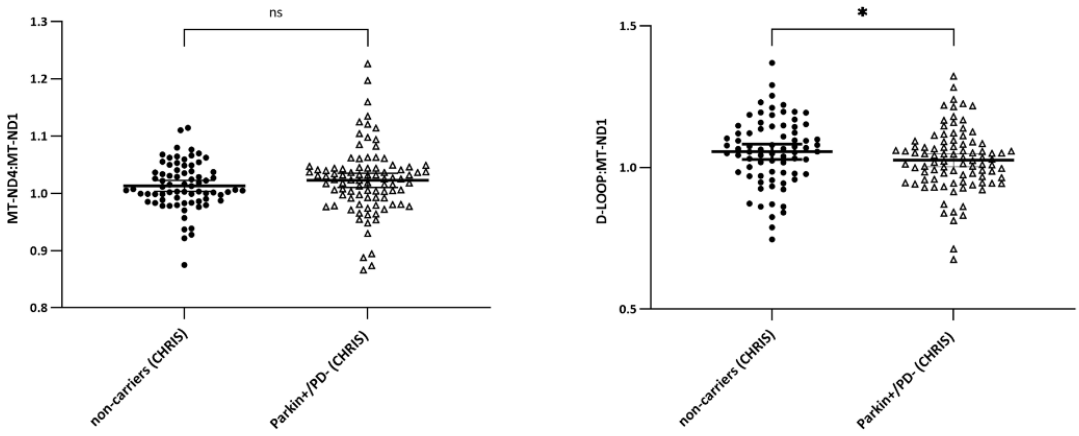

Figure 10. mtDNA major arc deletions and mtDNA transcription-associated 7S DNA normalized to MT-ND1 in individuals with a heterozygous mutation in Parkin. *Real-time PCR quantification of mtDNA sequences in the D-LOOP, the minor arc gene MT-ND1 and the major arc gene MT-ND4 in CHRIS participants carrying a heterozygous mutation in Parkin (Parkin+/PD-) (n = 91) and non-carriers (n = 75). Left: scatter plot showing mean with 95% confidence interval of the MT-ND4:MT-ND1 ratio, indicating major arc deletions. Right: scatter plot showing mean with 95% confidence interval of the D-LOOP:MT-ND1, indicating the amount of transcription-associated 7S DNA per mtDNA molecule. Statistical analysis was carried out by using the Mann-Whitney U test, * p≤0.05. ns = not significant.*

4.2.2 mtDNA variants and copy number in individuals with a heterozygous *Parkin* mutation

mtDNA alterations are known to cause a number of severe disorders, mainly associated with defects in the metabolic homeostasis. These disorders predominantly affect tissues and organs with high energetic demand like the brain (Monzio Compagnoni et al., 2020). Studies in *postmortem* brains or peripheral tissues of PD patients have led to the identification of three different types of mtDNA alterations: point mutations, deletions and copy number variations (Simon et al., 2000; W. Wei et al., 2017). Herein, I looked to characterize the mitochondrial genome in blood-derived DNA of unaffected carriers of heterozygous *Parkin* mutations and non-carriers, by assessing mtDNA mutation and mtDNA copy number. For this, mtDNA sequencing was performed in outsourcing (https://www.centogene.com), and the analysis was carried out in-house, in collaboration with the bioinformatics group, by using the mtDNA-server (https://mtdna-server.uibk.ac.at/index.html). Previous mtDNA sequencing analyses have shown that the frequency of a mitochondrial mutation must exceed a threshold between 60 – 80% to result in functional defects (Stewart et al., 2015). However, in this study I wanted to also assess whether a much lower percentage of mutated mtDNA is able to influence the penetrance of *Parkin* mutations in heterozygous carriers. Heteroplasmic frequency of the variants was used as a measure of mtDNA heteroplasmy, which was estimated as base heteroplasmy (mutant

allele frequency over the total coverage of all alleles). Identified mtDNA variants were compared between a group of heterozygous *Parkin* mutation carriers (n = 95) and a control group (n = 60). Individuals with heterozygous *Parkin* mutations (Parkin+/PD-) were found, surprisingly, to have a significantly lower heteroplasmic variant (p= 0.006) count compared to healthy controls (Figure 11). Additionally, mtDNA copy number was evaluated in a group of heterozygous *Parkin* mutation carriers (n =144) and compared to a group of non-carriers (n = 9,527), as part of a separate study. This was done through qPCR by measuring the mitochondrial gene ND1 (MT-ND1) relative to the nuclear-encoded single copy gene beta-2-microglobulin (B2M) and providing the quantification of the amount of wild-type mtDNA copies (MT-ND1:B2M). mtDNA copy number analysis revealed increased levels in the Parkin+/PD- group compared to the group of non-carriers (p= 0.0001, 148.8 vs. 134.9, respectively) (Figure 11). These results suggest an accumulation of mtDNA molecules in the individuals carrying a heterozygous mutation in *Parkin*, due to an impairment in the mitochondrial clearance process or an increase (potentially compensatory) in mitochondrial biogenesis.

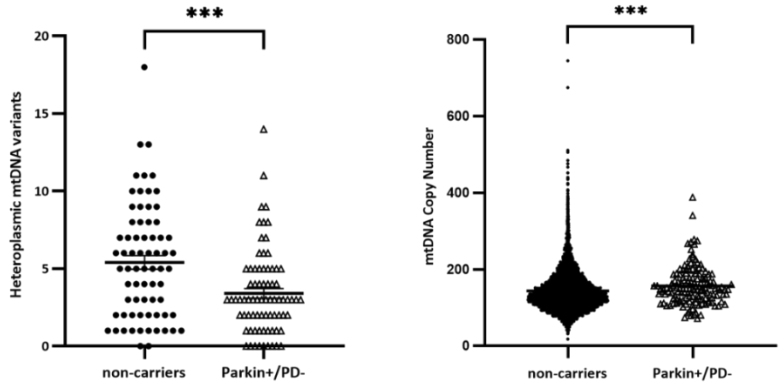

Figure 11. mtDNA analyses in blood-derived DNA from unaffected heterozygous carriers of mutations in Parkin and non-carriers. *Left: Scatter plot showing mean with 95% confidence of the number of heteroplasmic mtDNA variants for individuals carrying a heterozygous mutation in Parkin (Parkin+/PD-) (n= 95) vs. non-carriers (n=60). Right: scatter plot showing mean with 95% confidence interval of the MT-ND1:B2M, indicating the amount of mtDNA copies, for individuals carrying a heterozygous mutation in Parkin (Parkin+/PD-) (n = 144) and non-carriers (n = 9,527). Statistical analysis was carried out using the Mann-Whitney U test, *** p≤0.001.*

4.3 Assessment of mitochondrial function in lymphoblasts

The present section describes the results obtained from functional assays on immortalized lymphocytes (LCLs) as the first cellular model used in this study. This was performed for the 20

study participants described in section 3.1 of the materials and methods chapter (11 carriers of a heterozygous exon 7 deletion in *Parkin* and 9 non-carriers). None of these study subjects fulfilled the diagnostic criteria for a PD diagnosis.

4.3.1 Lymphoblastoid cell line generation through immortalization of PBMCs

Lymphoblastoid cell lines (LCLs) were successfully generated starting from the previously isolated PBMCs, as summarized in Figure 12A. Thawed PBMCs were infected with EBV as described in the materials and methods section 3.2.2. The time for the infected B-lymphocytes to show signs of transformation was approximately 7 days after infection. EBV infects specifically mature resting B-lymphocytes through their CR2/CD21 surface receptor (Hussain & Mulherkar, 2012). Successful immortalization was confirmed by the evident morphological changes, which included cell elongation, clumping and formation of the typical rosette shape. The cells were then allowed to proliferate and after 4 weeks in culture, big clumps (as shown in Figure 12B) were visible to the naked eye. The immortalization process was successful for all selected individuals, allowing the generation of 20 cell lines.

A)

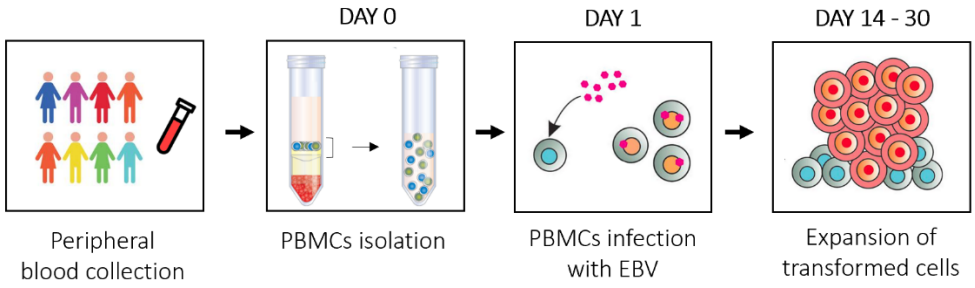

B)

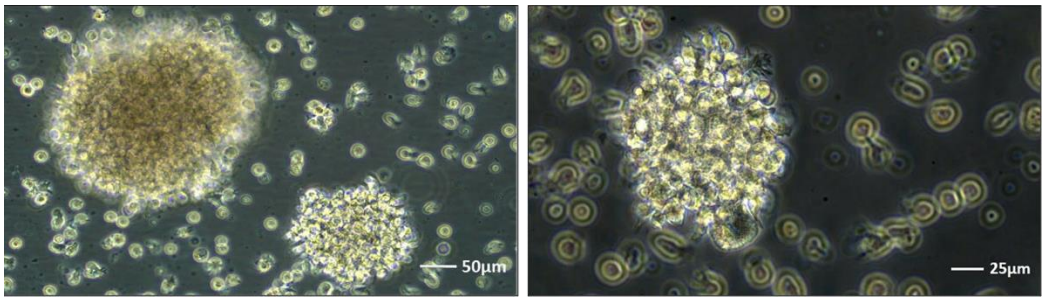

Figure 12. PBMCs immortalization with EBV to generate LCLs. *(A) Diagram showing the cell line generation process. (B) Visualization of LCLs by phase contrast inverted microscope; (left) cell clumps four weeks post-infection, scale bar: 50 µm; (right) typical rosette morphology, scale bar: 25 µm.*

4.3.2 Characterization of the lymphoblastoid cellular model

Upon LCLs generation, cells were subjected to molecular analysis in order to confirm whether the heterozygous exon 7 deletion was present in the lines of the 11 carrier individuals. This was done by droplet digital PCR.

The *Parkin* exon 7 deletion generates a truncated protein, which cannot be detected by the antibody against the C-terminus used in this study. Western blotting confirms that parkin expression was reduced in the LCLs of the heterozygous exon 7 deletion carriers (Figure 13).

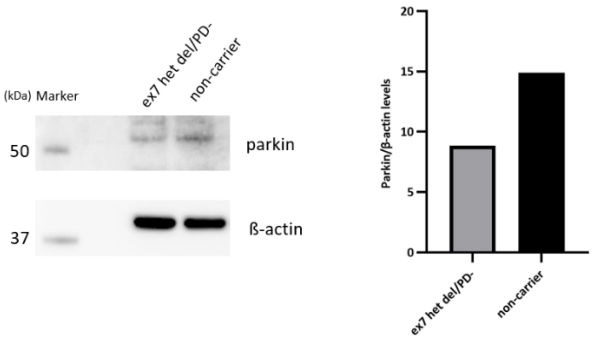

Figure 13. Evaluation of* parkin *levels in whole-cell lysates of LCLs*. Western blot and densitometric analysis, showing parkin protein expression in the generated lymphoblasts of a heterozygous deletion carrier (ex7 het del/PD-) and a non-carrier. n = 1. Parkin levels were analyzed with the indicated anti-parkin antibody, and β-actin was used as loading control. Molecular mass markers are in kilodaltons (kDa).*

4.3.3 Respirometry activity in LCLs of exon 7 heterozygous deletion carriers and non-carriers

Alterations in cellular respiration and changes in respiratory control may indicate significant mitochondrial defects. To investigate the respiratory capacity of LCLs in the set of 20 study participants, oxygen consumption was measured by means of high-resolution respirometry (Oxygraph-2K, Oroboros Instruments, Innsbruck, Austria). As described in the materials and methods section 3.2.16, the performed intact protocol conferred the evaluation of several respiratory states, based on the determination of oxygen concentration (µM) and oxygen flux per cell (amol $O_2 \cdot s^{-1} \cdot cell^{-1}$). As shown in Figure 14, the generated respirometry traces provided a bioenergetic profile, which included: (1) physiological respiratory activity in intact cells (routine

respiration), (2) LEAK respiration (residual respiration after inhibition of ATP synthase by oligomycin, compensating for proton leak, slippage and cationic cycling across the IMM), (3) electron transfer system capacity (ETS) (non-physiological maximal uncoupled respiration by addition of the uncoupler FCCP, not limited by ATP synthase activity), and (4) residual oxygen consumption (ROX) (respiration attributable to secondary cellular oxygen-consuming processes apart from the respiratory chain) by addition of the complex I inhibitor rotenone and antimycin A, an inhibitor of complex III of the electron transport chain. The administration of succinate, substrate of respiratory complex II, enabled to confirm the intactness of the membrane in the assayed LCLs, as there was no significant increase in oxygen consumption rate after its addition. Absolute respiration values were normalized for the total number of cells per measurement chamber as well as for the activity of citrate synthase enzyme, which was measured post-assay as described in the materials and methods section 3.2.17.

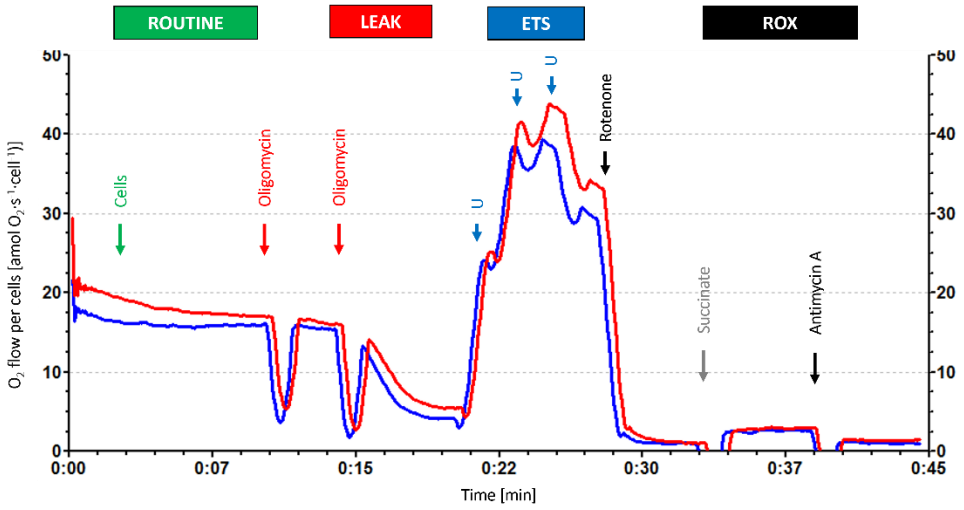

Figure 14. Representative traces of real-time high-resolution respirometry using an intact substrate-uncoupler-inhibitor titration (SUIT) protocol in LCLs. *The oxygen flow per cells (y-axis) is represented as a function of time (x-axis). Arrows indicate addition of cells and titrations of substrates and inhibitors, which comprised: addition of 5 x 10^{6} cells in each chamber; oligomycin (5 nM each step); FCCP (U) (0.5 µM each step); rotenone (0.5 µM); succinate (10 mM); antimycin A (2.5 µM). Representative trace for one non-carrier (blue trace) and one heterozygous deletion carrier (red trace). Oxygen fluxes were normalized per cell count and citrate synthase activity. ETS, electron transfer system; ROX, residual oxygen consumption.*

For all the experiments, LCLs were seeded at 3x10^{5} cells/mL in fresh RPMI medium 72 hours prior to performing the respirometry measurements. Before each assay, population doubling time was calculated in order to ensure similar proliferation rates between lines. Under

physiological conditions of non-permeabilized LCLs, individuals carrying a heterozygous exon 7 deletion in *Parkin* present a significantly increased oxygen consumption, identified during the routine respiratory state (p = 0.023) (Figure 15). This enhanced metabolic rate suggests a "hyperactive" respiratory state in comparison to the non-carriers. The trend of increased rate of oxygen consumption remained consistent through all the subsequent respiratory states (Table 12), nevertheless, group differences were not statistically significant. These data indicate an affected molecular phenotype in a peripheral tissue of heterozygous mutation carriers, detectable in the basal state. Notably, this goes in line with an elevation of basal respiration detected in LCLs of idiopathic PD patients compared to controls (Annesley et al., 2016). Absolute respiration values were normalized for the total number of cells per chamber and citrate synthase activity. The use of CS activity as mitochondrial marker for normalization of fluxes has been debated due on its modifiability under certain conditions such as development or exercise (Drahota et al., 2004); (Pesta et al., 2011). Nonetheless, when normalizing the oxygen fluxes of this study only by the total number of cells, the results were comparable (data not shown).

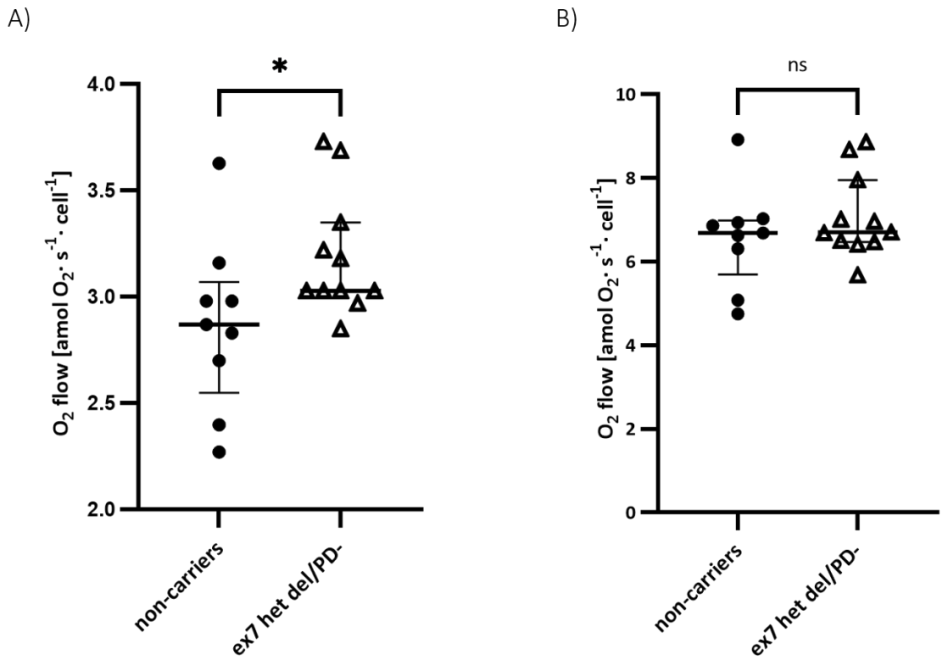

Figure 15. Hyperactive respiratory state at physiological conditions in heterozygous mutation carriers. *Group-wise comparison of respiration in LCLs from exon 7 heterozygous deletion carriers (n = 11) and non-carriers (n = 9), characterized by mitochondrial oxygen flow per cell. (A) routine respiration, (B) electron transfer system capacity (ETS). Each line was measured in at least three independent assays, each run was normalized to citrate synthase activity. Data are presented as scatter plots showing median with interquartile range. Statistical analysis was carried out by using the Mann-Whitney U test. (*) indicates significant group differences with an alpha level of 0.05. ns = not significant.*

Table 12. *Respiratory parameters assessed in LCLs of heterozygous Parkin exon 7 deletion carriers (n=11) and non-carriers (n=9)*

Respiratory parameters	***non-carriers (n = 11)***		***ex 7 het del/PD- (n = 9)***		
	mean	*median*	*mean*	*median*	*p-value*
Routine respiration (R)	2.87±0.40	2.87	3.19±0.28	3.05	**0.023**
Leak respiration (L)	0.88±0.13	0.90	0.95±0.16	0.98	0.382
Maximal respiratory capacity (E)	6.58±1.20	6.69	7.08±0.99	6.70	0.518
Residual Oxygen Consumption (ROX)					
Rotenone	0.18±0.04	0.17	0.20±0.03	0.20	0.305
Antimycin A	0.22±0.03	0.22	0.24±0.03	0.24	0.138
ATP Turnover (R-L)	1.99±0.39	1.93	2.25±0.30	2.17	0.159
Spare Respiratory Capacity (ET-R)	3.71±0.82	3.71	3.89±0.74	3.51	0.909

Values are given as mean ± s.d. and median. Statistical analysis was carried out by using the Mann-Whitney U test. Bold p-value indicates significance with an alpha level of 0.05.

4.3.4 Evaluation of mitochondrial Reactive Oxygen Species production in LCLs of heterozygous exon 7 deletion carriers

As previously reported in the literature, PD related gene products, including parkin, can influence mitochondrial function leading to an enhanced ROS production and susceptibility to oxidative stress (Dias et al., 2013). Additionally, considering the results of the bioenergetic profiling in the LCLs of the mutation carriers, which suggest an enhanced respiratory state, I sought to further characterize their mitochondrial function by looking into the production of ROS. One of these reactive oxygen species is the superoxide anion, which is mainly produced by complexes I and III of the mitochondrial electron transport system in the IMM (Dias et al., 2013). Therefore, LCLs of the carriers and non-carriers were co-stained with MitoSox Red and MitoTracker dyes as described in section 3.2.14, and mitochondrial superoxide levels (mROS) were measured by means of flow cytometry. The gating strategy consisted of several steps, including gating cell population by forward (FS-A) and sideward (SS-A) scatter, identifying single

cells using forward width (FS-W) and forward area (FS-A) scatter, selecting the MitoTracker green-positive population, followed by determination of MitoSox Red-positive cells and their mean fluorescence intensity. As depicted in Figure 16, the quantification of MitoSox Red signal showed an increase of mROS in the LCLs of heterozygous exon 7 deletion carriers, compared to the group of non-carriers (p= 0.054, 22.45 vs. 15.55 respectively). Although the difference between groups is borderline statistically significant, the trend of this result goes in line with the enhanced mitochondrial respiratory activity in the carrier group.

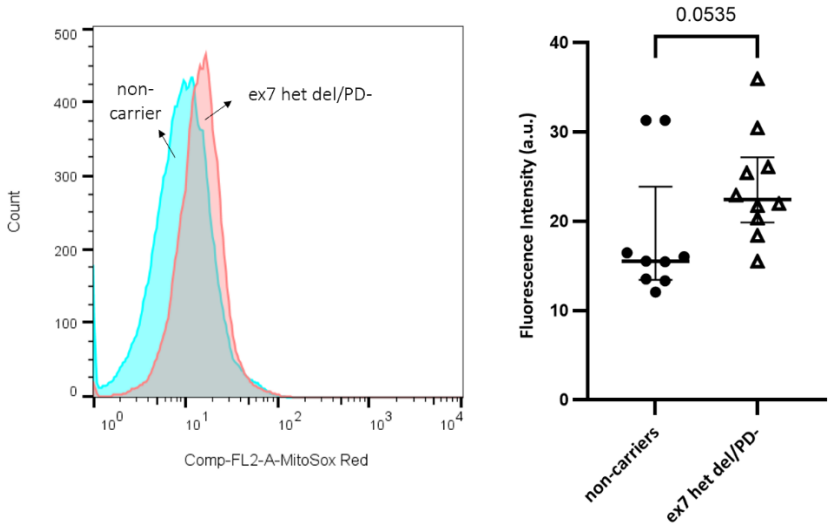

Figure 16. Mitochondrial ROS production is increased in LCLs of heterozygous Parkin exon 7 deletion carriers. *Left: representative flow cytometry histograms of MitoSox Red fluorescence (blue, non-carrier; red, carrier) in LCLs (20,000 cells). Right: group-wise comparison of mROS production in LCLs of heterozygous deletion carriers (n = 11) and non-carriers (n = 9). Data are from at least 3 independent experiments. Results are presented as scatter plots showing median with interquartile range; statistical analysis was carried out by using Mann-Whitney U test, p = 0.054. a.u.: arbitrary units.*

4.3.5 Mitochondrial membrane potential (MMP) assessment in LCLs of heterozygous exon 7 deletion carriers

Mitochondrial membrane potential is considered an important parameter that reflects mitochondrial integrity, thus offering an indicator of mitochondrial dysfunction in disease (Qadri et al., 2018). According to previous studies conducted in cells of peripheral tissue from PD patients with *Parkin* mutations, membrane potential is significantly decreased compared to the controls (Mortiboys et al., 2008). To account for the fact that mitochondrial function is altered in the LCLs of heterozygous exon 7 deletion carriers, MMP was evaluated, to determine the

overall oxidative phosphorylation activity of the electron transport system. Cells were stained using the cell permeant dye TMRM and further interrogated through flow cytometry as described in section 3.2.14. The gating strategy consisted of several steps, including gating cell population by forward (FS-A) and sideward (SS-A) scatter, identifying single cells using forward width (FS-W) and forward area (FS-A) scatter, selecting the VivaFix-positive population (live cells), followed by determination of TMRM-positive cells and their mean fluorescence intensity. MMP in the carrier group showed a trend towards a depolarized state compared to the non-carriers group, however this difference among groups was not statistically significant (p = 0.26, 715 vs. 755.7) (Figure 17).

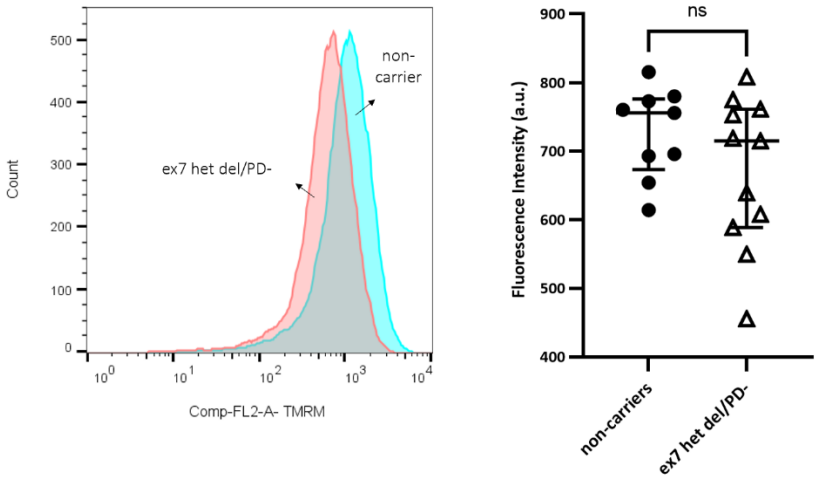

Figure 17. Mitochondrial membrane potential in LCLs of heterozygous exon 7 deletion carriers shows a trend towards a depolarized state. *Left: representative flow cytometry histograms of TMRM fluorescence (blue, non-carrier; red, carrier) in LCLs (20,000 cells). Right: group-wise comparison of MMP in LCLs from heterozygous deletion carriers (n = 11) and non-carriers (n = 9). Data are from at least 3 independent experiments. Results are presented as scatter plots showing median with interquartile range; statistical analysis was carried out with Mann-Whitney U test, p = 0.26. a.u.: arbitrary units. ns = not significant.*

4.4 Assessment of mitochondrial function in iPSC-derived neurons

In order to understand if the molecular phenotypes observed in the LCLs of the mutation carriers are more pronounced in neuronal cells, a subset of 4 individuals was selected and induced pluripotent stem cells (iPSC) were successfully generated by reprogramming their PBMCs. PBMCs from two healthy non-carriers (iPS-BC and iPS-DI) and two carriers of a heterozygous exon 7 deletion in *Parkin* (iPS-AD and iPS-BD) were reprogrammed into iPSCs and further differentiated into DA neurons. The following section describes the results generated by the

reprogramming process from PBMCs into iPSCs and the data obtained from the functional assays carried out in iPSC-derived DA neurons.

4.4.1 Reprogramming of PBMCs into iPSCs and characterization

Reprogramming of the PBMCs into iPSCs was carried out as described in section 3.2.4. Figure 18A shows a schematic representation of the applied protocol. After thawing the isolated PBMCs, cells were seeded in blood culture medium and further expanded for 14 days. As depicted in Figure 18B, the PBMCs increased markedly in size over the amplification period. On day 15, PBMCs were transfected with the episomal plasmids and after 10 – 15 days, small bright rounded colonies were visible. Approximately 20 – 30 days post-transfection, it was possible to observe compact colonies with well-defined borders, presenting a typical embryonic stem cell-like morphology (Figure 18B). iPSCs were successfully generated for the 4 selected individuals.

A)

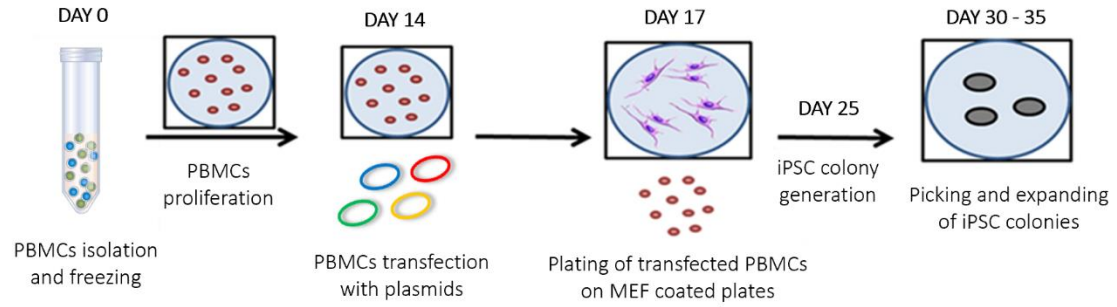

B)

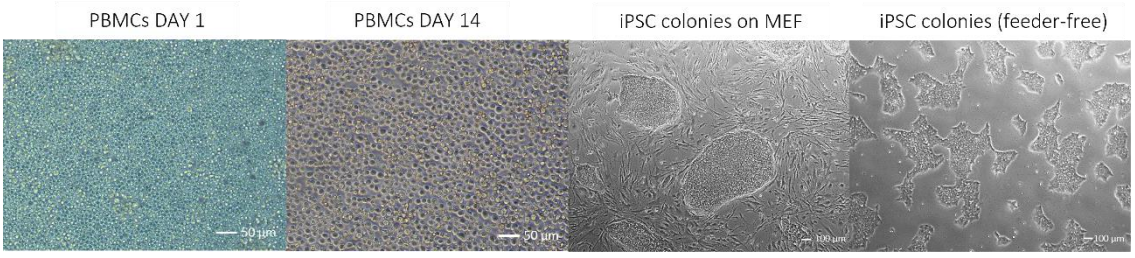

Figure 18. Generation of iPSCs from human PBMCs and cellular morphological changes. *(A) Scheme of the protocol used to generate iPSCs from frozen isolated PBMCs, using a single transfection of four non-integrating episomal plasmids. (B) From left to right: PBMCs in culture on day 1 of the reprograming process; PBMCs after expansion in culture for 14 days, before transfection (scale bar, 50 µm); iPSC colonies seeded on a MEF feeder layer (approximately 30 days after transfection); iPSCs cultured under feeder-free conditions (scale bar, 100 µm). iPSCs, induced pluripotent stem cells; PBMCs, peripheral blood mononuclear cells; MEF, mouse embryonic fibroblasts.*

Upon generation of the iPSC lines and their subsequent amplification, characterization of each line was carried out to assess their stemness state and pluripotency potential. Figure 19A shows iPSCs positive for alkaline phosphatase staining, indicating their self-renewal potential. Immunofluorescence staining depicts the expression and localization of pluripotency markers SSEA-4, TRA-1-60 (cell membrane surface markers) and OCT3/4 and SOX-2 (transcription factors located in the nucleus) (Figure 19B). To corroborate the successful reactivation of endogenous pluripotency markers, qPCR analysis was performed, revealing significantly higher expression levels of NANOG, GDF3, SOX-2, and OCT3/4 genes in the iPSCs compared to their precursor PBMCs (Figure 19C). Furthermore, *in vitro* pluripotency potential was evaluated by differentiating the iPSCs into embryoid bodies (EBs) with a spontaneous differentiation protocol. qRT-PCR measurements (Figure 19D) reveal that all 4 generated iPSC lines were able to differentiate into cells of the three germ layers. After 15 – 20 days of differentiation, EBs displayed up-regulation of specific endoderm (SOX17), mesoderm (RUNX1, MYH6) and ectoderm (NCAM, PAX6) markers. These results validated the pluripotent state of the iPSCs obtained from the PBMCs of the four selected individuals. In addition, the expression of exogenous episomal plasmids was assessed with qPCR using primers for the episomal plasmid specific *EBNA-1* gene. After 5 passaging steps, transgene expression was not detected anymore in the iPSCs. As depicted in Figure 19E, PBMCs indicated a strong transgene expression level 5 days post-transfection, while the PBMCs never exposed to the plasmids, as well as the generated iPSCs expressed significantly lower levels of exogenous episomal plasmids demonstrating the clearance of the exogenous transgenes. The presence of the heterozygous exon 7 deletion in *Parkin* in the iPSCs was confirmed by ddPCR. As depicted in Figure 19F, the iPSCs and PBMCs from individuals carrying the heterozygous deletion in exon 7 (AD and BD), show a copy number loss in the region of interest *Parkin*, where the concentration is approximately half of the reference gene *RPP30,* resulting in an approximate copy number of 1, thus validating the presence of the heterozygous deletion in the generated model. Finally, cytogenetic analyses confirmed a normal karyotype for the generated iPSC lines (Figure 19G).

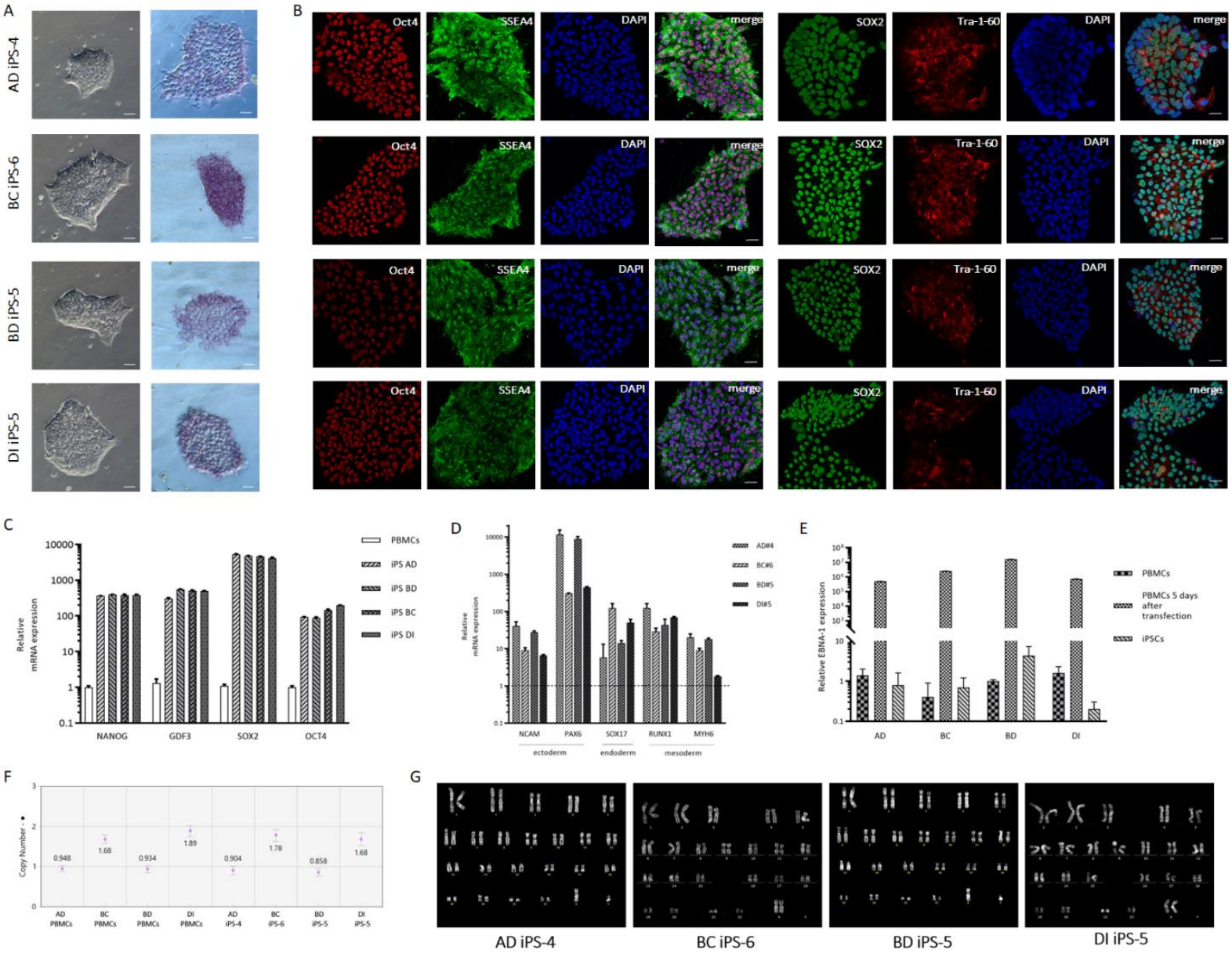
A
AD iPS-4
BC iPS-6
BD iPS-5
DI iPS-5
B
Oct4
SSEA4
DAPI
merge
SOX2
Tra-1-60
C
Relative mRNA expression
PBMCs
iPS AD
iPS BD
iPS BC
iPS DI
NANOG
GDF3
SOX2
OCT4
D
Relative mRNA expression
AD#4
BC#6
BD#5
DI#5
NCAM
PAX6
SOX17
RUNX1
MYH6
ectoderm
endoderm
mesoderm
E
Relative EBNA-1 expression
PBMCs
PBMCs 5 days after transfection
iPSCs
AD
BC
BD
DI
F
Copy Number
0.948
1.68
0.934
1.89
0.904
1.78
0.858
1.68
AD PBMCs
BC PBMCs
BD PBMCs
DI PBMCs
AD iPS-4
BC iPS-6
BD iPS-5
DI iPS-5
G
AD iPS-4
BC iPS-6
BD iPS-5
DI iPS-5

Figure 19. Characterization of four iPSC lines. *(A) Brightfield representative images of iPSC lines display a stem cell-like colony-forming morphology of small cells with large nuclei (left), and representative images showing a positive staining for alkaline phosphatase (right). Scale bar 50 µm. (B) Immunofluorescence analysis shows the presence of pluripotency markers OCT4, SSEA-4, SOX2 and Tra-1-60 in all four generated iPSC lines. Scale, scale bar 25 µm. (C) Expression levels of pluripotency markers NANOG, GDF3, SOX2 and OCT4 in PBMCs and iPSC lines relative to β-actin (as a loading control) as assessed by quantitative RT-PCR. The values for PBMCs were set to 1. (D) RT-PCR analyses of differentiation markers for the three germ layers (endoderm: SOX17; mesoderm: RUNX1, MHY6; ectoderm: NCAM, PAX6) in EBs from the four generated iPSC lines. The values are relative to β-actin and normalized to the parental iPSC line (set to 1) (not shown). (E) qPCR with episomal-specific primers (EBNA-1) (relative to FBXO15 control) shows no genome-integration of episomal vectors. (F) Confirmation of the presence of heterozygous Parkin exon 7 deletion in iPSC lines and their respective parental PBMCs by ddPCR. Data output shows copy number values determined with the ROI:REF ratio concentrations and multiplied by the number of copies of the reference gene RPP30. Reference gene copy number was set to 2. Error bars represent 95% Poisson confidence limits, generated by QuantaSoft software. (G) iPSCs derived from PBMCs of the two heterozygous deletion carries and two non-carriers displayed a normal karyotype.*

4.4.2 Generation and characterization of iPSC-derived neurons

The generated iPSC lines were subsequently differentiated into midbrain-type dopaminergic (DA) neurons as previously detailed in section 3.2.5 and summarized in the scheme of Figure 20A. With the aim of further characterizing the extent of differentiation in the neuronal model, immunofluorescence staining was performed for all four lines. I analyzed the co-staining of the DA neuronal marker tyrosine hydroxylase (TH), the rate-limiting enzyme in the synthesis of dopamine, together with the class III member of the beta tubulin family (TUJ1), which is involved in axon guidance and is frequently used as a neuronal marker (Tischfield et al., 2010). Figure 20B indicates high percentages of neurons co-expressing the neuron-specific marker TUJ1 and TH. Additionally, I assessed parkin protein expression levels in the differentiated neurons from the two individuals carrying a heterozygous exon 7 deletion (AD and BD) and the two non-carriers (BC and DI) by means of western blot analysis. The deletion of exon 7 in *Parkin* generates a truncated protein, which is unable to be detected by the antibody against the C-terminus used in this study. Western blot and densitometric analyses, shown in Figure 20C, confirmed that parkin expression was reduced in the iPSC-derived neurons of the heterozygous exon 7 deletion carriers.

A)

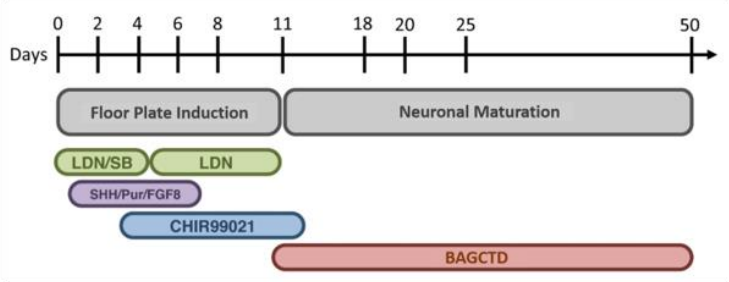
0
2
4
6
8
11
18
20
25
50
Days
Floor Plate Induction
Neuronal Maturation
LDN/SB
LDN
SHH/Pur/FGF8
CHIR99021
BAGCTD

B)

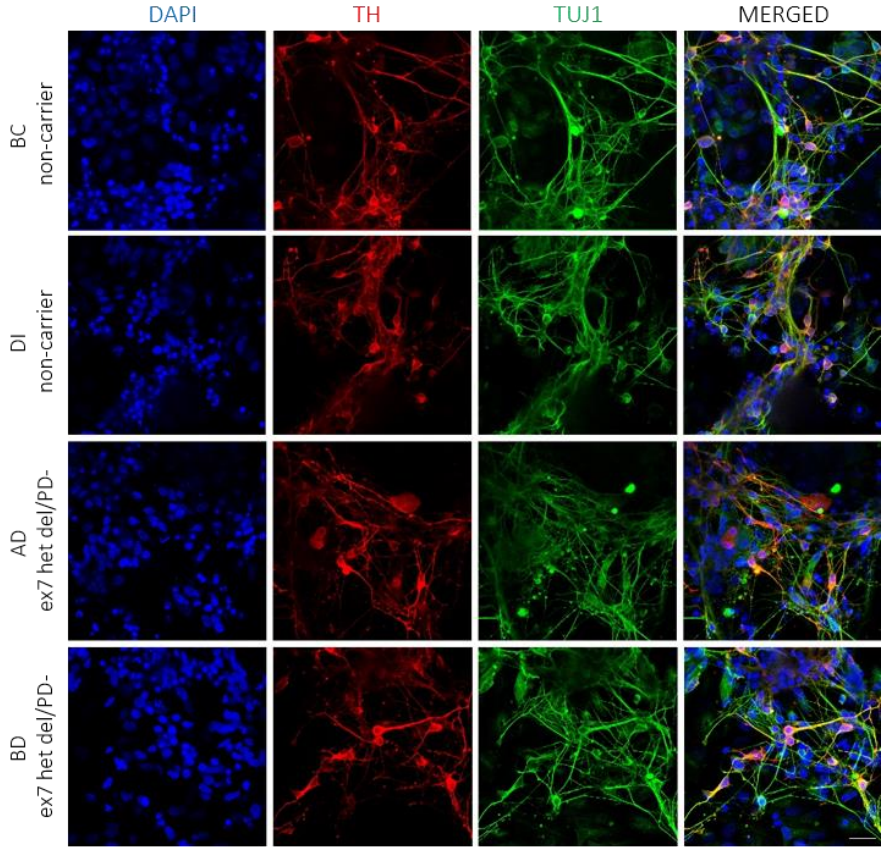
DAPI
TH
TUJ1
MERGED
BC non-carrier
DI non-carrier
AD ex7 het del/PD-
BD ex7 het del/PD-

C)

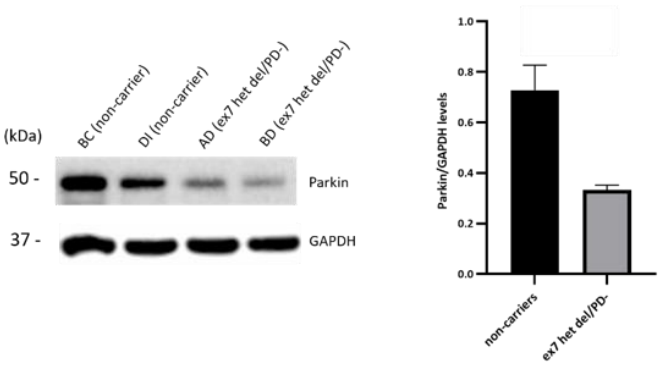
(kDa)
BC (non-carrier)
DI (non-carrier)
AD (ex7 het del/PD-)
BD (ex7 het del/PD-)
50 -
Parkin
37 -
GAPDH
Parkin/GAPDH levels
1.0
0.8
0.6
0.4
0.2
0.0
non-carriers
ex7 het del/PD-

Figure 20. Generation of iPSC-derived neurons and their characterization. *(A) Schematic summary of the differentiation protocol used to obtain DA neurons (Kriks et al., 2011). First stage indicates floor-plate induction through exposure to LDN and SB to trigger the Dual-SMAD inhibition. Purmorphamine (Pur), Sonic Hedgehog (SHH) and FGF8, together with CHIR99021 allow for a complete enrichment of DA precursors with A9 midbrain identity. Neural differentiation and maturation were achieved by applying the neurotrophic factors mix BAGCTD (BDNF, ascorbic acid, TGF- ß3, GDNF, cyclic-AMP, DAPT). (B) Immunofluorescence staining of neuronal cultures derived from iPSC-BC (non-carrier), iPSC-DI (non-carrier), iPSC-AD (ex 7 het del/PD-) and iPSC-BD (ex 7 het del/PD-) for neuron-specific TUJ1 (green), the DA marker TH (red), and nuclear DAPI (blue). Scale bar, 25 µm. (C) Western blot and densitometric analyses, showing parkin protein expression in iPSC-derived DA neurons of heterozygous Parkin exon 7 deletion carriers (AD, BD, ex7 het del/PD-) and non-carriers (BC, DI), n = 1. Parkin levels were analyzed with the indicated anti-parkin antibody, and GAPDH was used as loading control. Molecular mass markers are in kilodaltons (kDa).*

4.4.3 Evaluation of mitochondrial Reactive Oxygen Species production in iPSC-derived neurons

Increased levels of oxidative stress have been previously reported in several PD models (Nguyen et al., 2011; Palacino et al., 2004), also for PD patients with homozygous or compound heterozygous (biallelic) mutations in *Parkin* (Kamienieva et al., 2021). In addition, mROS measurements in the LCLs of the individuals carrying a heterozygous exon 7 deletion in *Parkin* showed a clear trend towards increased oxidative stress in this study. To explore possible functional alterations in the mitochondria of iPSC-derived neurons of individuals carrying a heterozygous deletion in *Parkin*, I measured mitochondrial-derived oxidants using the fluorogenic dye MitoSox Red as described in section 3.2.15. As depicted in Figure 21, iPSC-derived neurons obtained from the carriers (ex7 het del/PD-), as well as from a patient carrying a homozygous *Parkin* mutation (*Parkin* ++/PD+), displayed MitoSox positive mitochondria with a significantly higher mean fluorescence intensity as compared to the mean fluorescence intensity of the control populations (controls set to 1 vs. 1.18±0.04 vs. 1.32±0.05; p= 0.008, p= 0.001; respectively). This was confirmed also when comparing only the two non-carrier lines with the two-carrier lines generated in this study (non-carriers set to 1 vs. 1.14±0.02, p=0.007). When comparing the mean fluorescence intensity of the carriers group (ex7 het del/PD-) with the mean of the patient line there was not statistical significance (p= 0.074) but a clear trend. This phenotype of mitochondrial dysfunction in iPSC-derived neurons from *Parkin* PD individuals has been previously reported (Imaizumi et al., 2012), indicating increased levels of oxidative stress in these cells. The mitochondrial phenotype in the iPSC-derived neurons of the heterozygote mutation carriers suggest an increased oxidative stress compared to the non-carriers, similar to the phenotype observed in the PD patient. This could be interpreted as an

indicator of a gene-dosage effect for oxidative stress levels in heterozygous *Parkin* mutation carriers.

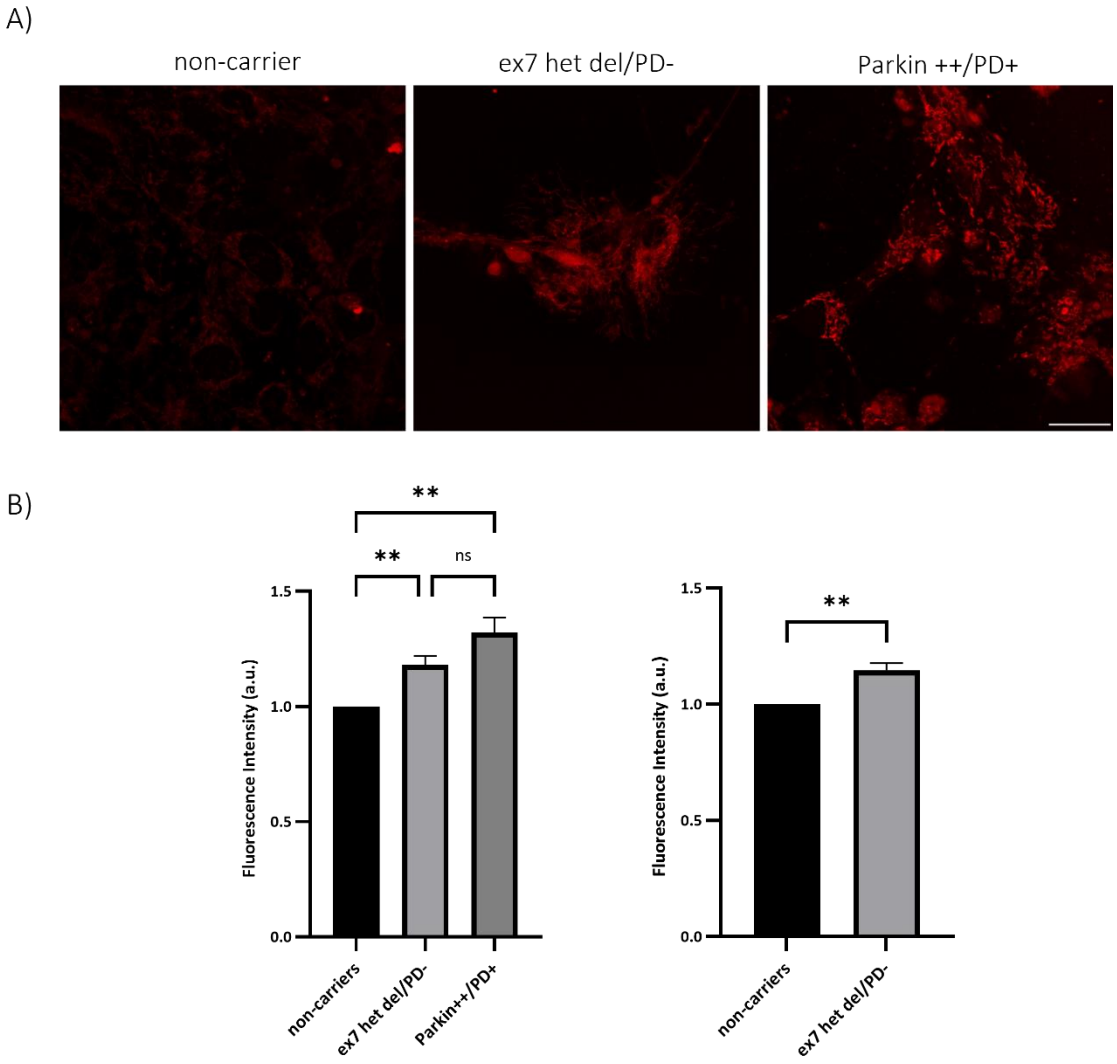

Figure 21. Measurement of mROS production in iPSC-derived neurons. *(A) Confocal live imaging of MitoSox red staining in iPSC-derived neurons at day 40 of differentiation. Scale bar: 25 µm. (B) Quantification of mean fluorescence intensity of MitoSox Red in iPSC-derived neurons; left: one PD patient line (iPSC-B125, Parkin++/PD+), two heterozygous carriers (ex7 het del/PD-) and the control group (three control lines including iPSC-SFC084-03-02 and the two non-carrier lines generated in this study); right: direct comparison between the two non-carriers (iPS-BC, iPS-DI) and the two carriers (iPS-AD, iPS-BD) generated in this study. Mean fluorescence intensity was analyzed in thresholded images, using the Image J software (n = 3-4 independent experiments); it was set to 1 in the control groups. Error bars represent the mean ± SEM. p values were determined using one-way ANOVA followed by Tukey's post hoc test to correct for multiple comparisons, as well as a two-sided t-test, when comparing only two groups. Significance levels are presented as comparisons with the control group. ** p≤0.01, ns = not significant. a.u.: arbitrary units.*

4.4.3.1 Assessment of superoxide dismutase levels in iPSC-derived neurons

Considering the results of mROS production, suggesting increased levels of oxidative stress in the neurons of the individuals carrying a heterozygous exon 7 deletion in *Parkin*, I further investigated the regulation of mROS in these cells. Superoxide is the predominant mROS generated and its levels are partly regulated by the antioxidant enzyme superoxide dismutase (SOD2) (Brand et al., 2004; Dias et al., 2013). To understand whether an increase in mROS in the iPSC-derived neurons of heterozygous deletion carriers is accompanied by modifications in the levels of the antioxidant enzyme, I quantified the protein levels of the mitochondrially located SOD2 by means of Western blot. When compared to the control group, the protein level of SOD2 was decreased in the neurons from the heterozygous exon 7 deletion carriers, as well as from the patient carrying a homozygous *Parkin* mutation, but did not differ significantly (Figure 22). Even though the difference is not statistically significant, these results could suggest deficiencies in the defense mechanism against oxidative stress in individuals lacking parkin or showing reduced parkin levels. Accordingly, Pacelli et. al, conducted a study where they observed increased ROS levels in fibroblasts from PD patients carrying mutations in *Parkin*, coupled with a decreased activity of mitochondrial SOD2 (Pacelli et al., 2011).

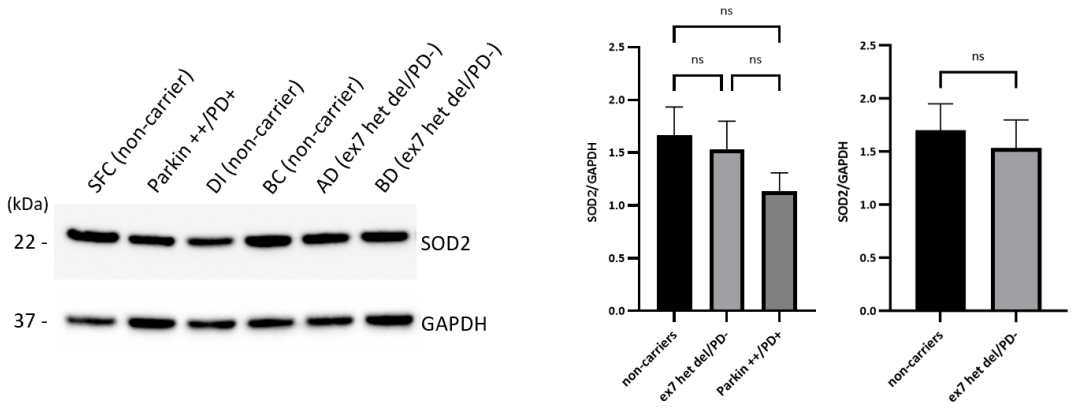

Figure 22. Evaluation of* SOD2 *levels in whole-cell lysates of iPSC-derived neurons*. Western blot and densitometric analysis, showing SOD2 protein expression in the generated iPSC-derived neurons. Densitometric analysis: (left) one PD patient line (iPSC-B125, Parkin++/PD+), two heterozygous carriers (ex7 het del/PD-) and the control group (three control lines including iPSC-SFC084-03-02 and the two non-carriers generated in this study); (right) direct comparison between the two non-carriers (iPS-BC, iPS-DI) and the two carriers (iPS-AD, iPS-BD) generated in this study. SOD2 levels were analyzed with the indicated anti-SOD2 antibody, and GAPDH was used as loading control. Molecular mass markers are in kilodaltons (kDa). n = 3 independent experiments. Error bars represent the mean ± SEM. Significance levels were determined using one-way ANOVA followed by Tukey's post hoc test to correct for multiple comparisons, as well as a two-sided t-test, when comparing only two groups. ns = not significant.*

4.4.4 Assessment of mitochondrial membrane potential (MMP) in iPSC-derived neurons

Next, I investigated the MMP in the iPSC-derived neurons, including the heterozygous *Parkin* exon 7 deletion carriers. MMP was assessed using the cell-permeant dye TMRM, which accumulates in healthy, active mitochondria with intact membrane potential, as described in section 3.2.15. The fluorescence intensity of TMRM clearly decreased both in exon 7 heterozygous deletion carrier neurons and PD patient neurons (Figure 23A), which indicates a reduced MMP in both sets of samples. Mean fluorescence intensity analysis revealed a statistically significant reduction of membrane potential for the carriers ($p= 0.032$), as well as for the PD patient neurons ($p= 0.003$), compared with the iPSC-derived neurons of the control group (control group set to 1 vs. 0.90±0.03 vs. 0.82±0.03). The same was true when comparing only the two non-carrier lines with the two-carrier lines generated in this study (non-carriers set to 1 vs. 0.91±0.03, $p=0.021$) (Figure 23B). Consistent with this outcome, Kumar et. al., observed a reduction in membrane potential in *Parkin* knockout iPSC-derived DA neurons (Kumar et al., 2020). Taken together, these results indicate an altered mitochondrial phenotype in the presence of a heterozygous *Parkin* mutation, which is milder when compared to the phenotype observed in the presence of disease, thus reinforcing the possibility of a gene-dosage effect.

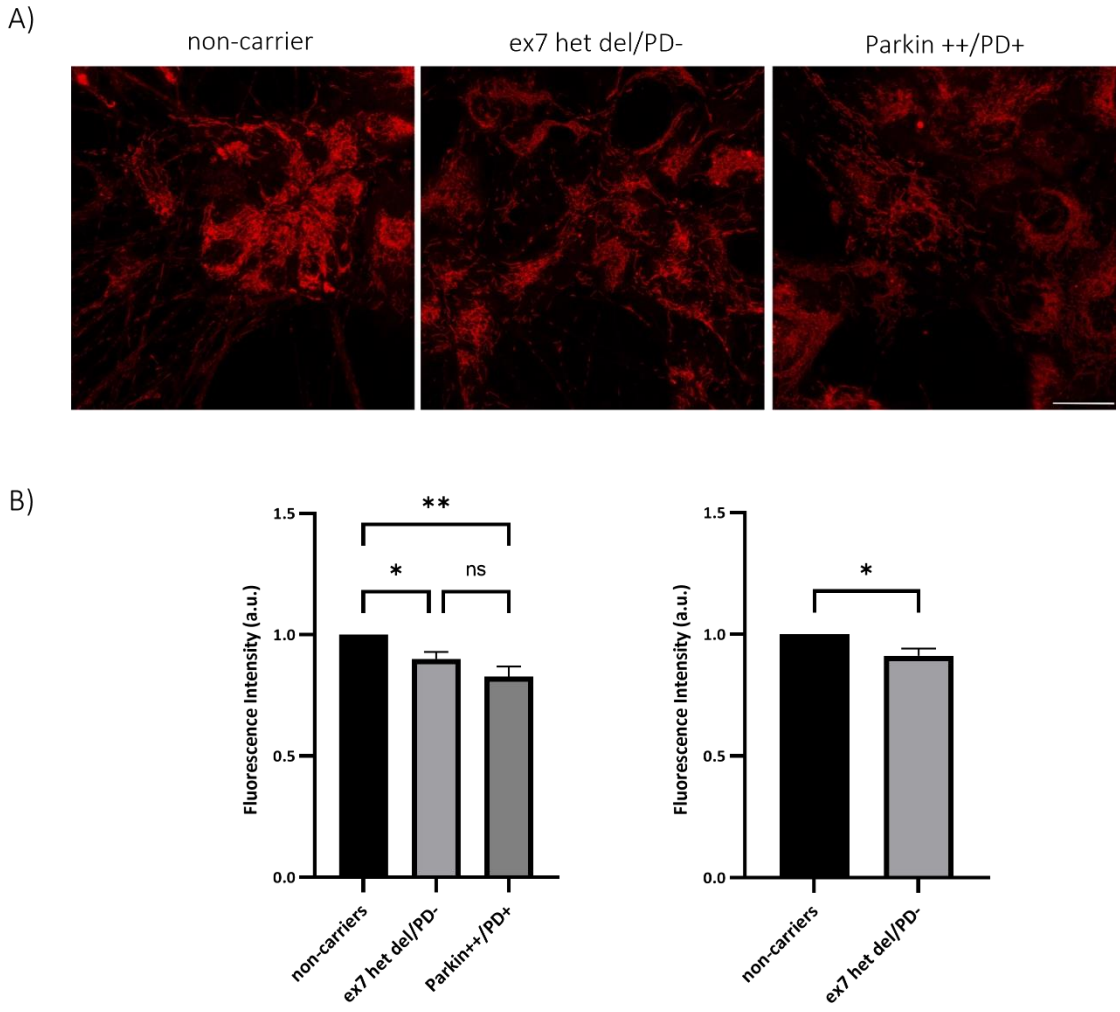

Figure 23. Assessment of MMP in iPSC-derived neurons. *(A) Confocal live imaging of iPSC-derived neurons at day 40 of differentiation, indicating mitochondria stained with TMRM. Scale bar: 25 µm. (B) Quantification of mean fluorescence intensity of TMRM in iPSC-derived neurons; left: one PD patient line (iPSC-B125, Parkin++/PD+), two heterozygous carriers (ex7 het del/PD-) and the control group (three control lines including iPSC-SFC084-03-02 and the two non-carriers generated in this study); right: direct comparison between the two non-carriers (iPS-BC, iPS-DI) and the two carriers (iPS-AD, iPS-BD) generated in this study. Mean fluorescence intensity was analyzed in thresholded images, using the Image J software. (n = 5 independent experiments); it was set to 1 in the control groups. Error bars represent the mean ± SEM. p values were determined using one-way ANOVA followed by Tukey's post hoc test to correct for multiple comparisons and a two-sided t-test, when comparing only two groups. Significance levels are presented as comparisons with the control group: * p≤0.05, ** p≤0.01, ns = not significant. a.u.: arbitrary units.*

4.4.5 Assessment of mitochondrial network morphology in iPSC-derived neurons

Considering the abnormalities in mitochondrial function observed so far in the neuronal model, in terms of oxidative stress and mitochondrial membrane potential, I performed morphological analysis of the mitochondrial network of the heterozygous *Parkin* exon 7 deletion carriers in

comparison with a *Parkin* PD line and control lines. Growing evidence has shown previously impaired mitochondrial function and morphology in parkin-deficient model systems (Mortiboys et al., 2008; Pinto et al., 2018). Assessment of mitochondrial network morphology was done by staining with the green-fluorescent dye MTG (Figure 24A), which specifically localizes to mitochondria regardless of their membrane potential. Mitochondrial network morphology assessment in iPSC-derived neurons of the *Parkin* exon 7 heterozygous deletion carriers revealed an increased mitochondrial fragmentation (quantified as total length of the modelled mitochondrial network divided by the number of unconnected parts), without a statistically significant group change ($p= 0.203$), compared to the iPSC-derived neurons from the control group (Figure 24C). On the other hand, the *Parkin* PD line showed a significant increased fragmentation when compared to the control group ($p= 0.030$). The same was true when the *Parkin* PD line was compared to the carriers group, although this comparison was not significant. Even if the difference between carriers and non-carries, is not statistically significant, the trend of this result coincides with the altered mitochondrial function observed for the carrier group. Moreover, I aimed to determine the degree of mitochondrial network fragmentation specifically in DA neurons. This was done by means of immunofluorescence staining of the mitochondrial network in iPSC-derived neurons with the anti-GRP75 antibody (Figure 24B) and network fragmentation was evaluated only in neurons expressing tyrosine hydroxylase, which were visualized by TH-staining. Again, this morphological assessment demonstrated no significant differences between carriers and non-carriers or with the *Parkin* PD line (Figure 24D), but confirmed the trend exhibited by the whole neuronal population examined with the fluorescent dye MTG.

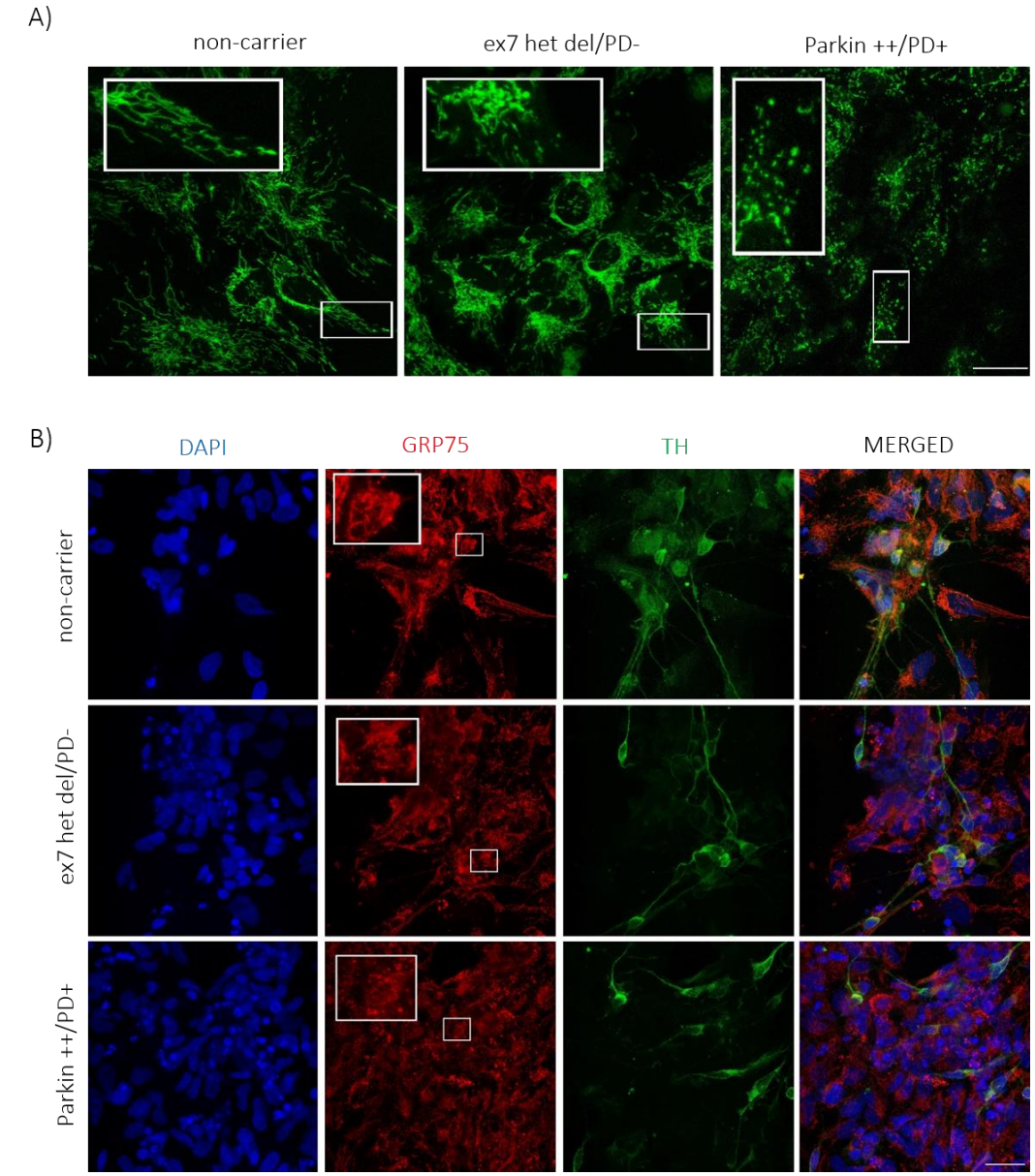
A)
non-carrier
ex7 het del/PD-
Parkin ++/PD+
B)
DAPI
GRP75
TH
MERGED
non-carrier
ex7 het del/PD-
Parkin ++/PD+
C)
Length/unconnected parts (a.u.)
1.5
1.0
0.5
0.0
*
ns
ns
non-carriers
ex7 het del/PD-
Parkin++/PD+
Length/unconnected parts (a.u.)
1.5
1.0
0.5
0.0
ns
non-carriers
ex7 het del/PD-
D)
Length/unconnected parts (a.u.)
5
4
3
2
1
0
ns
ns
ns
non-carriers
ex7 het del/PD-
Parkin++/PD+
Length/unconnected parts (a.u.)
5
4
3
2
1
0
ns
non-carriers
ex7 het del/PD-

Figure 24. Assessment of mitochondrial network morphology in iPSC-derived neurons. *Confocal live imaging of iPSC-derived neurons at day 50 of differentiation, stained with MitoTracker Green (A) and with anti-GRP75 and anti-TH antibodies (B). Scale bar: 25 µm. (C) Mitochondrial fragmentation measurements in iPSC-derived neurons; left: one PD patient line (iPSC-B125, Parkin++/PD+), two heterozygous carriers (ex7 het del/PD-) and the control group (three control lines including iPSC-SFC084-03-02 and the two non-carriers generated in this study); right: direct comparison between the two non-carriers (iPS-BC, iPS-DI) and the two carriers (iPS-AD, iPS-BD) generated in this study. n = 4 independent experiments; it was set to 1 in the control groups. (D) Mitochondrial fragmentation measurements in iPSC-derived DA neurons (TH^+), stained with anti-GRP75 antibody; left: one PD patient line (iPSC-B125, Parkin++/PD+), two heterozygous carriers (ex7 het del/PD-) and the control group (three control lines including iPSC-SFC084-03-02 and the two non-carriers generated in this study); right: direct comparison between the two non-carriers (iPS-BC, iPS-DI) and the two carriers (iPS-AD, iPS-BD) generated in this study. n = 2 independent experiments, fragmentation was assessed in at least 15 TH^+ neurons per experiment. Mitochondrial fragmentation was calculated with the filament function in Imaris Software: for each field, the total length of the modelled mitochondrial network was calculated and divided by the number of unconnected parts. Error bars represent the mean ± SEM. p values were determined using one-way ANOVA followed by Tukey's post hoc test to correct for multiple comparisons and a two-sided t-test, when only two groups were compared. Significance levels are presented as comparisons with the control group: * p≤0.05. a.u.: arbitrary units. ns = not significant.*

4.4.6 Evaluation of steady state levels of mitofusin 2 and TOM70 in iPSC-derived neurons

Stress-induced mitophagy is triggered by parkin translocation to dysfunctional mitochondria with low membrane potential (Narendra et al., 2008; Vives-Bauza et al., 2010). Following the mitochondrial translocation of parkin, ubiquitination of the mitochondrial fusion proteins is induced, followed by their degradation via the ubiquitin proteasome system (Gegg et al., 2010; Rakovic et al., 2011; Tanaka et al., 2010; Ziviani et al., 2010). Parkin ubiquitinates the OMM fusion protein MFN2 (mitofusin 2) to control its steady-state levels (Gegg et al., 2010; Rakovic et al., 2011; Tanaka et al., 2010; Ziviani et al., 2010), which were shown to be elevated in *Parkin* and *PINK1* knockout models (Ziviani et al., 2010). Furthermore, parkin activates the ubiquitin proteasome system for widespread degradation of outer mitochondrial membrane proteins (OMM), such as Tom20, Tom40, and Tom70 (Chan et al., 2011; Yoshii et al., 2011). Before it was shown that OMM rupture leads to the exposure of Prohibitin 2, which functions as a receptor for LC3 to form mitophagic vesicles (Y. Wei et al., 2017), it was not clear how OMM degradation and rupture could facilitate the initiation of mitophagy.

To further expand the knowledge concerning the possible consequences of carrying a heterozygous mutation in *Parkin*, the steady state levels of MFN2 (mitofusin 2) were evaluated in the iPSC-derived neurons of the *Parkin* mutation carriers. To this end, mitochondrial depolarization was induced in iPSC-derived neurons by treatment with the protonophore CCCP. Next, by Western blot analysis, the endogenous levels of MFN2 were determined in the neurons of the *Parkin* exon 7 heterozygous deletion carriers, PD patient, and the control group, under

(1) basal conditions and *(2)* after exposure to CCCP. The treatment with CCCP resulted in a drop of the protein levels of MFN2 in the control group and in the carrier group, but not in the neurons of the PD patient. Moreover, it was possible to observe a larger band above the non-modified MFN2 in the controls and heterozygous mutation carriers, possibly corresponding to the monoubiquitinated form of MFN2 (Figure 25A). For this experiment, MFN2 levels were quantified by calculating the ratio between MFN2 levels upon CCCP treatment and in basal conditions (MFN2 CCCP:MFN2 non treated). MFN2 levels in iPSC-derived neurons of the heterozygous deletion carriers revealed to be significantly increased (p= 0.007), as well as in the *Parkin* PD line (p= 0.0001), compared to the iPSC-derived neurons of the control group. When comparing the carriers group and the *Parkin* PD line, the latter revealed higher levels (p= 0.029). The same trend was observed when comparing only the two non-carrier lines with the two-carrier lines generated in this study, although without statistical significance (p=0.074) (Figure 25A). These results indicate that carrying a mutation in *Parkin* leads to elevated MFN2 levels under stress conditions, thus possibly suggesting reduced ubiquitination, which might negatively impact mitophagy initiation.

In this experiment, also the mitochondrial import receptor subunit TOM70, which is an abundant protein of the OMM, was investigated and showed comparable effects (Figure 25B). Densitometric analysis revealed a trend towards increased levels for the carriers´ group (p= 0.115), and a significant increase for the PD patient neurons (p= 0.002), compared with the iPSC-derived neurons of the control group. Likewise, when comparing TOM70 levels in iPSC-derived neurons of the carriers group with the levels in iPSC-derived neurons of the PD line, a significant difference (p= 0.031) was observed. When comparing only the two non-carrier lines with the two-carrier lines, the same trend was observed (Figure 25B). Even if the difference of MFN2 and TOM70 levels between carriers and non-carries is not statistically significant, these results correspond to the altered mitochondrial function observed in the carrier group.

Although not suitable for conclusively indicating mitophagy induction, these data might give a hint for pointing in the same direction as the mitophagy impairments detected in previous studies performed in iPSC-derived neurons of individuals carrying mutations in *Parkin* (Kumar et al., 2020; Rakovic et al., 2011; Suzuki et al., 2017). Notably, a recently published study reported a significant reduction in the mitophagy index for iPSC-derived neurons of *Parkin* mutants compared to controls (Kumar 2020).

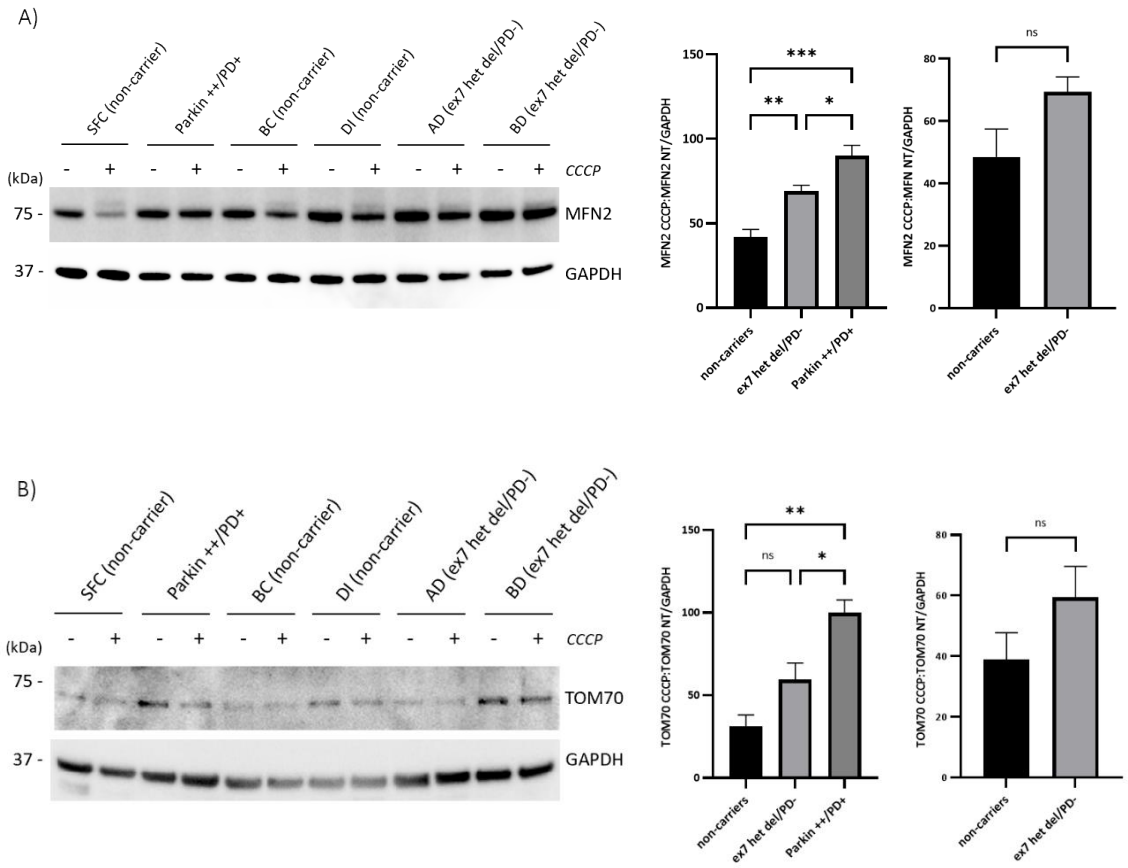

Figure 25. Evaluation of MFN2 and TOM70 steady state levels in whole-cell lysates of iPSC-derived DA neurons. *(A) Western blot and densitometric analysis, showing MFN2 protein levels in the generated iPSC-derived neurons under basal conditions (-) and treated with 20 μM CCCP (+) for 15 hours. Densitometric analysis: (left) one PD patient (iPS-B125, Parkin++/PD+), two heterozygous carriers (ex7 het del/PD-) and the control group (three control lines including iPSC-SFC084-03-02 and the two non-carriers generated in this study); (right) direct comparison between the two non-carriers (iPS-BC, iPS-DI) and the two carriers (iPS-AD, iPS-BD) generated in this study. MFN2 levels were analyzed with the indicated anti-MFN2 antibody and GAPDH was used as loading control. Molecular mass markers are in kilodaltons (kDa). Steady state levels were calculated as the ratio of MFN2 upon CCCP treatment over the levels of MFN2 under basal conditions (non-treated). n = 4 independent experiments. (B) Western blot and densitometric analysis, showing TOM70 protein levels in the generated iPSC-derived neurons under basal conditions (-) and treated with 20 μM CCCP (+) for 15 hours. Densitometric analysis: (left) one PD patient (iPSC-B125, Parkin++/PD+), two heterozygous carriers (ex7 het del/PD-) and the control group (three control lines including iPSC-SFC084-03-02 and the two non-carriers generated in this study); (right) direct comparison between the two non-carriers (iPS-BC, iPS-DI) and the two carriers (iPS-AD, iPS-BD) generated in this study. TOM70 levels were analyzed with the indicated anti-TOM70 antibody, and GAPDH was used as loading control. Molecular mass markers are in kilodaltons (kDa). Steady state levels were calculated as the ratio of TOM70 levels upon CCCP treatment over the levels of TOM70 under basal conditions (non-treated). n = 3 independent experiments. Error bar represents the mean ± SEM. Significance levels were determined using one-way ANOVA and Tukey's post hoc test to correct for multiple comparisons, as well as a two-sided t-test, when comparing only two groups. Significance levels are presented as comparisons with the control group: * p≤0.05, ** p≤0.01, *** p≤0.001. ns = not significant.*

4.4.7 Assessment of oxygen consumption rate in iPSC-derived neurons

The mitochondrial characterization performed so far in the iPSC-derived neurons of the *Parkin* exon 7 heterozygous deletion carriers has revealed abnormalities both in function and morphology. Several studies indicate that parkin is involved in the mitochondrial oxidative phosphorylation (OXPHOS) activity (Kumar et al., 2020; Zanon et al., 2017), and the bioenergetic profiling performed in this study in LCLs of individuals carrying a heterozygous deletion in *Parkin* has shown an affected respiratory phenotype. To ascertain whether the absence of parkin translates into functional consequences at the respiratory level, I measured oxygen consumption rate (OCR), which is an important indicator of OXPHOS activity and mitochondrial function. This was carried out in iPSC-derived neurons of the exon 7 heterozygous deletion carriers generated in this study, control lines and a *Parkin* PD line (Figure 26A, B). The respiration of iPSC-derived neurons was measured under basal conditions as well as upon treatment with the protonophore FCCP, leading to mitochondrial uncoupling. I conducted microplate respirometry assessment with a real-time kinetic assay for extracellular oxygen consumption rates, as described in section 3.2.18. Here, I observed a trend for a reduction in basal OCR for the neurons of individuals carrying a heterozygous deletion in *Parkin* compared with the control group, although not statistically significant (p=0.194). Nevertheless, the *Parkin* PD line showed a significant decrease of basal OCR levels (p=0.037) (Figure 26C). In addition, when challenging the neurons with FCCP to induce maximal respiration, both heterozygous deletion carriers and the PD patient iPSC-derived neurons, revealed a significant decrease of oxygen consumption (p=0.015, p=0.002 respectively), compared with the control group (Figure 26D). Consistent with these results, spare respiratory capacity, which is determined as the difference between maximal and routine respiration, was significantly reduced for the individuals with the heterozygous deletion in *Parkin* (p=0.041), as well as for the *Parkin* PD line (p=0.005) (Figure 26E). These alterations at the mitochondrial respiration level are in line with previously published studies conducted in peripheral tissues from patients with *Parkin* mutations (Gonzalez-Casacuberta et al., 2019), in *Parkin*-deficient animal models (Palacino et al., 2004; Stevens et al., 2015) and specifically in iPSCs-derived neurons from PD patients with *Parkin* mutations (Kumar et al., 2020).

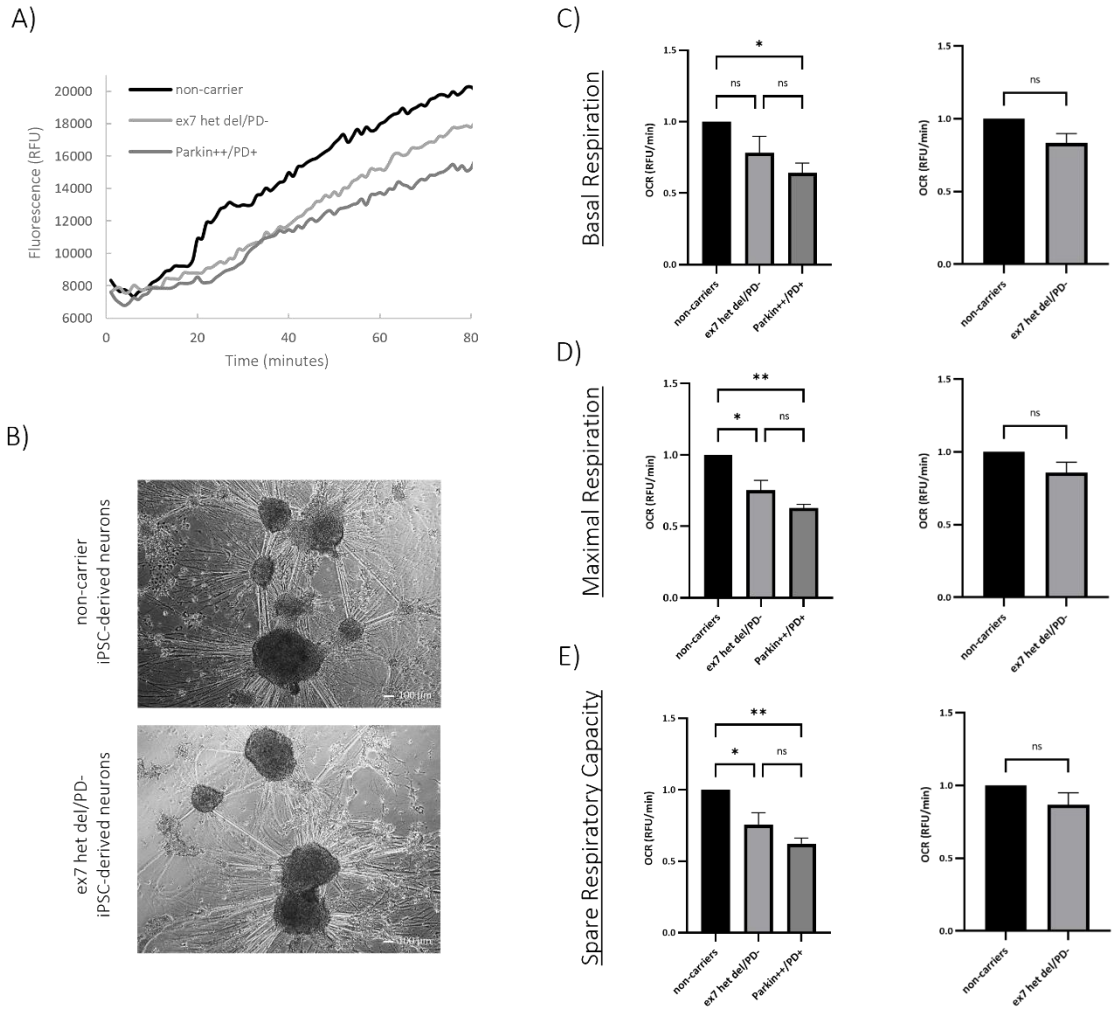

Figure 26. Oxygen consumption rates in iPSC-derived neurons*. (A) Representative maximal respiration curves of the fluorescence signal, generated by the oxygen probe after addition of 2.5 µM FCCP. Curves reflect dissolved oxygen in the culture medium of iPSC-derived neurons of a heterozygous Parkin exon 7 deletion carrier, a non-carrier, and a Parkin PD patient with homozygous mutation. (B) Representative images visualized by phase contrast inverted microscope of iPSC-derived neurons generated in this study and used for OCR assessment at day 34 of differentiation. Scale bar: 100 µm. (C, D, E) Relative quantification of respirometry parameters in iPSC-derived neurons; left: one PD patient (iPSC-2011, Parkin++/PD+), two heterozygous carriers (ex7 het del/PD-) and the control group (three control lines including iPSC-SFC084-03-02 and the two non-carriers generated in this study); right: direct comparison between the two non-carriers (iPS-BC, iPS-DI, and the two carriers (iPS-AD, iPS-BD) generated in this study. Basal respiration (C), maximal respiration measured after addition of 2.5 µM FCCP (D), and spare respiratory capacity (Maximal respiration – Basal respiration) (E). OCR was determined with the slope calculated on the linear portion of the signal profile of each well and normalized to the number of cells measured with the fluorescence of CyQuant direct nucleic acid stain; measurements were set to 1 in the control group of each experiment. n = 3 independent experiments. Error bars represent the mean ± SEM. p values were determined using one-way ANOVA followed by Tukey's post hoc test to correct for multiple comparisons and a two-sided t-test, when only two groups were compared. Significance levels are presented as comparisons with the control groups: *p≤0.05, **p<0.01, ns = not significant. RFU: relative fluorescence units.*

5. Discussion

The results generated in this thesis are discussed in the present chapter in the following order: identification of heterozygous *Parkin* variants in the CHRIS cohort and characterization of PD risk markers (section 5.1), evaluation of mtDNA integrity (section 5.2), and assessment of mitochondrial function in two cellular models of heterozygous *Parkin* mutation carriers (section 5.3).

5.1 Frequency of heterozygous *Parkin* variants and penetrance of Parkinson's disease risk markers in the population-based CHRIS cohort

Homozygous or compound-heterozygous mutations in the *Parkin* gene result in highly penetrant symptom expression, while several reports suggest that heterozygous mutations may also predispose to disease symptoms, albeit with highly reduced penetrance (Huttenlocher et al., 2015; Weissbach et al., 2017), similar to the pattern established for mutations in *GBA* (Avenali et al., 2020; Klein & Krainc, 2013). Previous studies have estimated the frequency of rare, heterozygous *Parkin* mutations in healthy control individuals in some populations up to 3.2%, with the frequency here in South Tyrolean being slightly higher, at around 3.9%, including two studies that identified no mutation in healthy control individuals (Bruggemann et al., 2009). In the population-based CHRIS study conducted in Val Venosta (South Tyrol, Italy), 3,603 individuals, free of overt clinical symptoms related to movement disorders, were screened by exome sequencing and CNV analysis, and I have identified heterozygous *Parkin* mutations to be carried in 4.55% of the study participants (n=164 individuals). Given the low residential mobility across generations in this restricted area of the Alps, rare variants might be overrepresented (Pattaro et al., 2007) as can be seen also from the comparison with gnomAD allele frequencies (Table 10). Given the structure of the population participating in CHRIS, a founder effect can be assumed for some of the *Parkin* mutations identified in this region. This might explain the higher frequency compared to previous studies. However, the CNV carrier frequency of 0.86% detected in this study is in keeping with previously published reports (Huttenlocher et al., 2015; Kay et al., 2010).

About 8% of all PD patients screened for *Parkin* mutations have been shown to carry a single heterozygous mutation (Klein et al., 2007). These observations raised the hypothesis that the relatively common heterozygous mutations in this 'recessive' PD gene may predispose to PD in

a dominant manner with highly reduced penetrance. Further supporting this notion, more recent studies have found an increased risk for PD in heterozygous *Parkin* CNV carriers as compared to non-carriers (OR= 2.11, $P = 2.54 \times 10^{-6}$) (Huttenlocher et al., 2015), with a large meta-analysis of case-control cohorts confirming an increased risk (OR= 1.65, $P = 3.69 \times 10^{-7}$), although possible confounding effects, such as cryptic biallelic mutation status, were highlighted (Lubbe et al., 2021). Phenotype expressivity in heterozygous mutation carriers is also extremely variable and includes overt symptoms of PD as well as subtle motor signs not allowing for a definitive clinical diagnosis of PD (Weissbach et al., 2017). Preclinical changes identified by neuroimaging studies and a reduced fluorodopa uptake in the striatum previously observed in asymptomatic heterozygous *Parkin* mutation carriers also support an increased risk of developing PD symptoms in heterozygous *Parkin* mutation carriers (Hilker et al., 2001); (Khan et al., 2005).

The presence of heterozygous *Parkin* mutations is one of the reported potential genetic risk factors for PD (Huttenlocher et al., 2015; Klein et al., 2007; Lubbe et al., 2021). Given the frequency (up to 4.5%) of heterozygous mutations in the population, it is essential to have better estimates of the penetrance of these variants and to investigate, which risk markers are manifesting in carriers and are thus potentially useful for identifying those individuals at greater risk of manifesting clinical symptoms later in life, or indeed of converting to disease positive. Using the identified carriers of Parkin mutations in CHRIS vs non-carriers, I screened for possible enrichment in validated PD risk markers of the *Movement Disorder Society (MDS)* (Heinzel et al., 2019). Diabetes has recently been defined as a novel PD risk marker as part of *The MDS Research Criteria for Prodromal PD* with a positive and negative likelihood ratio of 1.5 and 0.97, respectively (Heinzel et al., 2019). Notably, this PD risk marker was also associated with heterozygous *Parkin* mutation carrier status in my study (Table 11). Furthermore, a previous study has found a higher heart rate in PD subjects (Iwaki et al., 2020), while I observed a tendency for a lower heart rate in the heterozygous *Parkin* mutation carriers of the CHRIS study (Table 11). Therefore, diabetes status and potentially heart rate might be useful biomarkers to identify heterozygous *Parkin* variant carriers at greater risk of health issues due to carrier status.

5.2 mtDNA integrity assessment

Parkin has been shown to play an important role in mtDNA maintenance through different fronts, including regulation of PGC1α-mediated transcription of TFAM and TFB2M, two mtDNA transcription factors, or direct interaction with TFAM at the mtDNA D-Loop, enhancing

transcription and replication (Kuroda et al., 2006; Shin et al., 2011). In this study, I sought to investigate the possible impact of carrying a heterozygous *Parkin* mutation on the maintenance of mtDNA integrity. When assessing the abundance of somatic major arc deletions, by detecting the cellular concentration of MT-ND4 (situated in the common major arc deletion) and MT-ND1 (situated in the minor arc) and calculating the ratio (MT-ND4:MT-ND1), in DNA samples extracted from blood, I observed comparable values between the group of individuals carrying a heterozygous mutation in *Parkin* and the non-carrier group.

Conversely, the quantification of 7S DNA, a small DNA fragment binding in the D-loop during initiation of mtDNA transcription, which is therefore indicative of mtDNA molecules undergoing transcription, resulted in decreased levels in the carrier group. Interestingly, Wasner and colleagues quantified 7S DNA in iPSC-derived neuronal progenitors from *Parkin* mutant PD patients and observed significantly reduced levels (Wasner et al., 2020), confirming the result on the heterozygous *Parkin* mutation carriers of this study. The lower transcriptional activity could be explained as a consequence of reduced parkin function resulting from a heterozygous mutation. In 2006, Kuroda and colleagues found that parkin is associated with TFAM using co-immunoprecipitation in COS-1 cells (Kuroda et al., 2006). Mobility shift assays showed a shift in mtDNA in the presence of TFAM, possibly indicating that parkin associates with mtDNA indirectly via TFAM. A later study used genome-wide chromatin immunoprecipitation experiments in SH-SY5Y cells to show parkin's interaction with several mitochondrial genomic sequences including ATPase6, COXII, ND1, ND2 and D-LOOP (Kuroda et al., 2006; Rothfuss et al., 2009). These findings were however not further reproduced by additional studies using different models. In line with the results on mtDNA transcription, parkin was also shown to increase transcription of mitochondrial genes in cell lines stably overexpressing parkin (Kuroda et al., 2006; Rothfuss et al., 2009). Furthermore, a reduced function of the ubiquitin ligase parkin leads to the accumulation of Parkin Interacting Substrate (PARIS), which represses PGC1α expression and results in a decrease of the target genes nuclear respiratory factor 1 and 2 (NRF-1 and NRF-2) (Shin et al., 2011). NRF-1 and NRF-2 regulate the transcription of TFAM and TFB2M, which are required for the initiation of transcription and replication of the mtDNA (Gleyzer et al., 2005). Thus, my results confirm that mtDNA transcription (measured through 7S DNA) is a molecular biomarker capable of reflecting changes due to *Parkin* mutation status.

When assessing levels of mtDNA through copy number in blood-derived DNA of unaffected carriers of heterozygous *Parkin* mutations, I found it to be significantly increased compared to

the non-carriers group. These results suggest an accumulation of mtDNA molecules in the individuals carrying a heterozygous mutation in *Parkin*, which could result from an impairment in the mitochondrial clearance process or a compensatory increase in mitochondrial biogenesis. These findings go in line with a recent study by Delcambre et. al., 2020, where increased mtDNA copy number was observed in fibroblasts of PD patients with *LRRK2* mutations, which might be attributed to a faulty mitophagy system (Delcambre et al., 2020). This indicates that mtDNA copy number is also a suitable molecular biomarker capable of reflecting cellular consequences of carrying a single *Parkin* mutation.

Next, I investigated the number of heteroplasmic variants in the mtDNA of individuals carrying a heterozygous *Parkin* mutation. mtDNA mutations have been previously linked to the pathogenesis of PD, in fact, patients with sporadic PD have shown an increased number of functionally deleterious mtDNA mutations in neurons from the SN (Bender et al., 2006). Moreover, Suen et al., have previously demonstrated that overexpression of parkin reduces the level of heteroplasmic mutations by removing defective mitochondria carrying deleterious mutations (Suen et al., 2010). In this study, the carrier group presented a significantly reduced heteroplasmic variant count. This could suggest that the function of the non-mutated allele is still able to negatively select dysfunctional mitochondria in a highly proliferative tissue such as blood.

Overall, given the higher mtDNA copy number and lower 7S DNA, these data might suggest a more efficient replication and transcription in the *Parkin* mutation carriers, although the 7S DNA might be present in the mitochondrial replication cycle for less time. Taken together, reduced mtDNA transcriptional activity, reduced heteroplasmic variant count in blood, and increased mtDNA copy number may be different biomolecular signatures of impaired mitochondrial function in carriers of heterozygous *Parkin* mutations.

5.3 Mitochondrial functional characterization in cellular models of heterozygous *Parkin* deletion carriers

Mitochondria perform a wide range of critical functions in the cell. Growing evidence supports the involvement of mitochondrial dysfunction in the pathogenesis of PD. Moreover, mutations in the PD-causing gene *Parkin* have shown a compelling link to dysfunction of this multifaceted organelle, highlighting Parkin's crucial role in the maintenance of mitochondrial health.

Therefore, loss of parkin function, has been hypothesized to cause cellular degeneration via an aberrant accumulation of its substrates. Although PD is principally a neurodegenerative disorder, increasing awareness has been raised towards the peripheral mechanisms of the pathology. Growing evidence supports the fact that the pathology of PD is not strictly confined to the central nervous system but it is also detectable in the peripheral nervous system (Djaldetti et al., 2009). Of relevance, several studies show clear functional impairments in blood cells in the pathology of PD (Scherzer et al., 2007; Smith et al., 2018; Vida et al., 2019). Investigating disease processes in neurodegenerative disorders like PD, where the brain tissue is inaccessible, poses some limitations. Nevertheless, this has been partially tackled by using various cell models suitable to mirror the disease. In this study, assessments were performed in blood, in PBMC-derived LCLs, and in DA neurons, differentiated from iPSCs, which were reprogrammed from PBMCs (Figure 27).

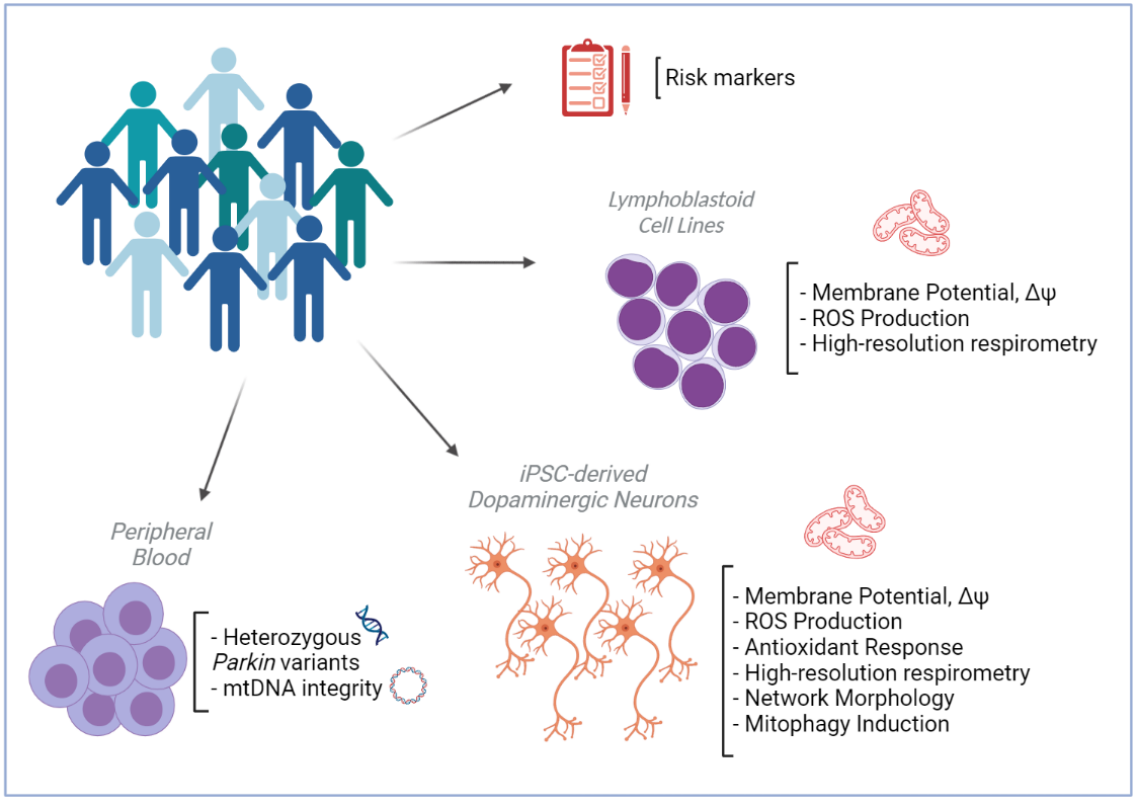

Figure 27. Cellular models derived from the participants enrolled in the CHRIS study *and the respective clinical and molecular assessments performed in the present study. This figure was designed by using BioRender Software (BioRender.com).*

5.3.1 Mitochondrial function assessment in LCLs of heterozygous exon 7 deletion carriers

Several studies have demonstrated the usefulness of peripheral tissues to investigate mitochondrial function and morphology in PD, reporting distinct abnormalities in mitochondria of fibroblasts (Carling et al., 2020; Grunewald et al., 2010; Milanese et al., 2019; Mortiboys et al., 2010; Mortiboys et al., 2008) as well as in leukocytes of genetic and idiopathic PD patients (Barroso et al., 1993; Michalak et al., 2017; Muftuoglu et al., 2004; Yoshino et al., 1992). Notably, one study has examined mitochondrial function in lymphoblastoid cells of idiopathic PD patients and age-matched controls and has found alterations in the patient cells (Annesley et al., 2016). Based on these data on peripheral tissues, I have generated a blood-derived cellular model aiming to reveal the potential molecular phenotype present in individuals without overt clinical symptoms, carrying a heterozygous mutation in *Parkin.* Epstein-Barr virus (EBV)-transformed lymphoblastoid cell lines (LCLs), derived from peripheral blood lymphocytes were developed as cellular model, enabling us to put together a functional mitochondrial profile in these individuals. Besides posing a viable alternative to solve the limited accessibility of primary cells, like skin fibroblasts, for research, LCLs have proven to be a suitable model to study mitochondrial function since they emulate metabolically active lymphoid cells, which might represent, in an accurate manner, activated lymphocytes *in vivo* (Ransohoff et al., 2015). Therefore, this model has been successfully used for several functional studies to unravel molecular mechanisms in complex diseases including autism, Alzheimer's disease, PD, Primary Open-Angle Glaucoma, among others (Abe et al., 1991; Annesley et al., 2016; Baron et al., 2006; Kobayashi et al., 2003; Lee et al., 2012; Ming et al., 2020). Importantly, in this study, none of the LCL cultures reached 10 passages before storage or use in experiments, in order to maintain genomic stability, which has been shown to be high at these low passage numbers (Hussain & Mulherkar, 2012).

In several studies, the presence of marked abnormalities in mitochondrial function has already been reported in peripheral tissues of *Parkin* mutant PD patients. Research performed in human fibroblasts has revealed traits including decreased complex I activity, lower ATP production, high levels of oxidized proteins, reduced membrane potential and higher mitochondrial network branching (Grunewald et al., 2010; Mortiboys et al., 2008; Zilocchi et al., 2020). In order to understand if there is a causal link between the presence of a heterozygous mutation in *Parkin,* and the appearance of a molecular phenotype in the LCLs of my study participants carrying a heterozygous exon 7 deletion, I investigated these cells for mitochondrial dysfunction, assessing

respirometry activity, reactive oxygen species production, and membrane potential. Previous studies conducted in peripheral tissues of monogenic and idiopathic PD patients have reported alterations at the bioenergetic level (Ambrosi et al., 2014; Muftuoglu et al., 2004; Piccoli et al., 2008), which were observed also in *Parkin*-deficient mice (Damiano et al., 2014). Interestingly, two studies performed in *Parkin* mutant skin fibroblasts from PD patients have reported a markedly higher mitochondrial respiratory rate compared to the controls (Gonzalez-Casacuberta et al., 2019; Haylett et al., 2016). In line with these data, my bioenergetic characterization by means of high-resolution respirometry demonstrated a significantly increased oxygen consumption at the routine respiratory state in the LCLs of the heterozygous exon 7 deletion carriers, compared to the non-carrier group, thus suggesting an altered mitochondrial function. Of note, my results are consistent with the results reported by Annesley et al., which observed a dramatically elevated basal mitochondrial respiration in idiopathic PD lymphoblasts, as an indication of a "hyperactive" state (Annesley et al., 2016). In the same study, the hyperactive state was observed independently of patient age, ongoing disease and disease severity, suggesting an early and stable switch to the "hyperactive" state. Additionally, in a recent study by Mor and colleagues, mitochondrial activity assessed in *Caenorhabditis elegans bcat-1*, an animal model known to recapitulate PD-like features, was characterized by a significantly increased respiration rate (Mor et al., 2020). My findings indicating an upregulation of basal cellular respiration in LCLs of heterozygous *Parkin* mutation carriers are suggestive of a cellular compensatory mechanism to overcome the changes occurring upon heterozygous *Parkin* mutation and go in line with the increased mtDNA copy number observed in the carrier group (section 5.2). In both cases, compensatory mechanisms might be activated aiming to preserve mitochondrial function. Furthermore, these results may suggest mitochondrial hyperactivity in peripheral tissues as a novel feature of mitochondrial dysfunction in PD.

To further assess mitochondrial function in the subpopulation of carriers, mitochondrial reactive oxygen species (mROS) production as well as mitochondrial membrane potential (MMP) were assessed in LCLs. As expected, considering the enhanced mitochondrial respiratory activity observed in the carrier group, these individuals presented an increased production of mROS compared to the control group. Even though the differences between groups are not statistically significant, I observed a strong upward trend, which is consistent with the hyperactive bioenergetic state, supporting the theory that an elevated mROS production may result from

increased electron transport rates. Likewise, Annesley et. al., reported an elevated ROS production coupled with the elevated mitochondrial respiration observed in their idiopathic PD lymphoblasts (Annesley et al., 2016). Notably, in a recent study by Ming et al., conducted in LCLs of *Parkin* mutation carriers, an oxidative stress phenotype was not reported under basal conditions, but vulnerability was detected when oxidative stress was induced by toxins (Ming et al., 2020). This suggests that a mutation in *Parkin* may confer vulnerability to the system, when subjected to environmental insults. A number of studies have proposed the upregulation of endogenous pathways of antioxidant defense or antioxidant supplements to counteract the impact of PD genetic predisposition (Grunewald et al., 2019). This could be an approach to consider in a condition where the lack of parkin is only partial and vulnerability appears mostly upon challenge with added factors.

Mitochondrial membrane potential in my heterozygous *Parkin* mutation carriers showed a trend towards a depolarized state but with no statistical significance. In the above mentioned studies, where mitochondrial oxygen consumption was decreased, also membrane potential was impaired (Ambrosi et al., 2014; Muftuoglu et al., 2004; Piccoli et al., 2008). On the contrary, an enhanced oxygen consumption phenotype has been shown to go in hand with no significant differences in mitochondrial membrane potential (Annesley et al., 2016; Gonzalez-Casacuberta et al., 2019; Haylett et al., 2016). An exception to this is the study by Zanellati and colleagues, who report a significant increment of oxygen consumption in the basal respiratory state in *Parkin* mutant fibroblasts of PD patients, coupled with a significant reduction of cellular ATP levels and altered membrane potential (Zanellati et al., 2015). In my study, when determining ATP turnover, the group of individuals carrying a heterozygous deletion in *Parkin* demonstrated values comparable with the control group, with a slight trend towards increase, thus suggesting no impairment in ATP levels nor in membrane potential.

Taken together, my data provide evidence for an altered mitochondrial function in a peripheral tissue model of unaffected individuals carrying a heterozygous exon 7 deletion in *Parkin.* Particularly, hyperactive mitochondrial respiration in the routine state, coupled with an increased ROS production, has the potential to cause higher damage rates in the system. This may suggest that mitochondria partially lacking parkin, a protein deeply involved in mitochondria homeostasis, reside in a potentially damaging state, which is regulated to the point of not turning into disease. Nevertheless, additional factors that challenge the system,

such as age or environmental toxins, could destabilize this compensatory system. Interestingly, it has been proposed that a possible reason for the reported enhanced mitochondrial respiration in peripheral cells of PD models could be their proliferative status and increased turnover. It was hypothesized that in early PD an elevated respiration as well as ROS production is present both in peripheral tissue and in the brain, accumulating deleterious effects in the post-mitotic cells of the brain, thus resulting in disease. In peripheral tissue, especially blood, cells might not accumulate long-term damage due to their highly proliferative nature and turnover but retain their hyperactive respiratory state (Annesley & Fisher, 2021). In the case of my heterozygous mutation carriers, this hyperactive respiration in peripheral tissues could remain as a sort of "silent" trait, without ever manifesting in clinical symptoms, unless and until additional factors exert an additive negative influence.

5.3.2 Mitochondrial function assessment in iPSC-derived neurons of heterozygous *Parkin* exon 7 deletion carriers

Mitochondrial function in the pathology of PD has been widely investigated in non-neuronal systems. Moreover, a number of animal models have been developed to study PD but most of these fail to recapitulate accurately the human disease (Dawson et al., 2010). Over the past decade, reprogramming and iPSC-technology have been substantially developed, allowing the evolution of patient-derived brain tissue engineering (Parr et al., 2017). The possibility of culturing and reprogramming patient-derived cells and differentiating them to patient-specific neurons *in vitro* has offered the opportunity to model PD cellular mechanisms in disease-relevant midbrain dopaminergic neurons, which are preferentially lost in PD. Several advantages characterize the iPSCs as model system to study PD, including its unlimited replicative potential and the presence of the genetic background of the donor, among others. Nonetheless, the field of iPSC-technology is relatively young, and protocols are constantly under modification for further improvements (Mertens et al., 2016). During the last years, several studies conducted on iPSC lines derived from PD patients have confirmed phenotypes associated with the pathology, but also revealed new ones, thus providing a considerable amount of valuable information. Importantly, approximately 80% of the iPSC-data generated has been used to model familial forms of PD, including mutations in *Parkin* (Tran et al., 2020).

In this study, I hypothesized that the altered molecular phenotype observed in the LCLs of the individuals carrying an exon 7 deletion in *Parkin* would appear more pronounced in neuronal

cells, modeling changes in PD-affected brain regions. To this end, a subset of 4 individuals (2 carriers and 2 non-carriers) was selected and iPSCs were successfully generated by reprogramming PBMCs extracted from these individuals. These newly generated lines were further differentiated to obtain iPSC-derived DA neurons and used for the functional characterization of their mitochondria. I investigated the presence of mitochondrial abnormalities in the iPSC-derived neurons of the two exon 7 heterozygous deletion carriers, as well as in the control group and in *Parkin* mutant PD patient lines by assessing the same features previously evaluated in the LCLs. Additionally, I looked for mitochondrial abnormalities that have been previously described in studies of iPSC-derived DA neurons of PD patients.

Several studies conducted on iPSC-derived neurons from PD patients have consistently reported mitochondrial dysfunction, including abnormalities in the organelle´s structure and function. In particular, since the development of iPSC technology, over 15 independent studies have generated iPSC-derived DA neurons from PD patients with mutations in the *Parkin* gene, most of them agreeing about the impact of *Parkin* mutations in mitochondrial dysfunction and PD development. The data generated in this thesis show that the iPSC-derived neurons of the heterozygous *Parkin* exon 7 deletion carriers present an overall decreased oxygen consumption rate when compared with the control group, which presented a statistically significant difference, when cells were forced to perform at maximal capacity. Moreover, the spare respiratory capacity is also significantly reduced for these individuals, suggesting a reduced capacity for mitochondrial respiration. This decreased capacity might result in a lack of energy in neurons, which present a substantial bioenergetic demand, especially true for dopaminergic neurons. This observed phenotype in the carrier group goes in parallel with the impaired oxygen consumption rate observed in the iPSC-derived neurons of the *Parkin* PD line, where the significance level appears even stronger. The impact of *Parkin* mutations on the respiration of iPSC-derived neurons has been assessed in previous studies, reporting deficits in mitochondrial respiration and complex I activity (Kumar et al., 2020; Zanon et al., 2017). Interestingly, a recent study employing mass spectrometry-based proteomics identified a strong dysregulation of mitochondrial proteins in iPSC-derived neurons lacking *Parkin*, from which several are important for energy metabolism, and the proteins involved in mitochondrial respiration were particularly decreased. Moreover, when assessing oxygen consumption rate in these neurons, a deficit in basal respiration and ATP production when providing lactate as energy source was confirmed

(Bogetofte et al., 2019). Furthermore, deficits in mitochondrial respiration have also been reported in ventral midbrain neurons of *Parkin*-mutant mice (Stevens et al., 2015). My results suggest a respiratory impairment in the neurons of the *Parkin* exon 7 heterozygous deletion carriers, which becomes considerable when stressors are provided, possibly again indicating that a diseased phenotype may become visible when additional factors are added to the genetic mutation.

Mitochondria in neurons are forced to meet an immense energetic demand, for which these organelles are required to maintain an intact membrane potential. Assessment of MMP in my cell lines revealed depolarized mitochondria both in the iPSC-derived neurons of the heterozygous *Parkin* exon 7 deletion carriers and the PD patient with a homozygous mutation in *Parkin*, when comparing to the iPSC-derived neurons of the control group. Consistent with this, Kumar et. al., observed a significant reduction in membrane potential in *Parkin* knockout iPSC-derived DA neurons (Kumar et al., 2020). Indeed, a decline in MMP has been reported in PD patient-derived fibroblasts with *Parkin* deficiency (Mortiboys et al., 2008), as well as in animal models of *Parkin* mutant *Drosophila*, where depolarized mitochondria seem to accumulate in DA neurons (Burman et al., 2012).

The presence of increased oxidative stress has been previously observed in several PD models (Jiang et al., 2012; Palacino et al., 2004), as well as in the LCLs of my study. I examined mitochondrial-derived oxidants in the iPSC-derived neurons of the heterozygous *Parkin* exon 7 deletion carriers as a readout of mitochondrial stress. iPSC-derived neurons obtained from the carriers, as well as from a patient carrying a homozygous *Parkin* mutation exhibited increased levels of oxidative stress when compared to the control group. Notably, the presence of the oxidative stress phenotype was also significant when comparing only the two non-carrier lines with the two-carrier lines generated in this study. This altered mitochondrial phenotype has been reported before by other groups using *Parkin*-mutant iPSC-derived neurons (Chung et al., 2016; Imaizumi et al., 2012; Suzuki et al., 2017), indicating increased levels of oxidative stress in these cells. Interestingly, Suzuki and colleagues measured ROS accumulation exclusively in enriched DA neurons fractions, obtaining a stronger level of significance, suggesting that DA neurons are selectively impaired in the absence of *Parkin* (Suzuki et al., 2017). By assessing oxidative stress in my iPSC-derived neurons, I can corroborate the clear phenotype in the

absence of parkin, which is measurable even in the presence of a heterozygous mutation of the gene.

The increased oxidative stress levels observed in parkin deficiency might give rise to a compensatory cellular response increasing antioxidant effectors such as catalase, SOD1/2, DJ-1, among others (Chang & Chen, 2020). Considering the results of increased ROS production in the iPSC-derived neurons obtained from the heterozygous mutation carriers and from the patient carrying a homozygous *Parkin* mutation, I investigated the levels of the antioxidant enzyme superoxide dismutase 2 (SOD2), which is exclusively located in mitochondria (Karnati et al., 2013). To this end, I quantified the protein levels of SOD2 by Western blotting. My results indicated that the protein level of SOD2 was decreased in the neurons from the heterozygous exon 7 deletion carriers, as well as in the neurons from the patient carrying a homozygous *Parkin* mutation, although this decrease did not reach statistical significance. The observed trend may suggest a deficiency at the level of the defense mechanisms against oxidative stress in situations of complete or partial deficiency of parkin. This trend goes in line with the results reported by Bogetofte et al., which, by investigating the mitochondrial proteome in parkin-deficient iPSC-derived neurons, observed a clear dysregulation at the level of proteins involved in the oxidative stress defense. These data were further confirmed by the significant down-regulation of DJ-1 and SOD1 assessed by Western blotting (Bogetofte et al., 2019). Accordingly, Pacelli and colleagues have shown a decreased activity of mitochondrial SOD2 in fibroblasts of PD patients with a *Parkin* mutation, paired with increased ROS levels (Pacelli et al., 2011). Similarly, in a mouse model with *Parkin* knockout, decreased levels of proteins involved in protection against oxidative stress were observed (Palacino et al., 2004). Altogether, these results indicate that the absence of parkin may confer a negative impact on the antioxidant enzyme levels, thus potentially contributing to an altered phenotype.

So far, the functional characterization of mitochondria in the iPSC-derived neurons of the individuals carrying a heterozygous exon 7 deletion in *Parkin* has revealed an altered profile, inclined towards the phenotype observed in the PD patients carrying a homozygous mutation in *Parkin*. Parkin also plays an important role in the regulation of mitochondrial network morphology. Accordingly, a number of studies conducted in parkin-deficient model systems report impaired mitochondrial function as well as altered morphology (Abou-Sleiman et al., 2006; Haylett et al., 2016; Mortiboys et al., 2008; Pinto et al., 2018; Zanon et al., 2017). Aiming

to broaden my knowledge on the performance of this multifunctional organelle, particularly in the setting of heterozygous mutations, I performed morphological analysis of the mitochondrial network. This was done by assessing mitochondrial fragmentation (quantified as total length of the modelled mitochondrial network divided by the number of unconnected parts), in the iPSC-derived neurons of the heterozygous exon 7 deletion carriers, the *Parkin* PD line and control lines. My results revealed a trend towards an increased mitochondrial fragmentation in the neurons of the heterozygous carriers, compared to the iPSC-derived neurons from the control group. I further assessed mitochondrial network fragmentation specifically in neurons expressing tyrosine hydroxylase, where the trend was confirmed, although without statistical significance. However, I found mitochondrial network fragmentation significantly increased in the iPSC-derived neurons of the Parkin PD line compared to the control group. This phenotype of altered mitochondrial morphology observed in the *Parkin* PD line has been previously reported in studies conducted in iPSC-derived neurons lacking parkin, described as swollen mitochondria, high electron-dense matrix, network fragmentation and increased perikaryal volume density (Chung et al., 2016; Imaizumi et al., 2012; Kumar et al., 2020; Shaltouki et al., 2015; Zanon et al., 2017). Interestingly, Imaizumi and colleagues performed a detailed morphological analysis of mitochondria in iPSC-derived neurons of *Parkin* mutant patients using electron microscopy and observed abnormal morphology as a clear feature in these cells, but not in parkin-deficient fibroblasts or in undifferentiated iPSCs of the same individuals (Imaizumi et al., 2012). This may suggest a selective impairment in neuronal cultures, even though several other studies have confirmed the aberrant morphology in *Parkin*-mutant fibroblasts (Mortiboys et al., 2008; Pacelli et al., 2011; Zanellati et al., 2015). Moreover, it has been shown that overexpression of parkin or PINK1 rescues mitochondrial fragmentation (Kamp et al., 2010). My results confirm what was previously reported in the literature, and even if the difference between heterozygous mutation carriers and non-carries is not statistically significant, the trend coincides with the altered mitochondrial function observed for the carrier group.

The E3 ubiquitin ligase parkin plays an important role in ubiquitinating proteins on damaged mitochondria and promoting their elimination by mitophagy. The role of *Parkin* mutations in mitophagy was studied broadly in cells overexpressing parkin but was confirmed also in iPSC-derived DA neurons with endogenous parkin levels (Imaizumi et al., 2012; Kumar et al., 2020; Suzuki et al., 2017). In the present thesis, I hypothesized that not only parkin-deficient iPSC-

derived neurons show an impaired “tagging” of depolarized mitochondria for degradation, but also the iPSC-derived neurons from heterozygous mutation carriers, partially lacking parkin. Based on this, I generated mitochondrial damage in these neurons by treating them with CCCP to trigger the loss of the membrane potential and induce parkin translocation to mitochondria. Steady state levels of the OMM proteins MFN2 and TOM70 were determined, under basal conditions and upon treatment with CCCP. As expected, levels of OMM proteins were significantly increased in the neurons of the *Parkin* PD line when comparing to the control neurons, as has been observed previously for both *Parkin* and *PINK1* knockout animals (Ziviani et al., 2010). Remarkably, I was able to also confirm the premise on the iPSC-derived neurons of individuals carrying a heterozygous exon 7 deletion in *Parkin*. This result was observed for both assayed proteins unveiling another molecular trait in these individuals, suggesting that even a partial deficiency of parkin might destabilize the initiation of the important mitochondrial quality control process. However, for being able to draw conclusive results on this, other approaches, including the use of fluorescent indicators of mitophagy such as mito-Keima and mito-QC, or electron microscopy, will need to be applied.

Additionally, even though the parkin-dependent mitophagy process might not be fully functional, the non-damaged mitochondria could potentially play a role in the compensation of this deficit. Furthermore, mitochondrial homeostasis might be maintained in the cells of these individuals thanks to alternative, parkin-independent mitophagy pathways, such as the receptor-mediated mitophagy or other ubiquitin ligases, which are known to run in parallel to the canonical PINK1/Parkin pathway (Villa et al., 2018).

The major finding of the functional assessment of mitochondria is the observation that in both cellular models the individuals carrying a heterozygous mutation in *Parkin* present detectable defects on several fronts. Importantly, the altered molecular phenotype in the unaffected heterozygous mutation carriers is milder as compared to the phenotype observed in the cells of PD patients lacking parkin and suggests the possibility of a gene-dosage effect.

Taken together, the results of this study not only confirm an impaired mitochondrial phenotype observed previously in iPSC-derived neurons of *Parkin* mutant patients, but it also suggests that a heterozygous mutation in *Parkin* is able to trigger changes in mitochondrial homeostasis in these clinically unaffected individuals. To what extent these alterations can affect the overall function of these organelles to the point of translating into disease remains to be investigated.

6. Conclusion

Homozygous or compound-heterozygous (biallelic) mutations in *Parkin* are the most common cause of autosomal recessive early-onset (< 45 years) familial PD. About 8% of all PD patients screened for *Parkin* mutations have been shown to carry a single heterozygous mutation (Klein et al., 2007). These observations raised the hypothesis that the relatively common heterozygous mutations in this 'recessive' PD gene may predispose to PD in a dominant manner with highly reduced penetrance. Further supporting this notion, carrying heterozygous *Parkin* mutations is one of the reported potential genetic risk factors for PD. Phenotype expressivity in heterozygous mutation carriers is extremely variable and includes overt symptoms of PD as well as subtle motor signs not allowing for a definitive clinical diagnosis of PD. Furthermore, neuroimaging or electrophysiology studies have demonstrated parkinsonian features in asymptomatic heterozygous mutation carriers. Therefore, identifying those individuals at possibly greater risk of disease development requires identification of biological and molecular markers that can be monitored in the prodromal phase. While data about conversion of individuals carrying heterozygous *Parkin* mutations to full disease is lacking, it is crucial to identify such markers, as these will be vital for testing potential neuroprotective therapies before progressive neurodegeneration advances. The prodromal phase of PD is clinically characterized not only by the presence of non-motor signs but also subtle motor disturbances as part of the phenotypic spectrum. In a subset of 27 heterozygous *Parkin* mutation carriers and 24 non-mutation carriers from the CHRIS study who were recalled based on their genetic profile, it was observed that sensor-based quantification of movements allows discrimination between unaffected heterozygous mutation carriers and mutation-free controls. Thereby, it is crucial to challenge the motor system with more difficult tasks to unmask these subtle motor alterations (Prasuhn et al., 2021). In this study, I have shown that asymptomatic heterozygous *Parkin* mutation carriers in the general population have increased occurrence of diabetes and decreased heart rate. Moreover, in a subset of individuals, I have identified an altered molecular phenotype, characterized by disparities at the level of mtDNA integrity and mitochondrial function in blood and two different cellular models derived from the mutation carriers and non-carriers from the same families. I postulate that a beginning disease process could be characterized by a hyperactive respiration in peripheral, rapidly turned over LCLs, where mitochondria seem to counteract or adapt to the insult, while in post-mitotic neurons, the damage of the insult might accumulate with time. I have observed that indeed, heterozygous carriers of *Parkin* mutations

manifest molecular effects that go in the same direction to those observed in PD patients caused by the same mutations on both alleles. Several mitochondrial biomarkers presented here appear therefore to be useful indicators of an increased vulnerability, and these can be used in further studies. Some of those biomarkers reveal statistically significant differences between non-carriers, carriers of one mutation and carriers of two mutations in homozygous or compound heterozygous states. Factors that negatively affect mitochondrial function may push carriers over a certain "threshold", whereby carriers convert from presenting mild, barely observable subclinical phenotypes, to becoming more symptomatic. In order to adequately understand individual disease conversion, there is a need for more longitudinal studies with both putatively healthy individuals, and symptomatic individuals carrying single *Parkin* mutations, coupled with more in-depth clinical phenotyping and measurements of the biomarkers presented here. The gradient of "mitochondrial function" biomarkers studied here suggests that there may well be a threshold of disrupted mitochondrial function, past which a *Parkin* mutation carrier may convert to a disease state. Given the results of this study, it would be worth studying the degree to which mitochondrial protection factors in the cell models described here may indicate a strategy that rescues mitochondrial function in mutation carriers with the herein described biomarkers. Such a strategy may delay, or possibly prevent, the conversion to full clinical phenotype.

7. References

Abe, K., St George-Hyslop, P. H., Tanzi, R. E., & Kogure, K. (1991). Induction of amyloid precursor protein mRNA after heat shock in cultured human lymphoblastoid cells. *Neurosci Lett*, *125*(2), 169-171. https://doi.org/10.1016/0304-3940(91)90019-p

Abou-Sleiman, P. M., Muqit, M. M., & Wood, N. W. (2006). Expanding insights of mitochondrial dysfunction in Parkinson's disease. *Nat Rev Neurosci*, *7*(3), 207-219. https://doi.org/10.1038/nrn1868

Ambrosi, G., Ghezzi, C., Sepe, S., Milanese, C., Payan-Gomez, C., Bombardieri, C. R., Armentero, M. T., Zangaglia, R., Pacchetti, C., Mastroberardino, P. G., & Blandini, F. (2014). Bioenergetic and proteolytic defects in fibroblasts from patients with sporadic Parkinson's disease. *Biochim Biophys Acta*, *1842*(9), 1385-1394. https://doi.org/10.1016/j.bbadis.2014.05.008

Annesley, S. J., & Fisher, P. R. (2021). Lymphoblastoid Cell Lines as Models to Study Mitochondrial Function in Neurological Disorders. *Int J Mol Sci*, *22*(9). https://doi.org/10.3390/ijms22094536

Annesley, S. J., Lay, S. T., De Piazza, S. W., Sanislav, O., Hammersley, E., Allan, C. Y., Francione, L. M., Bui, M. Q., Chen, Z. P., Ngoei, K. R., Tassone, F., Kemp, B. E., Storey, E., Evans, A., Loesch, D. Z., & Fisher, P. R. (2016). Immortalized Parkinson's disease lymphocytes have enhanced mitochondrial respiratory activity. *Dis Model Mech*, *9*(11), 1295-1305. https://doi.org/10.1242/dmm.025684

Avenali, M., Blandini, F., & Cerri, S. (2020). Glucocerebrosidase Defects as a Major Risk Factor for Parkinson's Disease. *Front Aging Neurosci*, *12*, 97. https://doi.org/10.3389/fnagi.2020.00097

Balestrino, R., & Schapira, A. H. V. (2020). Parkinson disease. *Eur J Neurol*, *27*(1), 27-42. https://doi.org/10.1111/ene.14108

Baron, C. A., Liu, S. Y., Hicks, C., & Gregg, J. P. (2006). Utilization of lymphoblastoid cell lines as a system for the molecular modeling of autism. *J Autism Dev Disord*, *36*(8), 973-982. https://doi.org/10.1007/s10803-006-0134-x

Barroso, N., Campos, Y., Huertas, R., Esteban, J., Molina, J. A., Alonso, A., Gutierrez-Rivas, E., & Arenas, J. (1993). Respiratory chain enzyme activities in lymphocytes from untreated patients with Parkinson disease. *Clin Chem*, *39*(4), 667-669. https://www.ncbi.nlm.nih.gov/pubmed/8386068

Bender, A., Krishnan, K. J., Morris, C. M., Taylor, G. A., Reeve, A. K., Perry, R. H., Jaros, E., Hersheson, J. S., Betts, J., Klopstock, T., Taylor, R. W., & Turnbull, D. M. (2006). High levels of mitochondrial DNA deletions in substantia nigra neurons in aging and Parkinson disease. *Nat Genet*, *38*(5), 515-517. https://doi.org/10.1038/ng1769

Berenguer-Escuder, C., Grossmann, D., Antony, P., Arena, G., Wasner, K., Massart, F., Jarazo, J., Walter, J., Schwamborn, J. C., Grunewald, A., & Kruger, R. (2020). Impaired mitochondrial-endoplasmic reticulum interaction and mitophagy in Miro1-mutant neurons in Parkinson's disease. *Hum Mol Genet*, *29*(8), 1353-1364. https://doi.org/10.1093/hmg/ddaa066

Bernardini, J. P., Brouwer, J. M., Tan, I. K., Sandow, J. J., Huang, S., Stafford, C. A., Bankovacki, A., Riffkin, C. D., Wardak, A. Z., Czabotar, P. E., Lazarou, M., & Dewson, G. (2019). Parkin inhibits BAK and BAX apoptotic function by distinct mechanisms during mitophagy. *EMBO J*, *38*(2). https://doi.org/10.15252/embj.201899916

Blauwendraat, C., Nalls, M. A., & Singleton, A. B. (2020). The genetic architecture of Parkinson's disease. *Lancet Neurol*, *19*(2), 170-178. https://doi.org/10.1016/S1474-4422(19)30287-X

Bloem, B. R., Okun, M. S., & Klein, C. (2021). Parkinson's disease. *The Lancet*. https://doi.org/https://doi.org/10.1016/S0140-6736(21)00218-X

Bogetofte, H., Jensen, P., Ryding, M., Schmidt, S. I., Okarmus, J., Ritter, L., Worm, C. S., Hohnholt, M. C., Azevedo, C., Roybon, L., Bak, L. K., Waagepetersen, H., Ryan, B. J., Wade-Martins, R., Larsen, M. R., & Meyer, M. (2019). PARK2 Mutation Causes Metabolic Disturbances and Impaired Survival of Human iPSC-Derived Neurons. *Front Cell Neurosci*, *13*, 297. https://doi.org/10.3389/fncel.2019.00297

Borghammer, P., & Van Den Berge, N. (2019). Brain-First versus Gut-First Parkinson's Disease: A Hypothesis. *J Parkinsons Dis*, *9*(s2), S281-S295. https://doi.org/10.3233/JPD-191721

Brand, M. D., Affourtit, C., Esteves, T. C., Green, K., Lambert, A. J., Miwa, S., Pakay, J. L., & Parker, N. (2004). Mitochondrial superoxide: production, biological effects, and activation of uncoupling proteins. *Free Radic Biol Med*, *37*(6), 755-767. https://doi.org/10.1016/j.freeradbiomed.2004.05.034

Bruggemann, N., Mitterer, M., Lanthaler, A. J., Djarmati, A., Hagenah, J., Wiegers, K., Winkler, S., Pawlack, H., Lohnau, T., Pramstaller, P. P., Klein, C., & Lohmann, K. (2009). Frequency of heterozygous Parkin mutations in healthy subjects: need for careful prospective follow-up examination of mutation carriers. *Parkinsonism Relat Disord*, *15*(6), 425-429. https://doi.org/10.1016/j.parkreldis.2008.11.014

Burman, J. L., Yu, S., Poole, A. C., Decal, R. B., & Pallanck, L. (2012). Analysis of neural subtypes reveals selective mitochondrial dysfunction in dopaminergic neurons from parkin mutants. *Proc Natl Acad Sci U S A*, *109*(26), 10438-10443. https://doi.org/10.1073/pnas.1120688109

Carling, P. J., Mortiboys, H., Green, C., Mihaylov, S., Sandor, C., Schwartzentruber, A., Taylor, R., Wei, W., Hastings, C., Wong, S., Lo, C., Evetts, S., Clemmens, H., Wyles, M., Willcox, S., Payne, T., Hughes, R., Ferraiuolo, L., Webber, C., Hide, W., Wade-Martins, R., Talbot, K., Hu, M. T., & Bandmann, O. (2020). Deep phenotyping of peripheral tissue facilitates mechanistic disease stratification in sporadic Parkinson's disease. *Prog Neurobiol*, *187*, 101772. https://doi.org/10.1016/j.pneurobio.2020.101772

Celardo, I., Martins, L. M., & Gandhi, S. (2014). Unravelling mitochondrial pathways to Parkinson's disease. *Br J Pharmacol*, *171*(8), 1943-1957. https://doi.org/10.1111/bph.12433

Cenini, G., Lloret, A., & Cascella, R. (2019). Oxidative Stress in Neurodegenerative Diseases: From a Mitochondrial Point of View. *Oxid Med Cell Longev*, *2019*, 2105607. https://doi.org/10.1155/2019/2105607

Chan, N. C., Salazar, A. M., Pham, A. H., Sweredoski, M. J., Kolawa, N. J., Graham, R. L., Hess, S., & Chan, D. C. (2011). Broad activation of the ubiquitin-proteasome system by Parkin is critical for mitophagy. *Hum Mol Genet*, *20*(9), 1726-1737. https://doi.org/10.1093/hmg/ddr048

Chang, K. H., & Chen, C. M. (2020). The Role of Oxidative Stress in Parkinson's Disease. *Antioxidants (Basel)*, *9*(7). https://doi.org/10.3390/antiox9070597

Cheng, H. C., Ulane, C. M., & Burke, R. E. (2010). Clinical progression in Parkinson disease and the neurobiology of axons. *Ann Neurol*, *67*(6), 715-725. https://doi.org/10.1002/ana.21995

Cheon, S. M., Park, M. J., Kim, W. J., & Kim, J. W. (2009). Non-motor off symptoms in Parkinson's disease. *J Korean Med Sci*, *24*(2), 311-314. https://doi.org/10.3346/jkms.2009.24.2.311

Chung, S. Y., Kishinevsky, S., Mazzulli, J. R., Graziotto, J., Mrejeru, A., Mosharov, E. V., Puspita, L., Valiulahi, P., Sulzer, D., Milner, T. A., Taldone, T., Krainc, D., Studer, L., & Shim, J. W. (2016). Parkin and PINK1 Patient iPSC-Derived Midbrain Dopamine Neurons Exhibit Mitochondrial Dysfunction and alpha-Synuclein Accumulation. *Stem Cell Reports*, *7*(4), 664-677. https://doi.org/10.1016/j.stemcr.2016.08.012

Connolly, N. M. C., Theurey, P., Adam-Vizi, V., Bazan, N. G., Bernardi, P., Bolaños, J. P., Culmsee, C., Dawson, V. L., Deshmukh, M., Duchen, M. R., Düssmann, H., Fiskum, G., Galindo, M. F., Hardingham, G. E., Hardwick, J. M., Jekabsons, M. B., Jonas, E. A., Jordán, J., Lipton, S. A., Manfredi, G., Mattson, M. P., McLaughlin, B., Methner, A., Murphy, A. N., Murphy, M. P., Nicholls, D. G., Polster, B. M., Pozzan, T., Rizzuto, R., Satrústegui, J., Slack, R. S., Swanson, R. A., Swerdlow, R. H., Will, Y., Ying, Z., Joselin, A., Gioran, A., Moreira Pinho, C., Watters, O., Salvucci, M., Llorente-Folch, I., Park, D. S., Bano, D., Ankarcrona, M., Pizzo, P., & Prehn, J. H. M. (2018). Guidelines on experimental methods to assess mitochondrial dysfunction in cellular models of neurodegenerative diseases. *Cell Death & Differentiation*, *25*(3), 542-572. https://doi.org/10.1038/s41418-017-0020-4

Coore, H. G., Denton, R. M., Martin, B. R., & Randle, P. J. (1971). Regulation of adipose tissue pyruvate dehydrogenase by insulin and other hormones. *Biochem J*, *125*(1), 115-127. https://doi.org/10.1042/bj1250115

Corti, O., Lesage, S., & Brice, A. (2011). What genetics tells us about the causes and mechanisms of Parkinson's disease. *Physiol Rev*, *91*(4), 1161-1218. https://doi.org/10.1152/physrev.00022.2010

D'Erchia, A. M., Atlante, A., Gadaleta, G., Pavesi, G., Chiara, M., De Virgilio, C., Manzari, C., Mastropasqua, F., Prazzoli, G. M., Picardi, E., Gissi, C., Horner, D., Reyes, A., Sbisa, E., Tullo, A., & Pesole, G. (2015). Tissue-specific mtDNA abundance from exome data and its correlation with mitochondrial transcription, mass and respiratory activity. *Mitochondrion*, *20*, 13-21. https://doi.org/10.1016/j.mito.2014.10.005

Da Poian, A. T., El-Bacha, T. & Luz, M. R. P. (2010). Nutrient Utilization in Humans: Metabolism Pathways. *Nature Education*, *3*.

Damiano, M., Gautier, C. A., Bulteau, A. L., Ferrando-Miguel, R., Gouarne, C., Paoli, M. G., Pruss, R., Auchere, F., L'Hermitte-Stead, C., Bouillaud, F., Brice, A., Corti, O., & Lombes, A. (2014). Tissue- and cell-specific mitochondrial defect in Parkin-deficient mice. *PLoS One*, *9*(6), e99898. https://doi.org/10.1371/journal.pone.0099898

Davies, K. M., Strauss, M., Daum, B., Kief, J. H., Osiewacz, H. D., Rycovska, A., Zickermann, V., & Kuhlbrandt, W. (2011). Macromolecular organization of ATP synthase and complex I in whole mitochondria. *Proc Natl Acad Sci U S A*, *108*(34), 14121-14126. https://doi.org/10.1073/pnas.1103621108

Davis, G. C., Williams, A. C., Markey, S. P., Ebert, M. H., Caine, E. D., Reichert, C. M., & Kopin, I. J. (1979). Chronic Parkinsonism secondary to intravenous injection of meperidine analogues. *Psychiatry Res*, *1*(3), 249-254. https://doi.org/10.1016/0165-1781(79)90006-4

Dawson, T. M., & Dawson, V. L. (2014). Parkin plays a role in sporadic Parkinson's disease. *Neurodegener Dis*, *13*(2-3), 69-71. https://doi.org/10.1159/000354307

Dawson, T. M., Ko, H. S., & Dawson, V. L. (2010). Genetic animal models of Parkinson's disease. *Neuron*, *66*(5), 646-661. https://doi.org/10.1016/j.neuron.2010.04.034

de Lau, L. M., & Breteler, M. M. (2006). Epidemiology of Parkinson's disease. *Lancet Neurol*, *5*(6), 525-535. https://doi.org/10.1016/S1474-4422(06)70471-9

Delcambre, S., Ghelfi, J., Ouzren, N., Grandmougin, L., Delbrouck, C., Seibler, P., Wasner, K., Aasly, J. O., Klein, C., Trinh, J., Pereira, S. L., & Grunewald, A. (2020). Mitochondrial Mechanisms of LRRK2 G2019S Penetrance. *Front Neurol*, *11*, 881. https://doi.org/10.3389/fneur.2020.00881

Desai, V. G., Feuers, R. J., Hart, R. W., & Ali, S. F. (1996). MPP(+)-induced neurotoxicity in mouse is age-dependent: evidenced by the selective inhibition of complexes of electron transport. *Brain Res*, *715*(1-2), 1-8. https://doi.org/10.1016/0006-8993(95)01255-9

Dias, V., Junn, E., & Mouradian, M. M. (2013). The role of oxidative stress in Parkinson's disease. *J Parkinsons Dis*, *3*(4), 461-491. https://doi.org/10.3233/JPD-130230

Djaldetti, R., Lev, N., & Melamed, E. (2009). Lesions outside the CNS in Parkinson's disease. *Mov Disord*, *24*(6), 793-800. https://doi.org/10.1002/mds.22172

Domingo, A., & Klein, C. (2018). Genetics of Parkinson disease. *Handb Clin Neurol*, *147*, 211-227. https://doi.org/10.1016/B978-0-444-63233-3.00014-2

Dowey, S. N., Huang, X., Chou, B. K., Ye, Z., & Cheng, L. (2012). Generation of integration-free human induced pluripotent stem cells from postnatal blood mononuclear cells by plasmid vector expression. *Nat Protoc*, *7*(11), 2013-2021. https://doi.org/10.1038/nprot.2012.121

Drahota, Z., Milerova, M., Stieglerova, A., Houstek, J., & Ostadal, B. (2004). Developmental changes of cytochrome c oxidase and citrate synthase in rat heart homogenate. *Physiol Res*, *53*(1), 119-122. https://www.ncbi.nlm.nih.gov/pubmed/14984324

Ekstrand, M. I., & Galter, D. (2009). The MitoPark Mouse - an animal model of Parkinson's disease with impaired respiratory chain function in dopamine neurons. *Parkinsonism Relat Disord*, *15 Suppl 3*, S185-188. https://doi.org/10.1016/S1353-8020(09)70811-9

Emre, N., Vidal, J. G., Elia, J., O'Connor, E. D., Paramban, R. I., Hefferan, M. P., Navarro, R., Goldberg, D. S., Varki, N. M., Marsala, M., & Carson, C. T. (2010). The ROCK inhibitor Y-27632 improves recovery of human embryonic stem cells after fluorescence-activated cell sorting with multiple cell surface markers. *PLoS One*, *5*(8), e12148. https://doi.org/10.1371/journal.pone.0012148

Fahn, S. (2000). The spectrum of levodopa-induced dyskinesias. *Ann Neurol*, *47*(4 Suppl 1), S2-9; discussion S9-11. https://www.ncbi.nlm.nih.gov/pubmed/10762127

Fereshtehnejad, S. M., Yao, C., Pelletier, A., Montplaisir, J. Y., Gagnon, J. F., & Postuma, R. B. (2019). Evolution of prodromal Parkinson's disease and dementia with Lewy bodies: a prospective study. *Brain*, *142*(7), 2051-2067. https://doi.org/10.1093/brain/awz111

Forno, L. S. (1996). Neuropathology of Parkinson's disease. *J Neuropathol Exp Neurol*, *55*(3), 259-272. https://doi.org/10.1097/00005072-199603000-00001

Friedman, L. G., Lachenmayer, M. L., Wang, J., He, L., Poulose, S. M., Komatsu, M., Holstein, G. R., & Yue, Z. (2012). Disrupted autophagy leads to dopaminergic axon and dendrite degeneration and promotes presynaptic accumulation of alpha-synuclein and LRRK2 in the brain. *J Neurosci*, *32*(22), 7585-7593. https://doi.org/10.1523/JNEUROSCI.5809-11.2012

Ge, P., Dawson, V. L., & Dawson, T. M. (2020). PINK1 and Parkin mitochondrial quality control: a source of regional vulnerability in Parkinson's disease. *Mol Neurodegener*, *15*(1), 20. https://doi.org/10.1186/s13024-020-00367-7

Gegg, M. E., Cooper, J. M., Chau, K. Y., Rojo, M., Schapira, A. H., & Taanman, J. W. (2010). Mitofusin 1 and mitofusin 2 are ubiquitinated in a PINK1/parkin-dependent manner upon induction of mitophagy. *Hum Mol Genet*, *19*(24), 4861-4870. https://doi.org/10.1093/hmg/ddq419

Gleyzer, N., Vercauteren, K., & Scarpulla, R. C. (2005). Control of mitochondrial transcription specificity factors (TFB1M and TFB2M) by nuclear respiratory factors (NRF-1 and NRF-2) and PGC-1 family coactivators. *Mol Cell Biol*, *25*(4), 1354-1366. https://doi.org/10.1128/MCB.25.4.1354-1366.2005

Gonzalez-Casacuberta, I., Juarez-Flores, D. L., Ezquerra, M., Fucho, R., Catalan-Garcia, M., Guitart-Mampel, M., Tobias, E., Garcia-Ruiz, C., Fernandez-Checa, J. C., Tolosa, E., Marti, M. J., Grau, J. M., Fernandez-Santiago, R., Cardellach, F., Moren, C., & Garrabou, G. (2019). Mitochondrial and autophagic alterations in skin fibroblasts from Parkinson disease patients with Parkin mutations. *Aging (Albany NY)*, *11*(11), 3750-3767. https://doi.org/10.18632/aging.102014

Grunewald, A., Kasten, M., Ziegler, A., & Klein, C. (2013). Next-generation phenotyping using the parkin example: time to catch up with genetics. *JAMA Neurol*, *70*(9), 1186-1191. https://doi.org/10.1001/jamaneurol.2013.488

Grunewald, A., Kumar, K. R., & Sue, C. M. (2019). New insights into the complex role of mitochondria in Parkinson's disease. *Prog Neurobiol*, *177*, 73-93. https://doi.org/10.1016/j.pneurobio.2018.09.003

Grunewald, A., Rygiel, K. A., Hepplewhite, P. D., Morris, C. M., Picard, M., & Turnbull, D. M. (2016). Mitochondrial DNA Depletion in Respiratory Chain-Deficient Parkinson Disease Neurons. *Ann Neurol*, *79*(3), 366-378. https://doi.org/10.1002/ana.24571

Grunewald, A., Voges, L., Rakovic, A., Kasten, M., Vandebona, H., Hemmelmann, C., Lohmann, K., Orolicki, S., Ramirez, A., Schapira, A. H., Pramstaller, P. P., Sue, C. M., & Klein, C. (2010). Mutant Parkin impairs mitochondrial function and morphology in human fibroblasts. *PLoS One*, *5*(9), e12962. https://doi.org/10.1371/journal.pone.0012962

Haas, R. H., Nasirian, F., Nakano, K., Ward, D., Pay, M., Hill, R., & Shults, C. W. (1995). Low platelet mitochondrial complex I and complex II/III activity in early untreated Parkinson's disease. *Ann Neurol*, *37*(6), 714-722. https://doi.org/10.1002/ana.410370604

Hattori, N., & Mizuno, Y. (2017). Twenty years since the discovery of the parkin gene. *J Neural Transm (Vienna)*, *124*(9), 1037-1054. https://doi.org/10.1007/s00702-017-1742-7

Hattori, N., Tanaka, M., Ozawa, T., & Mizuno, Y. (1991). Immunohistochemical studies on complexes I, II, III, and IV of mitochondria in Parkinson's disease. *Ann Neurol*, *30*(4), 563-571. https://doi.org/10.1002/ana.410300409

Hauser, D. N., & Hastings, T. G. (2013). Mitochondrial dysfunction and oxidative stress in Parkinson's disease and monogenic parkinsonism. *Neurobiol Dis*, *51*, 35-42. https://doi.org/10.1016/j.nbd.2012.10.011

Hauser, D. N., Primiani, C. T., & Cookson, M. R. (2017). The Effects of Variants in the Parkin, PINK1, and DJ-1 Genes along with Evidence for their Pathogenicity. *Curr Protein Pept Sci*, *18*(7), 702-714. https://doi.org/10.2174/1389203717666160311121954

Havelund, J. F., Heegaard, N. H. H., Faergeman, N. J. K., & Gramsbergen, J. B. (2017). Biomarker Research in Parkinson's Disease Using Metabolite Profiling. *Metabolites*, *7*(3). https://doi.org/10.3390/metabo7030042

Haylett, W., Swart, C., van der Westhuizen, F., van Dyk, H., van der Merwe, L., van der Merwe, C., Loos, B., Carr, J., Kinnear, C., & Bardien, S. (2016). Altered Mitochondrial Respiration and Other Features of Mitochondrial Function in Parkin-Mutant Fibroblasts from Parkinson's Disease Patients. *Parkinsons Dis*, *2016*, 1819209. https://doi.org/10.1155/2016/1819209

Hedrich, K., Eskelson, C., Wilmot, B., Marder, K., Harris, J., Garrels, J., Meija-Santana, H., Vieregge, P., Jacobs, H., Bressman, S. B., Lang, A. E., Kann, M., Abbruzzese, G., Martinelli, P., Schwinger, E., Ozelius, L. J., Pramstaller, P. P., Klein, C., & Kramer, P. (2004). Distribution, type, and origin of Parkin mutations: review and case studies. *Mov Disord*, *19*(10), 1146-1157. https://doi.org/10.1002/mds.20234

Hedrich, K., Kann, M., Lanthaler, A. J., Dalski, A., Eskelson, C., Landt, O., Schwinger, E., Vieregge, P., Lang, A. E., Breakefield, X. O., Ozelius, L. J., Pramstaller, P. P., & Klein, C. (2001). The importance of gene dosage studies: mutational analysis of the parkin gene in early-onset parkinsonism. *Hum Mol Genet*, *10*(16), 1649-1656. https://doi.org/10.1093/hmg/10.16.1649

Heinzel, S., Berg, D., Gasser, T., Chen, H., Yao, C., Postuma, R. B., & Disease, M. D. S. T. F. o. t. D. o. P. s. (2019). Update of the MDS research criteria for prodromal Parkinson's disease. *Mov Disord*, *34*(10), 1464-1470. https://doi.org/10.1002/mds.27802

Hilker, R., Klein, C., Ghaemi, M., Kis, B., Strotmann, T., Ozelius, L. J., Lenz, O., Vieregge, P., Herholz, K., Heiss, W. D., & Pramstaller, P. P. (2001). Positron emission tomographic analysis of the nigrostriatal dopaminergic system in familial parkinsonism associated with mutations in the parkin gene. *Ann Neurol*, *49*(3), 367-376. https://www.ncbi.nlm.nih.gov/pubmed/11261512

Hirota, Y., Yamashita, S., Kurihara, Y., Jin, X., Aihara, M., Saigusa, T., Kang, D., & Kanki, T. (2015). Mitophagy is primarily due to alternative autophagy and requires the MAPK1 and

MAPK14 signaling pathways. *Autophagy*, *11*(2), 332-343. https://doi.org/10.1080/15548627.2015.1023047

Hoppins, S., Lackner, L., & Nunnari, J. (2007). The machines that divide and fuse mitochondria. *Annu Rev Biochem*, *76*, 751-780. https://doi.org/10.1146/annurev.biochem.76.071905.090048

Hussain, T., & Mulherkar, R. (2012). Lymphoblastoid Cell lines: a Continuous in Vitro Source of Cells to Study Carcinogen Sensitivity and DNA Repair. *Int J Mol Cell Med*, *1*(2), 75-87. https://www.ncbi.nlm.nih.gov/pubmed/24551762

Huttenlocher, J., Stefansson, H., Steinberg, S., Helgadottir, H. T., Sveinbjornsdottir, S., Riess, O., Bauer, P., & Stefansson, K. (2015). Heterozygote carriers for CNVs in PARK2 are at increased risk of Parkinson's disease. *Hum Mol Genet*, *24*(19), 5637-5643. https://doi.org/10.1093/hmg/ddv277

Imaizumi, Y., Okada, Y., Akamatsu, W., Koike, M., Kuzumaki, N., Hayakawa, H., Nihira, T., Kobayashi, T., Ohyama, M., Sato, S., Takanashi, M., Funayama, M., Hirayama, A., Soga, T., Hishiki, T., Suematsu, M., Yagi, T., Ito, D., Kosakai, A., Hayashi, K., Shouji, M., Nakanishi, A., Suzuki, N., Mizuno, Y., Mizushima, N., Amagai, M., Uchiyama, Y., Mochizuki, H., Hattori, N., & Okano, H. (2012). Mitochondrial dysfunction associated with increased oxidative stress and alpha-synuclein accumulation in PARK2 iPSC-derived neurons and postmortem brain tissue. *Mol Brain*, *5*, 35. https://doi.org/10.1186/1756-6606-5-35

Iwaki, H., Leonard, H. L., Bandrés-Ciga, S., Blauwendraat, C., Makarious, M. B., Scholz, S. W., Nishikawa, N., Faghri, F., Frasier, M., Gibbs, J. R., Singleton, A. B., Nalls, M. A., & Hernandez, D. G. (2020). Biomarkers of Parkinson's Disease: Screening Vital Signs and Routine Blood Tests. *medRxiv*, 2020.2005.2018.20103085. https://doi.org/10.1101/2020.05.18.20103085

Jang, Y. H., & Lim, K. I. (2018). Recent Advances in Mitochondria-Targeted Gene Delivery. *Molecules*, *23*(9). https://doi.org/10.3390/molecules23092316

Jiang, H., Ren, Y., Yuen, E. Y., Zhong, P., Ghaedi, M., Hu, Z., Azabdaftari, G., Nakaso, K., Yan, Z., & Feng, J. (2012). Parkin controls dopamine utilization in human midbrain dopaminergic neurons derived from induced pluripotent stem cells. *Nat Commun*, *3*, 668. https://doi.org/10.1038/ncomms1669

Kamienieva, I., Duszynski, J., & Szczepanowska, J. (2021). Multitasking guardian of mitochondrial quality: Parkin function and Parkinson's disease. *Transl Neurodegener*, *10*(1), 5. https://doi.org/10.1186/s40035-020-00229-8

Kamp, F., Exner, N., Lutz, A. K., Wender, N., Hegermann, J., Brunner, B., Nuscher, B., Bartels, T., Giese, A., Beyer, K., Eimer, S., Winklhofer, K. F., & Haass, C. (2010). Inhibition of mitochondrial fusion by alpha-synuclein is rescued by PINK1, Parkin and DJ-1. *EMBO J*, *29*(20), 3571-3589. https://doi.org/10.1038/emboj.2010.223

Karnati, S., Luers, G., Pfreimer, S., & Baumgart-Vogt, E. (2013). Mammalian SOD2 is exclusively located in mitochondria and not present in peroxisomes. *Histochem Cell Biol*, *140*(2), 105-117. https://doi.org/10.1007/s00418-013-1099-4

Kasten, M., Hartmann, C., Hampf, J., Schaake, S., Westenberger, A., Vollstedt, E. J., Balck, A., Domingo, A., Vulinovic, F., Dulovic, M., Zorn, I., Madoev, H., Zehnle, H., Lembeck, C. M., Schawe, L., Reginold, J., Huang, J., Konig, I. R., Bertram, L., Marras, C., Lohmann, K., Lill, C. M., & Klein, C. (2018). Genotype-Phenotype Relations for the Parkinson's Disease Genes Parkin, PINK1, DJ1: MDSGene Systematic Review. *Mov Disord*, *33*(5), 730-741. https://doi.org/10.1002/mds.27352

Kay, D. M., Stevens, C. F., Hamza, T. H., Montimurro, J. S., Zabetian, C. P., Factor, S. A., Samii, A., Griffith, A., Roberts, J. W., Molho, E. S., Higgins, D. S., Gancher, S., Moses, L., Zareparsi, S., Poorkaj, P., Bird, T., Nutt, J., Schellenberg, G. D., & Payami, H. (2010). A comprehensive analysis of deletions, multiplications, and copy number variations in PARK2. *Neurology*, *75*(13), 1189-1194. https://doi.org/10.1212/WNL.0b013e3181f4d832

Keeney, P. M., Xie, J., Capaldi, R. A., & Bennett, J. P., Jr. (2006). Parkinson's disease brain mitochondrial complex I has oxidatively damaged subunits and is functionally impaired and misassembled. *J Neurosci*, *26*(19), 5256-5264. https://doi.org/10.1523/JNEUROSCI.0984-06.2006

Khan, N. L., Scherfler, C., Graham, E., Bhatia, K. P., Quinn, N., Lees, A. J., Brooks, D. J., Wood, N. W., & Piccini, P. (2005). Dopaminergic dysfunction in unrelated, asymptomatic carriers of a single parkin mutation. *Neurology*, *64*(1), 134-136. https://doi.org/10.1212/01.WNL.0000148725.48740.6D

Kircher, M., Witten, D. M., Jain, P., O'Roak, B. J., Cooper, G. M., & Shendure, J. (2014). A general framework for estimating the relative pathogenicity of human genetic variants. *Nat Genet*, *46*(3), 310-315. https://doi.org/10.1038/ng.2892

Kitada, T., Asakawa, S., Hattori, N., Matsumine, H., Yamamura, Y., Minoshima, S., Yokochi, M., Mizuno, Y., & Shimizu, N. (1998). Mutations in the parkin gene cause autosomal recessive juvenile parkinsonism. *Nature*, *392*(6676), 605-608. https://doi.org/10.1038/33416

Klein, C., & Krainc, D. (2013). Glucocerebrosidase mutations: tipping point toward Parkinson disease and dementia? *JAMA Neurol*, *70*(6), 686-688. https://doi.org/10.1001/jamaneurol.2013.87

Klein, C., Lohmann-Hedrich, K., Rogaeva, E., Schlossmacher, M. G., & Lang, A. E. (2007). Deciphering the role of heterozygous mutations in genes associated with parkinsonism. *Lancet Neurol*, *6*(7), 652-662. https://doi.org/10.1016/S1474-4422(07)70174-6

Klein, C., & Westenberger, A. (2012). Genetics of Parkinson's disease. *Cold Spring Harb Perspect Med*, *2*(1), a008888. https://doi.org/10.1101/cshperspect.a008888

Kobayashi, H., Kruger, R., Markopoulou, K., Wszolek, Z., Chase, B., Taka, H., Mineki, R., Murayama, K., Riess, O., Mizuno, Y., & Hattori, N. (2003). Haploinsufficiency at the alpha-synuclein gene underlies phenotypic severity in familial Parkinson's disease. *Brain*, *126*(Pt 1), 32-42. https://doi.org/10.1093/brain/awg010

Kocer, A., Yaman, A., Niftaliyev, E., Duruyen, H., Eryilmaz, M., & Kocer, E. (2013). Assessment of platelet indices in patients with neurodegenerative diseases: mean platelet volume was increased in patients with Parkinson's disease. *Curr Gerontol Geriatr Res*, *2013*, 986254. https://doi.org/10.1155/2013/986254

Kouli, A., Torsney, K. M., & Kuan, W. L. (2018). Parkinson's Disease: Etiology, Neuropathology, and Pathogenesis. In T. B. Stoker & J. C. Greenland (Eds.), *Parkinson's Disease: Pathogenesis and Clinical Aspects*. https://doi.org/10.15586/codonpublications.parkinsonsdisease.2018.ch1

Kovalchuke, L., Mosharov, E. V., Levy, O. A., & Greene, L. A. (2019). Stress-induced phospho-ubiquitin formation causes parkin degradation. *Sci Rep*, *9*(1), 11682. https://doi.org/10.1038/s41598-019-47952-5

Kraytsberg, Y., Kudryavtseva, E., McKee, A. C., Geula, C., Kowall, N. W., & Khrapko, K. (2006). Mitochondrial DNA deletions are abundant and cause functional impairment in aged human substantia nigra neurons. *Nat Genet*, *38*(5), 518-520. https://doi.org/10.1038/ng1778

Kriks, S., Shim, J. W., Piao, J., Ganat, Y. M., Wakeman, D. R., Xie, Z., Carrillo-Reid, L., Auyeung, G., Antonacci, C., Buch, A., Yang, L., Beal, M. F., Surmeier, D. J., Kordower, J. H., Tabar, V., & Studer, L. (2011). Dopamine neurons derived from human ES cells efficiently engraft in animal models of Parkinson's disease. *Nature*, *480*(7378), 547-551. https://doi.org/10.1038/nature10648

Kuan, W. L., Stott, K., He, X., Wood, T. C., Yang, S., Kwok, J. C. F., Hall, K., Zhao, Y., Tietz, O., Aigbirhio, F. I., Vernon, A. C., & Barker, R. A. (2021). Systemic alpha-synuclein injection triggers selective neuronal pathology as seen in patients with Parkinson's disease. *Mol Psychiatry*, *26*(2), 556-567. https://doi.org/10.1038/s41380-019-0608-9

Kuhlbrandt, W. (2015). Structure and function of mitochondrial membrane protein complexes. *BMC Biol*, *13*, 89. https://doi.org/10.1186/s12915-015-0201-x

Kumar, M., Acevedo-Cintron, J., Jhaldiyal, A., Wang, H., Andrabi, S. A., Eacker, S., Karuppagounder, S. S., Brahmachari, S., Chen, R., Kim, H., Ko, H. S., Dawson, V. L., & Dawson, T. M. (2020). Defects in Mitochondrial Biogenesis Drive Mitochondrial Alterations in PARKIN-Deficient Human Dopamine Neurons. *Stem Cell Reports*, *15*(3), 629-645. https://doi.org/10.1016/j.stemcr.2020.07.013

Kuroda, Y., Mitsui, T., Kunishige, M., Shono, M., Akaike, M., Azuma, H., & Matsumoto, T. (2006). Parkin enhances mitochondrial biogenesis in proliferating cells. *Hum Mol Genet*, *15*(6), 883-895. https://doi.org/10.1093/hmg/ddl006

Langston, J. W., Ballard, P., Tetrud, J. W., & Irwin, I. (1983). Chronic Parkinsonism in humans due to a product of meperidine-analog synthesis. *Science*, *219*(4587), 979-980. https://doi.org/10.1126/science.6823561

Lee, A., & Gilbert, R. M. (2016). Epidemiology of Parkinson Disease. *Neurol Clin*, *34*(4), 955-965. https://doi.org/10.1016/j.ncl.2016.06.012

Lee, S., Sheck, L., Crowston, J. G., Van Bergen, N. J., O'Neill, E. C., O'Hare, F., Kong, Y. X., Chrysostomou, V., Vincent, A. L., & Trounce, I. A. (2012). Impaired complex-I-linked respiration and ATP synthesis in primary open-angle glaucoma patient lymphoblasts. *Invest Ophthalmol Vis Sci*, *53*(4), 2431-2437. https://doi.org/10.1167/iovs.12-9596

Lee, S. B., Kim, J. J., Han, S. A., Fan, Y., Guo, L. S., Aziz, K., Nowsheen, S., Kim, S. S., Park, S. Y., Luo, Q., Chung, J. O., Choi, S. I., Aziz, A., Yin, P., Tong, S. Y., Fiesel, F. C., Springer, W., Zhang, J. S., & Lou, Z. (2019). The AMPK-Parkin axis negatively regulates necroptosis and

tumorigenesis by inhibiting the necrosome. *Nat Cell Biol*, *21*(8), 940-951. https://doi.org/10.1038/s41556-019-0356-8

Levitt, P., Pintar, J. E., & Breakefield, X. O. (1982). Immunocytochemical demonstration of monoamine oxidase B in brain astrocytes and serotonergic neurons. *Proc Natl Acad Sci U S A*, *79*(20), 6385-6389. https://doi.org/10.1073/pnas.79.20.6385

Li, D., Aung-Htut, M. T., Ham, K. A., Fletcher, S., & Wilton, S. D. (2020). A Splice Intervention Therapy for Autosomal Recessive Juvenile Parkinson's Disease Arising from Parkin Mutations. *Int J Mol Sci*, *21*(19). https://doi.org/10.3390/ijms21197282

Lill, C. M. (2016). Genetics of Parkinson's disease. *Mol Cell Probes*, *30*(6), 386-396. https://doi.org/10.1016/j.mcp.2016.11.001

Lin, K. J., Lin, K. L., Chen, S. D., Liou, C. W., Chuang, Y. C., Lin, H. Y., & Lin, T. K. (2019). The Overcrowded Crossroads: Mitochondria, Alpha-Synuclein, and the Endo-Lysosomal System Interaction in Parkinson's Disease. *Int J Mol Sci*, *20*(21). https://doi.org/10.3390/ijms20215312

Liu, J., Liu, W., Li, R., & Yang, H. (2019). Mitophagy in Parkinson's Disease: From Pathogenesis to Treatment. *Cells*, *8*(7). https://doi.org/10.3390/cells8070712

Llopis, J., McCaffery, J. M., Miyawaki, A., Farquhar, M. G., & Tsien, R. Y. (1998). Measurement of cytosolic, mitochondrial, and Golgi pH in single living cells with green fluorescent proteins. *Proc Natl Acad Sci U S A*, *95*(12), 6803-6808. https://doi.org/10.1073/pnas.95.12.6803

Lonskaya, I., Hebron, M. L., Algarzae, N. K., Desforges, N., & Moussa, C. E. (2013). Decreased parkin solubility is associated with impairment of autophagy in the nigrostriatum of sporadic Parkinson's disease. *Neuroscience*, *232*, 90-105. https://doi.org/10.1016/j.neuroscience.2012.12.018

Lubbe, S. J., Bustos, B. I., Hu, J., Krainc, D., Joseph, T., Hehir, J., Tan, M., Zhang, W., Escott-Price, V., Williams, N. M., Blauwendraat, C., Singleton, A. B., Morris, H. R., & for International Parkinson's Disease Genomics, C. (2021). Assessing the relationship between monoallelic PRKN mutations and Parkinson's risk. *Hum Mol Genet*, *30*(1), 78-86. https://doi.org/10.1093/hmg/ddaa273

Lucking, C. B., Durr, A., Bonifati, V., Vaughan, J., De Michele, G., Gasser, T., Harhangi, B. S., Meco, G., Denefle, P., Wood, N. W., Agid, Y., Brice, A., French Parkinson's Disease Genetics Study, G., & European Consortium on Genetic Susceptibility in Parkinson's, D. (2000). Association between early-onset Parkinson's disease and mutations in the parkin gene. *N Engl J Med*, *342*(21), 1560-1567. https://doi.org/10.1056/NEJM200005253422103

Luo, S., Valencia, C. A., Zhang, J., Lee, N. C., Slone, J., Gui, B., Wang, X., Li, Z., Dell, S., Brown, J., Chen, S. M., Chien, Y. H., Hwu, W. L., Fan, P. C., Wong, L. J., Atwal, P. S., & Huang, T. (2018). Biparental Inheritance of Mitochondrial DNA in Humans. *Proc Natl Acad Sci U S A*, *115*(51), 13039-13044. https://doi.org/10.1073/pnas.1810946115

Lutz-Bonengel, S., & Parson, W. (2019). No further evidence for paternal leakage of mitochondrial DNA in humans yet. *Proc Natl Acad Sci U S A*, *116*(6), 1821-1822. https://doi.org/10.1073/pnas.1820533116

Mali, P., Chou, B. K., Yen, J., Ye, Z., Zou, J., Dowey, S., Brodsky, R. A., Ohm, J. E., Yu, W., Baylin, S. B., Yusa, K., Bradley, A., Meyers, D. J., Mukherjee, C., Cole, P. A., & Cheng, L. (2010). Butyrate greatly enhances derivation of human induced pluripotent stem cells by promoting epigenetic remodeling and the expression of pluripotency-associated genes. *Stem Cells*, *28*(4), 713-720. https://doi.org/10.1002/stem.402

Matheoud, D., Sugiura, A., Bellemare-Pelletier, A., Laplante, A., Rondeau, C., Chemali, M., Fazel, A., Bergeron, J. J., Trudeau, L. E., Burelle, Y., Gagnon, E., McBride, H. M., & Desjardins, M. (2016). Parkinson's Disease-Related Proteins PINK1 and Parkin Repress Mitochondrial Antigen Presentation. *Cell*, *166*(2), 314-327. https://doi.org/10.1016/j.cell.2016.05.039

Matsuda, N., Sato, S., Shiba, K., Okatsu, K., Saisho, K., Gautier, C. A., Sou, Y. S., Saiki, S., Kawajiri, S., Sato, F., Kimura, M., Komatsu, M., Hattori, N., & Tanaka, K. (2010). PINK1 stabilized by mitochondrial depolarization recruits Parkin to damaged mitochondria and activates latent Parkin for mitophagy. *J Cell Biol*, *189*(2), 211-221. https://doi.org/10.1083/jcb.200910140

Mazzulli, J. R., Zunke, F., Isacson, O., Studer, L., & Krainc, D. (2016). alpha-Synuclein-induced lysosomal dysfunction occurs through disruptions in protein trafficking in human midbrain synucleinopathy models. *Proc Natl Acad Sci U S A*, *113*(7), 1931-1936. https://doi.org/10.1073/pnas.1520335113

McLaren, W., Gil, L., Hunt, S. E., Riat, H. S., Ritchie, G. R., Thormann, A., Flicek, P., & Cunningham, F. (2016). The Ensembl Variant Effect Predictor. *Genome Biol*, *17*(1), 122. https://doi.org/10.1186/s13059-016-0974-4

McLelland, G. L., Soubannier, V., Chen, C. X., McBride, H. M., & Fon, E. A. (2014). Parkin and PINK1 function in a vesicular trafficking pathway regulating mitochondrial quality control. *EMBO J*, *33*(4), 282-295. https://doi.org/10.1002/embj.201385902

Mendoza-Velasquez, J. J., Flores-Vazquez, J. F., Barron-Velazquez, E., Sosa-Ortiz, A. L., Illigens, B. W., & Siepmann, T. (2019). Autonomic Dysfunction in alpha-Synucleinopathies. *Front Neurol*, *10*, 363. https://doi.org/10.3389/fneur.2019.00363

Meraviglia, V., Zanon, A., Lavdas, A. A., Schwienbacher, C., Silipigni, R., Di Segni, M., Chen, H. S., Pramstaller, P. P., Hicks, A. A., & Rossini, A. (2015). Generation of Induced Pluripotent Stem Cells from Frozen Buffy Coats using Non-integrating Episomal Plasmids. *J Vis Exp*(100), e52885. https://doi.org/10.3791/52885

Mertens, J., Marchetto, M. C., Bardy, C., & Gage, F. H. (2016). Evaluating cell reprogramming, differentiation and conversion technologies in neuroscience. *Nat Rev Neurosci*, *17*(7), 424-437. https://doi.org/10.1038/nrn.2016.46

Michalak, S., Florczak-Wyspianska, J., Rybacka-Mossakowska, J., Ambrosius, W., Osztynowicz, K., Baszczuk, A., Kozubski, W., & Wysocka, E. (2017). Mitochondrial Respiration in Intact Peripheral Blood Mononuclear Cells and Sirtuin 3 Activity in Patients with Movement Disorders. *Oxid Med Cell Longev*, *2017*, 9703574. https://doi.org/10.1155/2017/9703574

Milanese, C., Payan-Gomez, C., Galvani, M., Molano Gonzalez, N., Tresini, M., Nait Abdellah, S., van Roon-Mom, W. M. C., Figini, S., Marinus, J., van Hilten, J. J., & Mastroberardino, P. G. (2019). Peripheral mitochondrial function correlates with clinical severity in

idiopathic Parkinson's disease. *Mov Disord*, *34*(8), 1192-1202. https://doi.org/10.1002/mds.27723

Ming, F., Tan, J., Qin, L., Zhang, H., Tang, J., Tan, X., & Wang, C. (2020). The PARK2 Mutation Associated with Parkinson's Disease Enhances the Vulnerability of Peripheral Blood Lymphocytes to Paraquat. *Biomed Res Int*, *2020*, 4658109. https://doi.org/10.1155/2020/4658109

Mittler, R., Vanderauwera, S., Suzuki, N., Miller, G., Tognetti, V. B., Vandepoele, K., Gollery, M., Shulaev, V., & Van Breusegem, F. (2011). ROS signaling: the new wave? *Trends Plant Sci*, *16*(6), 300-309. https://doi.org/10.1016/j.tplants.2011.03.007

Monzio Compagnoni, G., Di Fonzo, A., Corti, S., Comi, G. P., Bresolin, N., & Masliah, E. (2020). The Role of Mitochondria in Neurodegenerative Diseases: the Lesson from Alzheimer's Disease and Parkinson's Disease. *Mol Neurobiol*, *57*(7), 2959-2980. https://doi.org/10.1007/s12035-020-01926-1

Mor, D. E., Sohrabi, S., Kaletsky, R., Keyes, W., Tartici, A., Kalia, V., Miller, G. W., & Murphy, C. T. (2020). Metformin rescues Parkinson's disease phenotypes caused by hyperactive mitochondria. *Proc Natl Acad Sci U S A*, *117*(42), 26438-26447. https://doi.org/10.1073/pnas.2009838117

Morais, S., Bastos-Ferreira, R., Sequeiros, J., & Alonso, I. (2016). Genomic mechanisms underlying PARK2 large deletions identified in a cohort of patients with PD. *Neurol Genet*, *2*(3), e73. https://doi.org/10.1212/NXG.0000000000000073

Mortiboys, H., Johansen, K. K., Aasly, J. O., & Bandmann, O. (2010). Mitochondrial impairment in patients with Parkinson disease with the G2019S mutation in LRRK2. *Neurology*, *75*(22), 2017-2020. https://doi.org/10.1212/WNL.0b013e3181ff9685

Mortiboys, H., Thomas, K. J., Koopman, W. J., Klaffke, S., Abou-Sleiman, P., Olpin, S., Wood, N. W., Willems, P. H., Smeitink, J. A., Cookson, M. R., & Bandmann, O. (2008). Mitochondrial function and morphology are impaired in parkin-mutant fibroblasts. *Ann Neurol*, *64*(5), 555-565. https://doi.org/10.1002/ana.21492

Moscovich, M., Heinzel, S., Postuma, R. B., Reilmann, R., Klockgether, T., Jacobi, H., Hoglinger, G., & Berg, D. (2020). How specific are non-motor symptoms in the prodrome of Parkinson's disease compared to other movement disorders? *Parkinsonism Relat Disord*, *81*, 213-218. https://doi.org/10.1016/j.parkreldis.2020.10.003

Moustafa, A. A., Chakravarthy, S., Phillips, J. R., Gupta, A., Keri, S., Polner, B., Frank, M. J., & Jahanshahi, M. (2016). Motor symptoms in Parkinson's disease: A unified framework. *Neurosci Biobehav Rev*, *68*, 727-740. https://doi.org/10.1016/j.neubiorev.2016.07.010

Mouton-Liger, F., Jacoupy, M., Corvol, J. C., & Corti, O. (2017). PINK1/Parkin-Dependent Mitochondrial Surveillance: From Pleiotropy to Parkinson's Disease. *Front Mol Neurosci*, *10*, 120. https://doi.org/10.3389/fnmol.2017.00120

Mrozek-Gorska, P., Buschle, A., Pich, D., Schwarzmayr, T., Fechtner, R., Scialdone, A., & Hammerschmidt, W. (2019). Epstein-Barr virus reprograms human B lymphocytes immediately in the prelatent phase of infection. *Proc Natl Acad Sci U S A*, *116*(32), 16046-16055. https://doi.org/10.1073/pnas.1901314116

Muftuoglu, M., Elibol, B., Dalmizrak, O., Ercan, A., Kulaksiz, G., Ogus, H., Dalkara, T., & Ozer, N. (2004). Mitochondrial complex I and IV activities in leukocytes from patients with parkin mutations. *Mov Disord*, *19*(5), 544-548. https://doi.org/10.1002/mds.10695

Narendra, D., Tanaka, A., Suen, D. F., & Youle, R. J. (2008). Parkin is recruited selectively to impaired mitochondria and promotes their autophagy. *J Cell Biol*, *183*(5), 795-803. https://doi.org/10.1083/jcb.200809125

Nguyen, H. N., Byers, B., Cord, B., Shcheglovitov, A., Byrne, J., Gujar, P., Kee, K., Schule, B., Dolmetsch, R. E., Langston, W., Palmer, T. D., & Pera, R. R. (2011). LRRK2 mutant iPSC-derived DA neurons demonstrate increased susceptibility to oxidative stress. *Cell Stem Cell*, *8*(3), 267-280. https://doi.org/10.1016/j.stem.2011.01.013

Nicklas, W. J., Vyas, I., & Heikkila, R. E. (1985). Inhibition of NADH-linked oxidation in brain mitochondria by 1-methyl-4-phenyl-pyridine, a metabolite of the neurotoxin, 1-methyl-4-phenyl-1,2,5,6-tetrahydropyridine. *Life Sci*, *36*(26), 2503-2508. https://doi.org/10.1016/0024-3205(85)90146-8

Nuytemans, K., Theuns, J., Cruts, M., & Van Broeckhoven, C. (2010). Genetic etiology of Parkinson disease associated with mutations in the SNCA, PARK2, PINK1, PARK7, and LRRK2 genes: a mutation update. *Hum Mutat*, *31*(7), 763-780. https://doi.org/10.1002/humu.21277

Oertel, W., & Schulz, J. B. (2016). Current and experimental treatments of Parkinson disease: A guide for neuroscientists. *J Neurochem*, *139 Suppl 1*, 325-337. https://doi.org/10.1111/jnc.13750

Ohlei, O., Dobricic, V., Lohmann, K., Klein, C., Lill, C. M., & Bertram, L. (2018). Field synopsis and systematic meta-analyses of genetic association studies in isolated dystonia. *Parkinsonism Relat Disord*, *57*, 50-57. https://doi.org/10.1016/j.parkreldis.2018.07.018

Okamoto, K., & Shaw, J. M. (2005). Mitochondrial morphology and dynamics in yeast and multicellular eukaryotes. *Annu Rev Genet*, *39*, 503-536. https://doi.org/10.1146/annurev.genet.38.072902.093019

Ovallath, S., & Deepa, P. (2013). The history of parkinsonism: descriptions in ancient Indian medical literature. *Mov Disord*, *28*(5), 566-568. https://doi.org/10.1002/mds.25420

Pacelli, C., De Rasmo, D., Signorile, A., Grattagliano, I., di Tullio, G., D'Orazio, A., Nico, B., Comi, G. P., Ronchi, D., Ferranini, E., Pirolo, D., Seibel, P., Schubert, S., Gaballo, A., Villani, G., & Cocco, T. (2011). Mitochondrial defect and PGC-1alpha dysfunction in parkin-associated familial Parkinson's disease. *Biochim Biophys Acta*, *1812*(8), 1041-1053. https://doi.org/10.1016/j.bbadis.2010.12.022

Palacino, J. J., Sagi, D., Goldberg, M. S., Krauss, S., Motz, C., Wacker, M., Klose, J., & Shen, J. (2004). Mitochondrial dysfunction and oxidative damage in parkin-deficient mice. *J Biol Chem*, *279*(18), 18614-18622. https://doi.org/10.1074/jbc.M401135200

Palmer, C. S., Osellame, L. D., Laine, D., Koutsopoulos, O. S., Frazier, A. E., & Ryan, M. T. (2011). MiD49 and MiD51, new components of the mitochondrial fission machinery. *EMBO Rep*, *12*(6), 565-573. https://doi.org/10.1038/embor.2011.54

Park, J. S., Davis, R. L., & Sue, C. M. (2018). Mitochondrial Dysfunction in Parkinson's Disease: New Mechanistic Insights and Therapeutic Perspectives. *Curr Neurol Neurosci Rep*, *18*(5), 21. https://doi.org/10.1007/s11910-018-0829-3

Parker, W. D., Jr., Parks, J. K., & Swerdlow, R. H. (2008). Complex I deficiency in Parkinson's disease frontal cortex. *Brain Res*, *1189*, 215-218. https://doi.org/10.1016/j.brainres.2007.10.061

Parr, C. J. C., Yamanaka, S., & Saito, H. (2017). An update on stem cell biology and engineering for brain development. *Mol Psychiatry*, *22*(6), 808-819. https://doi.org/10.1038/mp.2017.66

Pattaro, C., Gogele, M., Mascalzoni, D., Melotti, R., Schwienbacher, C., De Grandi, A., Foco, L., D'Elia, Y., Linder, B., Fuchsberger, C., Minelli, C., Egger, C., Kofink, L. S., Zanigni, S., Schafer, T., Facheris, M. F., Smarason, S. V., Rossini, A., Hicks, A. A., Weiss, H., & Pramstaller, P. P. (2015). The Cooperative Health Research in South Tyrol (CHRIS) study: rationale, objectives, and preliminary results. *J Transl Med*, *13*, 348. https://doi.org/10.1186/s12967-015-0704-9

Pattaro, C., Marroni, F., Riegler, A., Mascalzoni, D., Pichler, I., Volpato, C. B., Dal Cero, U., De Grandi, A., Egger, C., Eisendle, A., Fuchsberger, C., Gogele, M., Pedrotti, S., Pinggera, G. K., Stefanov, S. A., Vogl, F. D., Wiedermann, C. J., Meitinger, T., & Pramstaller, P. P. (2007). The genetic study of three population microisolates in South Tyrol (MICROS): study design and epidemiological perspectives. *BMC Med Genet*, *8*, 29. https://doi.org/10.1186/1471-2350-8-29

Penno, M. B., Pedrotti-Krueger, M., & Ray, T. (1993). Cryopreservation of whole blood and isolated lymphocytes for B-cell immortalization. *Journal of tissue culture methods*, *15*(1), 43-47. https://doi.org/10.1007/BF02387289

Perrier, A. L., Tabar, V., Barberi, T., Rubio, M. E., Bruses, J., Topf, N., Harrison, N. L., & Studer, L. (2004). Derivation of midbrain dopamine neurons from human embryonic stem cells. *Proc Natl Acad Sci U S A*, *101*(34), 12543-12548. https://doi.org/10.1073/pnas.0404700101

Pesta, D., Hoppel, F., Macek, C., Messner, H., Faulhaber, M., Kobel, C., Parson, W., Burtscher, M., Schocke, M., & Gnaiger, E. (2011). Similar qualitative and quantitative changes of mitochondrial respiration following strength and endurance training in normoxia and hypoxia in sedentary humans. *Am J Physiol Regul Integr Comp Physiol*, *301*(4), R1078-1087. https://doi.org/10.1152/ajpregu.00285.2011

Piccoli, C., Sardanelli, A., Scrima, R., Ripoli, M., Quarato, G., D'Aprile, A., Bellomo, F., Scacco, S., De Michele, G., Filla, A., Iuso, A., Boffoli, D., Capitanio, N., & Papa, S. (2008). Mitochondrial respiratory dysfunction in familiar parkinsonism associated with PINK1 mutation. *Neurochem Res*, *33*(12), 2565-2574. https://doi.org/10.1007/s11064-008-9729-2

Pickrell, A. M., Huang, C. H., Kennedy, S. R., Ordureau, A., Sideris, D. P., Hoekstra, J. G., Harper, J. W., & Youle, R. J. (2015). Endogenous Parkin Preserves Dopaminergic Substantia Nigral Neurons following Mitochondrial DNA Mutagenic Stress. *Neuron*, *87*(2), 371-381. https://doi.org/10.1016/j.neuron.2015.06.034

Pinto, M., Nissanka, N., & Moraes, C. T. (2018). Lack of Parkin Anticipates the Phenotype and Affects Mitochondrial Morphology and mtDNA Levels in a Mouse Model of Parkinson's Disease. *J Neurosci*, *38*(4), 1042-1053. https://doi.org/10.1523/JNEUROSCI.1384-17.2017

Poewe, W., Seppi, K., Tanner, C. M., Halliday, G. M., Brundin, P., Volkmann, J., Schrag, A. E., & Lang, A. E. (2017). Parkinson disease. *Nat Rev Dis Primers*, *3*, 17013. https://doi.org/10.1038/nrdp.2017.13

Polymeropoulos, M. H., Lavedan, C., Leroy, E., Ide, S. E., Dehejia, A., Dutra, A., Pike, B., Root, H., Rubenstein, J., Boyer, R., Stenroos, E. S., Chandrasekharappa, S., Athanassiadou, A., Papapetropoulos, T., Johnson, W. G., Lazzarini, A. M., Duvoisin, R. C., Di Iorio, G., Golbe, L. I., & Nussbaum, R. L. (1997). Mutation in the alpha-synuclein gene identified in families with Parkinson's disease. *Science*, *276*(5321), 2045-2047. https://doi.org/10.1126/science.276.5321.2045

Pramstaller, P. P., Falk, M., Schoenhuber, R., & Poewe, W. (1999). Validation of a mail questionnaire for parkinsonism in two languages (German and Italian). *J Neurol*, *246*(2), 79-86. https://doi.org/10.1007/s004150050312

Pramstaller, P. P., Schlossmacher, M. G., Jacques, T. S., Scaravilli, F., Eskelson, C., Pepivani, I., Hedrich, K., Adel, S., Gonzales-McNeal, M., Hilker, R., Kramer, P. L., & Klein, C. (2005). Lewy body Parkinson's disease in a large pedigree with 77 Parkin mutation carriers. *Ann Neurol*, *58*(3), 411-422. https://doi.org/10.1002/ana.20587

Prasuhn, J., Borsche, M., Hicks, A. A., Gogele, M., Egger, C., Kritzinger, C., Pichler, I., Castelo-Rueda, M. P., Langlott, L., Kasten, M., Mascalzoni, D., Klein, C., Pramstaller, P. P., & Bruggemann, N. (2021). Task matters - challenging the motor system allows distinguishing unaffected Parkin mutation carriers from mutation-free controls. *Parkinsonism Relat Disord*, *86*, 101-104. https://doi.org/10.1016/j.parkreldis.2021.03.028

Qadri, R., Namdeo, M., Behari, M., Goyal, V., Sharma, S., & Mukhopadhyay, A. K. (2018). Alterations in mitochondrial membrane potential in peripheral blood mononuclear cells in Parkinson's Disease: Potential for a novel biomarker. *Restor Neurol Neurosci*, *36*(6), 719-727. https://doi.org/10.3233/RNN-180852

Qiu, X., Xiao, Y., Wu, J., Gan, L., Huang, Y., & Wang, J. (2019). C-Reactive Protein and Risk of Parkinson's Disease: A Systematic Review and Meta-Analysis. *Front Neurol*, *10*, 384. https://doi.org/10.3389/fneur.2019.00384

Rakovic, A., Grunewald, A., Kottwitz, J., Bruggemann, N., Pramstaller, P. P., Lohmann, K., & Klein, C. (2011). Mutations in PINK1 and Parkin impair ubiquitination of Mitofusins in human fibroblasts. *PLoS One*, *6*(3), e16746. https://doi.org/10.1371/journal.pone.0016746

Ransohoff, R. M., Schafer, D., Vincent, A., Blachere, N. E., & Bar-Or, A. (2015). Neuroinflammation: Ways in Which the Immune System Affects the Brain. *Neurotherapeutics*, *12*(4), 896-909. https://doi.org/10.1007/s13311-015-0385-3

Reeve, A., Simcox, E., & Turnbull, D. (2014). Ageing and Parkinson's disease: why is advancing age the biggest risk factor? *Ageing Res Rev*, *14*, 19-30. https://doi.org/10.1016/j.arr.2014.01.004

Rodolfo, C., Campello, S., & Cecconi, F. (2018). Mitophagy in neurodegenerative diseases. *Neurochem Int*, *117*, 156-166. https://doi.org/10.1016/j.neuint.2017.08.004

Rothfuss, O., Fischer, H., Hasegawa, T., Maisel, M., Leitner, P., Miesel, F., Sharma, M., Bornemann, A., Berg, D., Gasser, T., & Patenge, N. (2009). Parkin protects mitochondrial genome integrity and supports mitochondrial DNA repair. *Hum Mol Genet*, *18*(20), 3832-3850. https://doi.org/10.1093/hmg/ddp327

Saiki, R. K., Scharf, S., Faloona, F., Mullis, K. B., Horn, G. T., Erlich, H. A., & Arnheim, N. (1985). Enzymatic amplification of beta-globin genomic sequences and restriction site analysis for diagnosis of sickle cell anemia. *Science*, *230*(4732), 1350-1354. https://doi.org/10.1126/science.2999980

Sanjari Moghaddam, H., Ghazi Sherbaf, F., Mojtahed Zadeh, M., Ashraf-Ganjouei, A., & Aarabi, M. H. (2018). Association Between Peripheral Inflammation and DATSCAN Data of the Striatal Nuclei in Different Motor Subtypes of Parkinson Disease. *Front Neurol*, *9*, 234. https://doi.org/10.3389/fneur.2018.00234

Santos, M., Morais, S., Pereira, C., Sequeiros, J., & Alonso, I. (2019). Parkin truncating variants result in a loss-of-function phenotype. *Sci Rep*, *9*(1), 16150. https://doi.org/10.1038/s41598-019-52534-6

Saxton, W. M., & Hollenbeck, P. J. (2012). The axonal transport of mitochondria. *J Cell Sci*, *125*(Pt 9), 2095-2104. https://doi.org/10.1242/jcs.053850

Schapira, A. H. (1993). Mitochondrial complex I deficiency in Parkinson's disease. *Adv Neurol*, *60*, 288-291. https://www.ncbi.nlm.nih.gov/pubmed/8420145

Schapira, A. H., Mann, V. M., Cooper, J. M., Dexter, D., Daniel, S. E., Jenner, P., Clark, J. B., & Marsden, C. D. (1990). Anatomic and disease specificity of NADH CoQ1 reductase (complex I) deficiency in Parkinson's disease. *J Neurochem*, *55*(6), 2142-2145. https://doi.org/10.1111/j.1471-4159.1990.tb05809.x

Scherzer, C. R., Eklund, A. C., Morse, L. J., Liao, Z., Locascio, J. J., Fefer, D., Schwarzschild, M. A., Schlossmacher, M. G., Hauser, M. A., Vance, J. M., Sudarsky, L. R., Standaert, D. G., Growdon, J. H., Jensen, R. V., & Gullans, S. R. (2007). Molecular markers of early Parkinson's disease based on gene expression in blood. *Proc Natl Acad Sci U S A*, *104*(3), 955-960. https://doi.org/10.1073/pnas.0610204104

Seirafi, M., Kozlov, G., & Gehring, K. (2015). Parkin structure and function. *FEBS J*, *282*(11), 2076-2088. https://doi.org/10.1111/febs.13249

Shaltouki, A., Sivapatham, R., Pei, Y., Gerencser, A. A., Momcilovic, O., Rao, M. S., & Zeng, X. (2015). Mitochondrial alterations by PARKIN in dopaminergic neurons using PARK2 patient-specific and PARK2 knockout isogenic iPSC lines. *Stem Cell Reports*, *4*(5), 847-859. https://doi.org/10.1016/j.stemcr.2015.02.019

Shin, J. H., Ko, H. S., Kang, H., Lee, Y., Lee, Y. I., Pletinkova, O., Troconso, J. C., Dawson, V. L., & Dawson, T. M. (2011). PARIS (ZNF746) repression of PGC-1alpha contributes to neurodegeneration in Parkinson's disease. *Cell*, *144*(5), 689-702. https://doi.org/10.1016/j.cell.2011.02.010

Sie, L., Loong, S., & Tan, E. K. (2009). Utility of lymphoblastoid cell lines. *J Neurosci Res*, *87*(9), 1953-1959. https://doi.org/10.1002/jnr.22000

Simon, D. K., Mayeux, R., Marder, K., Kowall, N. W., Beal, M. F., & Johns, D. R. (2000). Mitochondrial DNA mutations in complex I and tRNA genes in Parkinson's disease. *Neurology*, *54*(3), 703-709. https://doi.org/10.1212/wnl.54.3.703

Singh, A., Zhi, L., & Zhang, H. (2019). LRRK2 and mitochondria: Recent advances and current views. *Brain Res*, *1702*, 96-104. https://doi.org/10.1016/j.brainres.2018.06.010

Sliter, D. A., Martinez, J., Hao, L., Chen, X., Sun, N., Fischer, T. D., Burman, J. L., Li, Y., Zhang, Z., Narendra, D. P., Cai, H., Borsche, M., Klein, C., & Youle, R. J. (2018). Parkin and PINK1 mitigate STING-induced inflammation. *Nature*, *561*(7722), 258-262. https://doi.org/10.1038/s41586-018-0448-9

Smith, A. M., Depp, C., Ryan, B. J., Johnston, G. I., Alegre-Abarrategui, J., Evetts, S., Rolinski, M., Baig, F., Ruffmann, C., Simon, A. K., Hu, M. T. M., & Wade-Martins, R. (2018). Mitochondrial dysfunction and increased glycolysis in prodromal and early Parkinson's blood cells. *Mov Disord*, *33*(10), 1580-1590. https://doi.org/10.1002/mds.104

Spillantini, M. G., Crowther, R. A., Jakes, R., Hasegawa, M., & Goedert, M. (1998). alpha-Synuclein in filamentous inclusions of Lewy bodies from Parkinson's disease and dementia with lewy bodies. *Proc Natl Acad Sci U S A*, *95*(11), 6469-6473. https://doi.org/10.1073/pnas.95.11.6469

Stevens, D. A., Lee, Y., Kang, H. C., Lee, B. D., Lee, Y. I., Bower, A., Jiang, H., Kang, S. U., Andrabi, S. A., Dawson, V. L., Shin, J. H., & Dawson, T. M. (2015). Parkin loss leads to PARIS-dependent declines in mitochondrial mass and respiration. *Proc Natl Acad Sci U S A*, *112*(37), 11696-11701. https://doi.org/10.1073/pnas.1500624112

Storch, A., Ludolph, A. C., & Schwarz, J. (2004). Dopamine transporter: involvement in selective dopaminergic neurotoxicity and degeneration. *J Neural Transm (Vienna)*, *111*(10-11), 1267-1286. https://doi.org/10.1007/s00702-004-0203-2

Suen, D. F., Narendra, D. P., Tanaka, A., Manfredi, G., & Youle, R. J. (2010). Parkin overexpression selects against a deleterious mtDNA mutation in heteroplasmic cybrid cells. *Proc Natl Acad Sci U S A*, *107*(26), 11835-11840. https://doi.org/10.1073/pnas.0914569107

Suzuki, S., Akamatsu, W., Kisa, F., Sone, T., Ishikawa, K. I., Kuzumaki, N., Katayama, H., Miyawaki, A., Hattori, N., & Okano, H. (2017). Efficient induction of dopaminergic neuron differentiation from induced pluripotent stem cells reveals impaired mitophagy in PARK2 neurons. *Biochem Biophys Res Commun*, *483*(1), 88-93. https://doi.org/10.1016/j.bbrc.2016.12.188

Tanaka, A., Cleland, M. M., Xu, S., Narendra, D. P., Suen, D. F., Karbowski, M., & Youle, R. J. (2010). Proteasome and p97 mediate mitophagy and degradation of mitofusins induced by Parkin. *J Cell Biol*, *191*(7), 1367-1380. https://doi.org/10.1083/jcb.201007013

Tischfield, M. A., Baris, H. N., Wu, C., Rudolph, G., Van Maldergem, L., He, W., Chan, W. M., Andrews, C., Demer, J. L., Robertson, R. L., Mackey, D. A., Ruddle, J. B., Bird, T. D., Gottlob, I., Pieh, C., Traboulsi, E. I., Pomeroy, S. L., Hunter, D. G., Soul, J. S., Newlin, A., Sabol, L. J., Doherty, E. J., de Uzcategui, C. E., de Uzcategui, N., Collins, M. L., Sener, E. C., Wabbels, B., Hellebrand, H., Meitinger, T., de Berardinis, T., Magli, A., Schiavi, C., Pastore-Trossello, M., Koc, F., Wong, A. M., Levin, A. V., Geraghty, M. T., Descartes, M., Flaherty, M., Jamieson, R. V., Moller, H. U., Meuthen, I., Callen, D. F., Kerwin, J., Lindsay, S., Meindl, A., Gupta, M. L., Jr., Pellman, D., & Engle, E. C. (2010). Human TUBB3

mutations perturb microtubule dynamics, kinesin interactions, and axon guidance. *Cell*, *140*(1), 74-87. https://doi.org/10.1016/j.cell.2009.12.011

Toyofuku, T., Okamoto, Y., Ishikawa, T., Sasawatari, S., & Kumanogoh, A. (2020). LRRK2 regulates endoplasmic reticulum-mitochondrial tethering through the PERK-mediated ubiquitination pathway. *EMBO J*, *39*(2), e100875. https://doi.org/10.15252/embj.2018100875

Tran, J., Anastacio, H., & Bardy, C. (2020). Genetic predispositions of Parkinson's disease revealed in patient-derived brain cells. *NPJ Parkinsons Dis*, *6*, 8. https://doi.org/10.1038/s41531-020-0110-8

Trempe, J. F., Sauve, V., Grenier, K., Seirafi, M., Tang, M. Y., Menade, M., Al-Abdul-Wahid, S., Krett, J., Wong, K., Kozlov, G., Nagar, B., Fon, E. A., & Gehring, K. (2013). Structure of parkin reveals mechanisms for ubiquitin ligase activation. *Science*, *340*(6139), 1451-1455. https://doi.org/10.1126/science.1237908

Trinh, D., Israwi, A. R., Arathoon, L. R., Gleave, J. A., & Nash, J. E. (2021). The multi-faceted role of mitochondria in the pathology of Parkinson's disease. *J Neurochem*, *156*(6), 715-752. https://doi.org/10.1111/jnc.15154

Valdinocci, D., Simoes, R. F., Kovarova, J., Cunha-Oliveira, T., Neuzil, J., & Pountney, D. L. (2019). Intracellular and Intercellular Mitochondrial Dynamics in Parkinson's Disease. *Front Neurosci*, *13*, 930. https://doi.org/10.3389/fnins.2019.00930

Valente, E. M., Abou-Sleiman, P. M., Caputo, V., Muqit, M. M., Harvey, K., Gispert, S., Ali, Z., Del Turco, D., Bentivoglio, A. R., Healy, D. G., Albanese, A., Nussbaum, R., Gonzalez-Maldonado, R., Deller, T., Salvi, S., Cortelli, P., Gilks, W. P., Latchman, D. S., Harvey, R. J., Dallapiccola, B., Auburger, G., & Wood, N. W. (2004). Hereditary early-onset Parkinson's disease caused by mutations in PINK1. *Science*, *304*(5674), 1158-1160. https://doi.org/10.1126/science.1096284

Van Laar, V. S., & Berman, S. B. (2009). Mitochondrial dynamics in Parkinson's disease. *Exp Neurol*, *218*(2), 247-256. https://doi.org/10.1016/j.expneurol.2009.03.019

Verstreken, P., Ly, C. V., Venken, K. J., Koh, T. W., Zhou, Y., & Bellen, H. J. (2005). Synaptic mitochondria are critical for mobilization of reserve pool vesicles at Drosophila neuromuscular junctions. *Neuron*, *47*(3), 365-378. https://doi.org/10.1016/j.neuron.2005.06.018

Vicario, M., Cieri, D., Brini, M., & Cali, T. (2018). The Close Encounter Between Alpha-Synuclein and Mitochondria. *Front Neurosci*, *12*, 388. https://doi.org/10.3389/fnins.2018.00388

Vida, C., Kobayashi, H., Garrido, A., Martinez de Toda, I., Carro, E., Molina, J. A., & De la Fuente, M. (2019). Lymphoproliferation Impairment and Oxidative Stress in Blood Cells from Early Parkinson's Disease Patients. *Int J Mol Sci*, *20*(3). https://doi.org/10.3390/ijms20030771

Villa, E., Marchetti, S., & Ricci, J. E. (2018). No Parkin Zone: Mitophagy without Parkin. *Trends Cell Biol*, *28*(11), 882-895. https://doi.org/10.1016/j.tcb.2018.07.004

Vives-Bauza, C., Zhou, C., Huang, Y., Cui, M., de Vries, R. L., Kim, J., May, J., Tocilescu, M. A., Liu, W., Ko, H. S., Magrane, J., Moore, D. J., Dawson, V. L., Grailhe, R., Dawson, T. M., Li, C., Tieu, K., & Przedborski, S. (2010). PINK1-dependent recruitment of Parkin to

mitochondria in mitophagy. *Proc Natl Acad Sci U S A*, *107*(1), 378-383. https://doi.org/10.1073/pnas.0911187107

Vulinovic, F., Krajka, V., Hausrat, T. J., Seibler, P., Alvarez-Fischer, D., Madoev, H., Park, J. S., Kumar, K. R., Sue, C. M., Lohmann, K., Kneussel, M., Klein, C., & Rakovic, A. (2018). Motor protein binding and mitochondrial transport are altered by pathogenic TUBB4A variants. *Hum Mutat*, *39*(12), 1901-1915. https://doi.org/10.1002/humu.23602

Wasner, K., Grunewald, A., & Klein, C. (2020). Parkin-linked Parkinson's disease: From clinical insights to pathogenic mechanisms and novel therapeutic approaches. *Neurosci Res*, *159*, 34-39. https://doi.org/10.1016/j.neures.2020.09.001

Wei, W., & Chinnery, P. F. (2020). Inheritance of mitochondrial DNA in humans: implications for rare and common diseases. *J Intern Med*, *287*(6), 634-644. https://doi.org/10.1111/joim.13047

Wei, W., Keogh, M. J., Wilson, I., Coxhead, J., Ryan, S., Rollinson, S., Griffin, H., Kurzawa-Akanbi, M., Santibanez-Koref, M., Talbot, K., Turner, M. R., McKenzie, C. A., Troakes, C., Attems, J., Smith, C., Al Sarraj, S., Morris, C. M., Ansorge, O., Pickering-Brown, S., Ironside, J. W., & Chinnery, P. F. (2017). Mitochondrial DNA point mutations and relative copy number in 1363 disease and control human brains. *Acta Neuropathol Commun*, *5*(1), 13. https://doi.org/10.1186/s40478-016-0404-6

Wei, Y., Chiang, W. C., Sumpter, R., Jr., Mishra, P., & Levine, B. (2017). Prohibitin 2 Is an Inner Mitochondrial Membrane Mitophagy Receptor. *Cell*, *168*(1-2), 224-238 e210. https://doi.org/10.1016/j.cell.2016.11.042

Weissbach, A., Konig, I. R., Huckelheim, K., Pramstaller, P. P., Werner, E., Bruggemann, N., Tadic, V., Lohmann, K., Baumer, T., Munchau, A., Kasten, M., & Klein, C. (2017). Influence of L-dopa on subtle motor signs in heterozygous Parkin- and PINK1 mutation carriers. *Parkinsonism Relat Disord*, *42*, 95-99. https://doi.org/10.1016/j.parkreldis.2017.07.003

Wenzel, D. M., Lissounov, A., Brzovic, P. S., & Klevit, R. E. (2011). UBCH7 reactivity profile reveals parkin and HHARI to be RING/HECT hybrids. *Nature*, *474*(7349), 105-108. https://doi.org/10.1038/nature09966

Westermann, B. (2012). Bioenergetic role of mitochondrial fusion and fission. *Biochim Biophys Acta*, *1817*(10), 1833-1838. https://doi.org/10.1016/j.bbabio.2012.02.033

Winklhofer, K. F., & Haass, C. (2010). Mitochondrial dysfunction in Parkinson's disease. *Biochim Biophys Acta*, *1802*(1), 29-44. https://doi.org/10.1016/j.bbadis.2009.08.013

Wishart, S., & Macphee, G. J. (2011). Evaluation and management of the non-motor features of Parkinson's disease. *Ther Adv Chronic Dis*, *2*(2), 69-85. https://doi.org/10.1177/2040622310387847

Yi, W., MacDougall, E. J., Tang, M. Y., Krahn, A. I., Gan-Or, Z., Trempe, J. F., & Fon, E. A. (2019). The landscape of Parkin variants reveals pathogenic mechanisms and therapeutic targets in Parkinson's disease. *Hum Mol Genet*, *28*(17), 2811-2825. https://doi.org/10.1093/hmg/ddz080

Yoshii, S. R., Kishi, C., Ishihara, N., & Mizushima, N. (2011). Parkin mediates proteasome-dependent protein degradation and rupture of the outer mitochondrial membrane. *J Biol Chem*, *286*(22), 19630-19640. https://doi.org/10.1074/jbc.M110.209338

Yoshino, H., Nakagawa-Hattori, Y., Kondo, T., & Mizuno, Y. (1992). Mitochondrial complex I and II activities of lymphocytes and platelets in Parkinson's disease. *Journal of Neural Transmission - Parkinson's Disease and Dementia Section*, *4*(1), 27-34. https://doi.org/10.1007/BF02257619

Zahoor, I., Shafi, A., & Haq, E. (2018). Pharmacological Treatment of Parkinson's Disease. In T. B. Stoker & J. C. Greenland (Eds.), *Parkinson's Disease: Pathogenesis and Clinical Aspects*. https://doi.org/10.15586/codonpublications.parkinsonsdisease.2018.ch7

Zanellati, M. C., Monti, V., Barzaghi, C., Reale, C., Nardocci, N., Albanese, A., Valente, E. M., Ghezzi, D., & Garavaglia, B. (2015). Mitochondrial dysfunction in Parkinson disease: evidence in mutant PARK2 fibroblasts. *Front Genet*, *6*, 78. https://doi.org/10.3389/fgene.2015.00078

Zanon, A., Kalvakuri, S., Rakovic, A., Foco, L., Guida, M., Schwienbacher, C., Serafin, A., Rudolph, F., Trilck, M., Grunewald, A., Stanslowsky, N., Wegner, F., Giorgio, V., Lavdas, A. A., Bodmer, R., Pramstaller, P. P., Klein, C., Hicks, A. A., Pichler, I., & Seibler, P. (2017). SLP-2 interacts with Parkin in mitochondria and prevents mitochondrial dysfunction in Parkin-deficient human iPSC-derived neurons and Drosophila. *Hum Mol Genet*, *26*(13), 2412-2425. https://doi.org/10.1093/hmg/ddx132

Zanon, A., Pramstaller, P. P., Hicks, A. A., & Pichler, I. (2018). Environmental and Genetic Variables Influencing Mitochondrial Health and Parkinson's Disease Penetrance. *Parkinsons Dis*, *2018*, 8684906. https://doi.org/10.1155/2018/8684906

Zanon, A., Riekschnitz, D., von Troyer, M., Volpato, C., Picard, A., Cantaloni, C., Di Segni, M., Silipigni, R., Pramstaller, P. P., Hicks, A. A., & Pichler, I. (2019). Generation of an induced pluripotent stem cell line (EURACi005-A) from a Parkinson's disease patient carrying a homozygous exon 3 deletion in the PRKNgene. *Stem Cell Res*, *41*, 101624. https://doi.org/10.1016/j.scr.2019.101624

Zhang, W., Hu, X., Shen, Q., & Xing, D. (2019). Mitochondria-specific drug release and reactive oxygen species burst induced by polyprodrug nanoreactors can enhance chemotherapy. *Nature Communications*, *10*(1), 1704. https://doi.org/10.1038/s41467-019-09566-3

Zhao, R. Z., Jiang, S., Zhang, L., & Yu, Z. B. (2019). Mitochondrial electron transport chain, ROS generation and uncoupling (Review). *Int J Mol Med*, *44*(1), 3-15. https://doi.org/10.3892/ijmm.2019.4188

Zheng, L., Bernard-Marissal, N., Moullan, N., D'Amico, D., Auwerx, J., Moore, D. J., Knott, G., Aebischer, P., & Schneider, B. L. (2017). Parkin functionally interacts with PGC-1alpha to preserve mitochondria and protect dopaminergic neurons. *Hum Mol Genet*, *26*(3), 582-598. https://doi.org/10.1093/hmg/ddw418

Zilocchi, M., Colugnat, I., Lualdi, M., Meduri, M., Marini, F., Corasolla Carregari, V., Moutaoufik, M. T., Phanse, S., Pieroni, L., Babu, M., Garavaglia, B., Fasano, M., & Alberio, T. (2020). Exploring the Impact of PARK2 Mutations on the Total and Mitochondrial Proteome of Human Skin Fibroblasts. *Front Cell Dev Biol*, *8*, 423. https://doi.org/10.3389/fcell.2020.00423

Ziviani, E., Tao, R. N., & Whitworth, A. J. (2010). Drosophila parkin requires PINK1 for mitochondrial translocation and ubiquitinates mitofusin. *Proc Natl Acad Sci U S A*, *107*(11), 5018-5023. https://doi.org/10.1073/pnas.0913485107

8. Acknowledgments

I would like to thank all the people who have supported me during my PhD.

I would like to thank Dr. Andrew A. Hicks for giving me the opportunity to perform my PhD at the Institute for Biomedicine at the European Academy of Bozen and for all his support and guidance. I also thank Professor Simona Casarosa for her help and availability.

I would also like to express my gratitude to Dr. Irene Pichler for her supervision, advice, and support during my PhD studies. Additionally, I would like to thank Dr. Alessandra Zanon for her unconditional support through this process and to all my lab friends and colleagues, for creating an encouraging and creative environment.

A heartfelt thanks goes to Ale, Julia, Giada and Gio, who have always been there for me, through thick and thin.

I would like to thank the bioinformatic group, Dr. Athina Raftopoulou and Dr. Alexandros Lavdas for all the support with the analyses.

My love and endless gratitude go to my family for their unconditional support and great encouragement through all these years.

9. Appendix

9.1 List of abbreviations

AAO – age at onset

AP - Alkaline phosphatase

CCCP - Carbonyl cyanide 4-(trifluoromethoxy) phenylhydrazone

CHRIS - Cooperative Health Research in South Tyrol

CNVs - copy number variations

COMT – catechol-o-methyltransferase

CS - citrate synthase

DA – Dopaminergic

ddPCR - Droplet digital PCR

Drp1 - dynamin-related protein 1

DT - doubling time

EBs - embryoid bodies

EBV - Epstein Barr Virus

ERRs - estrogen related receptors

ETC - electron transport chain

FBS - fetal bovine serum

FCCP - carbonyl cyanide-p-trifluoromethoxyphenylhydrazone

GFR - Growth Factor Reduced

HDAC - histone deacetylases

HF - frequency of heteroplasmy

IMM – inner mitochondrial membrane

IMS - intermembrane space

iPD – idiopathic PD

iPSC - induced pluripotent stem cell

KSR - knockout serum replacement

LBs – Lewy bodies

LCLs - lymphoblastoid cell lines

L-Dopa – levodopa

mROS – mitochondrial reactive oxygen species

MAO – monoamine oxidase

MDV – mitochondrial derived vesicle

MEF - mouse embryonic fibroblasts

MFN1 - mitofusin 1

MFN2 - mitofusin 2

MMP, Δψ – mitochondrial membrane potential

MnSOD - manganese superoxide dismutase

MPP+ - cation 1-methyl-4-phenylpyridinium

MPPP - 1-methyl-4-phenyl-4-propionoxy-piperine

MPTP – 1-methyl-4-phenyl tetrahydropyridine

mtDNA – mitochondrial DNA

MTG - Mito Tracker™ Green

NaB - sodium butyrate

NADH

NRFs - nuclear respiratory factors

O2k - Oxygraph-2k

OCR - oxygen consumption rates

OMM – outer mitochondrial membrane

Opa1 - optic atrophy protein

OXPHOS - oxidative phosphorylation

PARIS – parkin interacting substrate

PARL – presenilin-associated rhomboid-like protein

PBMCs - peripheral blood mononuclear cells

PD – Parkinson´s Disease

PGC-1 α - peroxisome proliferator-activated receptor gamma coactivator 1α

PHA – phytohemagglutinin

PVDF - polyvinylidene fluoride

qRT-PCR - quantitative RT-PCR

REP – repressor element of parkin

ROCK - Rho-associated, coiled-coil containing protein kinase

ROS – reactive oxygen species

RQI - RNA quality indicator

SNpc – substantia nigra pars compacta

SNPs – single nucleotide polymorphisms

SOD2 - superoxide dismutase

TCA - tricarboxylic acid

TFAM – mitochondrial transcription factor A

TH - tyrosine hydroxylase

TMRM - Tetramethylrhodamine, methyl ester

TOM70 - mitochondrial import receptor subunit

UbL – ubiquitin-like

Declaration

I, Maria Paulina Castelo, confirm that this is my own work and the use of all material from other sources has been properly and fully acknowledged.

To protect the specific know-how (point 7 of the "Convenzione per il finanziamento di n. 1 borsa di studio Dottorato di Ricerca in Scienze Biomolecolari 33° ciclo, a.a. 2017/2018"), this doctoral thesis is subject to a 36 months embargo starting from the submission of the thesis on June 3, 2021. Consequently, the doctoral thesis shall be considered as confidential material until the end of the embargo period.